NTNU
Norwegian University of
Science and Technology

Initial Design and Analysis of a Floating Bridge Concept

Simon Gundegjerde

Marine Technology
Submission date: June 2017
Supervisor: Bernt Johan Leira, IMT
Co-supervisor: Rune Risnes, Risnes Innovation AS

Norwegian University of Science and Technology
Department of Marine Technology

NTNU
Norwegian University of Science and Technology
Department of Marine Technology

Master Thesis, Spring 2017
for
Master Student Simon Gundegjerde

Initial Design and Analysis of a Floating Bridge Concept

Innledende Design og Analyse av et Flytebrokonsept

The estimated cost for *Coastal Highway Route E39* has increased significantly over the last three years. Some of the cost drivers are linked to the high complexity of the bridge concepts. Rune Risnes in Risnes Innovation AS has come up with an alternative concept called *X-bridge.* This concept is designed to reduce the cost by utilizing well-known Norwegian marine and technology solutions. The *X-bridge* concept is designed to reduce cost especially within the fields of heavy lift operations and subsea operations as well as by removing large bridge towers.

The following subjects are to be addressed as part of this work:

1. Describe the background for the *Coastal Highway Route E39* and give a brief introduction to the concept of floating bridges. Some examples of existing floating bridges are to be included.
2. The relevant theoretical basis is to be outlined and some of the key algorithims utlized by the relevant computer software are to be described.
3. Explain the concept behind the *X-bridge*. Emphasis should be on the difference relative to ordinary floating bridges.
4. Come up with a suggested design based on the given input given by the designer Rune Risnes. Use data from similar constructions for the items where more accurate information is not available.
5. Perform a hydrodynamic analysis, using an appropriate software, for the floating parts of the bridge. Create a bridge model including the results from the hydrodynamic analysis as a coupled SIMO/RIFLEX model using SIMA.
6. Perform a static response analysis of the bridge followed by an eigenmode analysis. It should be aimed at identifying important eigenmodes. Dynamic analyses of the model subjected to relevant loading are also to be perfomred.
7. Depending on the development of the project and the concept, other design aspects may also be investigated.

The work scope may prove to be larger than initially anticipated. Subject to approval from the supervisor, topics may be deleted from the list above or reduced in extent.

In the thesis, the candidate shall present his personal contribution to the resolution of problems within the scope of the thesis work. Theories and conclusions should be based on mathematical derivations and/or logic reasoning identifying the various steps in the deduction.

The candidate should utilise the existing possibilities for obtaining relevant literature.

The thesis should be organised in a rational manner to give a clear exposition of results, assessments, and conclusions. The text should be brief and to the point, with a clear language. Telegraphic language should be avoided.

The thesis shall contain the following elements: A text defining the scope, preface, list of contents, summary, main body of thesis, conclusions with recommendations for further work, list of symbols and acronyms, references and (optional) appendices. All figures, tables and equations shall be numbered.

The supervisor may require that the candidate, in an early stage of the work, presents a written plan for the completion of the work. The original contribution of the candidate and material taken from other sources shall be clearly defined. Work from other sources shall be properly referenced using an acknowledged referencing system.

The thesis shall be submitted in 3 copies:

- Signed by the candidate
- The text defining the scope included
- In bound volume(s)
- Drawings and/or computer prints which cannot be bound should be organised in a separate folder.

Supervisor: Professor Bernt J. Leira

Deadline: June 11th 2017

Trondheim, January, 2017

Bernt J. Leira

Preface

This thesis within marine structures is the final work of a five-year master's degree in marine technology. It is written at the Department of Marine Technology at the Norwegian University of Science and Technology (NTNU). The thesis investigates a new concept for floating bridges suggested for the *Ferry-free coastal route E39*.

Rune Risnes is the person behind the floating bridge concept investigated in this thesis. I would like to thank him for giving me the opportunity to work with a new and exciting concept. His help during the work is also much appreciated.

My main supervisor at the Department of Marine Technology during my thesis work has been Professor Bernt Johan Leira. I would like to thank him for his guidance and for giving me the opportunity to shape my master thesis according to my interests.

I would also like to give a special thanks to PhD Candidate Thomas Hansen Viuff at the Department of Marine Technology who has spent endless hours helping me with my bridge model.

Trondheim, June 11, 2017

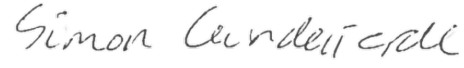

Simon Gundegjerde

Summary

The Norwegian government has an ambitious goal of connecting the Western coast of Norway with a ferry free road stretching from Kristiansand in the south to Trondheim in the north. This road has eight fjords which has to be crossed with ferries today. In order to reach their goal, it has been initiated several projects studying the possibility of crossing some of the widest and deepest fjords with floating bridges.

One of the biggest challenges, in addition to the technical, lies in the economical aspect of the project. Over the last three years, the estimated cost for the project *Coastal Highway Route E39* has increased from 150 to 340 billion NOK. The X-Bridge concept by Rune Risnes tries to utilize well known solutions in order to reduce the cost.

This thesis will describe the concept behind the X-Bridge, the initial design process and how the different dimensions are decided. The focus will be on clarifying the choices made, how the model is built and the overall behaviour with wave loadings.

The hydrodynamic analysis is performed in Wadam using the software HydroD. The bridge model is created as a coupled Simo/Riflex model using the software Sima. The model is analysed in static conditions and with regular dynamic waves. In addition, an eigenvalue analysis is performed.

Results show that the suggested bridge girder is too weak for the concept due to large static bending moments and shear forces. The wall thickness of the girder should be increased. Static stresses dominate the results due to the long spans. The model response behaves linearly, making it possible to estimate the response for several wave heights with the same period.

It is not possible to see any effect of the cables connecting the two arches in the results. Further work should focus on the unique features of the concept. This study has shown that including too many aspects in the model makes it more difficult to identify the special properties of the concept.

Sammendrag

Den norske regjeringern har Den norske regjeringen har sett seg et ambisiøst mål om å forbinde kysten av Vestlandet med en ferjefri vei fra Kristiansand i sør til Trondheim i nord. Strekningen har i dag åtte fjorder som må krysses med ferjer. For å nå målet deres er det blitt satt i gang flere prosjekter som studerer mulighetene for å krysse noen av de videste og dypeste fjordene med flytebroer.

En av de største utfordringene, i tillegg til det tekniske, ligger i de økonomiske aspektene ved prosjektet. Over de tre siste årene har den estimerte kostnaden for prosjektet *Ferjefri E39* økt fra 150 til 340 milliarder NOK. X-Bridge konseptet av Rune Risnes forsøker å utnytte kjente løsninger for å redusere kostnadene.

Denne avhandlingen vil beskrive konseptet bak X-Bridge, den innledende design prosessen og hvordan de ulike dimensjonene er bestemt. Fokus vil være på å klargjøre de valgene som er tatt, hvordan modellen er bygget opp og den generelle oppførselen under bølgelaster.

Den hydrodynamiske analysen er utført i Wadam ved å benytte programvaren HydroD. Bromodellen er laget som en koblet SimoRiflex-modell i programvaren Sima. Modellen er analysert statisk og ved regulære bølger. I tillegg er det utført en egenverdianalyse av modellen.

Resultater viser at den foreslåtte brobjelken er for svak for konseptet på grunn av høye statiske bøyemomenter og skjærkrefter. Veggtykkelsen av brobjelken bør derfor økes. Statiske spenninger dominerer resultatene på grunn av de lange spennene. Modellresponsen er lineær, noe som gjør det mulig å estimere responsen for flere bølgehøyder med samme periode.

Det er ikke mulig å se noe effekt av kablene som forbinder de to bro-buene i resultatene. Videre arbeid bør fokusere på de unike egenskapene ved konseptet. Denne studien har vist at det blir vanskelig å identifisere disse spesielle egenskapene når for mange aspekter i modellen er tatt med.

Contents

List of Figures

List of Tables

List of Equations

Abbreviations

Notation	Description
JONSWAP	Joint North Sea Wave Observation Project.
MARINTEK	Norwegian Marine Technology Research Institute.
CoB	Centre of Buoyancy.
CoG	Centre of Gravity.
DoF	Degrees of Freedom.
EoM	Equation of Motion.
FEM	Finite Element Method.
GUI	Graphical User Interface.
NTNU	Norwegian University of Science and Technology.
VLFS	Very Large Floating Structures.

Nomenclature

Notation	Description
MATLAB	Programming language developed by MathWorks. It started out as a matrix programming language where linear algebra programming was simple.
RIFLEX	Program used for analyse slender systems.
SIMA	Program used for modeling and analysis within marine technology.
SIMO	Non-linear motions and station keeping analysis of multibody systems.
WAMIT	Advanced software for analysing wave interactions with offshore platforms and other structures or vessels.
E39	European route E39 (road).
GeniE	A tool for design and analysis of offshore and maritime structures made up of beams and plates.
HydroD	A program for advanced stability and hydrodynamic analysis of offshore structures.
Krifast	Mainland connection between Kristiansund and Freis.
Wadam	General hydrodynamic analysis program for calculating wave-structure interaction for fixed and floating structures of arbitrary shape.
X-Bridge	Name on floating bridge concept developed by Rune Risnes in Risnes Innovation.

Latin Symbols

Notation	Description
A	Cross-sectional area.
$\boldsymbol{A}$	Genaral matrix, used in eigenvalue calculations.
a	Fluid acceleration.
C	Restoring coefficient.
$\boldsymbol{C}$	Damping matrix.
$\boldsymbol{c}$	Local damping matrix.
D	Cross-sectional diameter.
E	Young's modulus, also known as the elastic modulus.
F	Force.
$\boldsymbol{F}$	External loading.
G	Shear modulus.
g	Gravitational acceleration, $9.81\,\mathrm{m/s^2}$.
$\overline{\mathrm{GM}}$	Metacentric height.
H	Wave height.
h	Height.
H_s	Significant wave height, the mean of the highest third of the waves in a time-series.
I	Second moment of area, area moment of inertia.
$\boldsymbol{I}$	Identity matrix.
K	Shear force parallel to the axis.
$\boldsymbol{K}$	Stiffness matrix.
k	Stiffness, also used as wave number.
L	Length.

Notation	Description
l	Length.
$\boldsymbol{m}$	Local mass matrix.
$\boldsymbol{M}$	Mass matrix.
m	Mass.
M	Moment.
N	Axial force.
p	Pressure.
$\boldsymbol{Q}$	External force vector.
q	Distributed load.
$\boldsymbol{R}$	Reaction force vector.
$\boldsymbol{r}$	Response vector.
$\dot{\boldsymbol{r}}$	Velocity vector.
$\ddot{\boldsymbol{r}}$	Acceleration vector.
S	First moment of area, $S = A\bar{y}$.
T	Wave period or torsional moment.
t	Thickness.
T_p	Peak period, the wave period with the highest energy.
u	Fluid velocity.
$\boldsymbol{V}$	Velocity vector.
V	Volume.

Greek Symbols

Notation	Description
α	Angle or damping ratio coefficient.
β	Angle, also used as parameter in Newmarks's procedure.
ν	The signed ratio of transverse strain to axial strain.
ε	Strai, $\varepsilon = \Delta l/L$.
γ	Parameter for Newmark's procedure.
κ	Curvature.
$\boldsymbol{\lambda}$	Eigenvalue vector.
λ	Wave length, also used to eigenvalues in eigenvalue problems and damping ratio.
∇	Del, or nabla operator. Used as a vector differential operator. Also used for volume displacement.
$\boldsymbol{\omega}$	Angular frequency vector.
ω	Angular frequency.
$\boldsymbol{\phi}$	Mode shape vector.
ϕ	Velocity potential, also used for mode shape.
ρ	Material density.
σ	Stress.
τ	Shear stress.
ζ	Wave elevation.

Chapter 1

Introduction

This chapter gives a short introduction to the problem investigated in this thesis. It also contains the objectives and gives the structure of this report.

1.1 Background

On the 12th of April 2013, the Norwegian Government presented the *National Transport Plan 2014-2023* to the Norwegian parliament. The National Transport plan sets the Government's transport policy and goals for the next ten years. In this paper, the Government presented their ambition to link Western Norway with a ferry-free E39 (Norwegian Ministry of Transport and Communications, 2013).

According to Ellevset (2012), the coastal road E39 from Kristiansand in the south, to Trondheim in the north is approximately 1100 km long and includes eight ferry connections. The project *Coastal Highway E39* has been initiated to investigate the technological challenges and possibilities, and to explore the benefits of reducing the travelling time and remove all ferry connections. The goal is to reduce the travelling time with 7 - 9 hours, to a total of 12 - 13 hours (Ellevset, 2012).

To realise the Government's ambition about no ferries, the fjords must be crossed with bridges, underwater tunnels, floating tunnels or a combination. Due to the

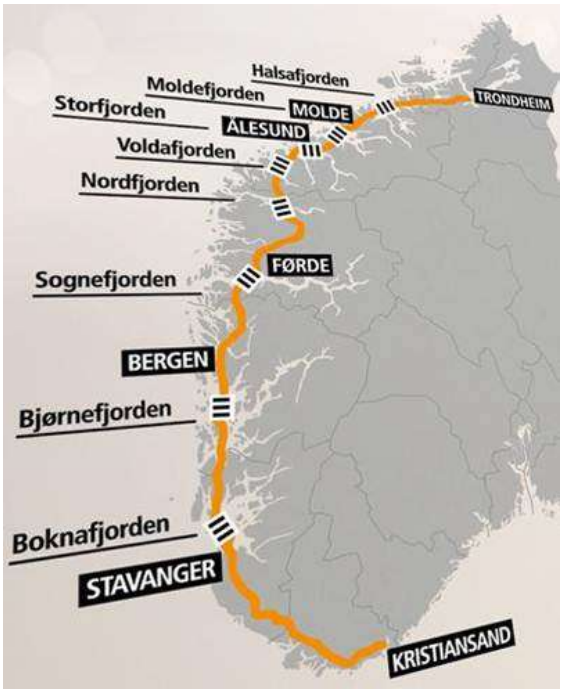

Figure 1.1: Coastal Highway Route E39 from Kristiansand in south to Trondheim in north. Image from Norwegian Public Roads Administration (2012)

long crossings and deep fjords, a lot of new technology is required. Therefore, it was established a subproject called *Fjord Crossings*.

Fjord Crossings was initially started in 2009 to investigate the possibilities of crossing Bjørnafjorden, but was later extended to include all fjord along the E39 being crossed by ferries (Norwegian Public Roads Administration, 2016).

High Costs

In addition to all the technological challenges with an ambitious project like *Costal Highway E39*, there is a significant economic issue as well. According to an article published by *NRK* in 2016, the estimated cost for the entire project increased from 150 to 340 billion NOK in just three years (Rydland & Sado, 2016). The high costs are now causing politicians to withdraw their promise of ferry free E39 within 20 years (Gillesvik, 2017).

The issue with high costs have been a motivator for Rune Risnes in Risnes Innovation to come up with an alternative bridge design to reduce the high cost connected to the floating bridges designed for crossing the wide and deep fjords at the west coast of Norway.

Risnes vision is to utilize proven technology in combination with avoiding large cost drivers as subsea operations, heavy lifting operations and large bridge towers.

1.2 Objective

The objective of this thesis is to come up with a suggestion for initial design for the floating bridge concept by Risnes Innovation. The initial design will be used to develop a model and conduct an early stage analysis of the design to see how the concept work. This includes, but are not limited to, identifying eigenperiod and mode shapes, relevant wave interactions and load distribution at the bridge.

1.3 Structure of the Report

The following chapters starts with a general chapter about floating bridges. It gives some information about the concept of floating bridges and investigates existing floating bridge concepts. It also addresses some of the other floating bridge concepts suggested along the road E39.

The next chapter focuses on relevant theory for floating bridges. This includes both theory used in the software and for calculations done by hand. The chapter addresses some solution algorithm utilized by the software.

Chapter 4 gives a thorough description of the X-Bridge concept. It also contains a section describing how some main parameters are decided.

The different methods used throughout the project are described in Chapter 5. This includes how most dimensions for the initial design are decided and analysis methods as well as methods of calculating results.

In Chapter 6 the whole modelling process in the different software is described. Starting with the pontoon analysis using GeniE and HydroD followed by how the entire bridge model is built using Simo.

Chapter 7 contains all the results found. It start with all the dimensions and properties for the different parts of the bridge. Static and dynamic analysis results follow together with the results from the eigenvalue analysis. As the result section contains a range of different results, it is decided to discuss the result consecutively for better readability.

A short summary of the most important results and a conclusion is given in Chapter 8. The chapter also contains a section with recommendations for further work.

All references are given in the Bibliography printed on page 121.

Chapter 2

Floating Bridges

The following Chapter contains information on floating bridges and descriptions of existing floating bridges in Norway and other places in the world as well as a short description of some of the suggested bridges for ferry free E39.

2.1 The Concept of Floating Bridges

Floating bridges are practical for long crossings of water where the conditions make it difficult to build a bottom supported bridge. This could be the case for both deep water and water where the bottom is too soft for pillars. Both the crossing of Bjørnafjorden and Sognefjorden along E39 requires crossing of deep and wide fjords. Floating bridges is therefore a natural alternative for these crossings.

2.1.1 Structure of Floating Bridges

The basic concept of floating bridges is simple: the piers or foundations are replaced with floating elements floating freely or with mooring lines. These floating elements holds the vertical loading of the bridge. The transverse and longitudinal loading is carried by the structural system and/or mooring lines. The floating elements, or pontoons, are usually made of concrete due to its capability of resisting the

highly corrosive environment in seawater. Concrete also has some other beneficial properties as good damping from vibrations and strong resistance to fire compared to wood and steel (Lwin, 1999).

According to Lwin (1999) the floating elements, hereafter referred to as pontoons, can either be separated or continuous. The continuous type consists of long pontoons connected to each other to form a bridge, while the separated type consists of individual pontoons spanned by a superstructure. For the continuous pontoon solution, the road beam is located closer to the sea, making is vulnerable for large waves. By rising the road beam, this problem is omitted, but it could introduce higher wind loads along the bridge girder.

Another important aspect of floating bridges is how it affects the ship traffic. Some bridges have solved this issue by creating movable spans, but this interrupt the traffic on the bridge. This is not a good solution to the suggested bridges over Bjørnafjorden and the other crossing due to combination of ship traffic and the large traffic on E39. It is therefore suggested different methods to elevate the bridge at certain points to allow for ship traffic to pass. This method is used on the Nordhordland Bridge as seen in Figure 2.1a. When a fairway is made, it is necessary to do a risk analysis of the ship traffic and the potential of ship collision (Norwegian Public Roads Administration, 2015a). This includes finding the probability of an event and the consequences of the event.

As mentioned, to withstand lateral loads there are mainly two methods. For long straight bridges it is necessary with pre-tensioned mooring lines in the transverse direction. An alternative is to curve the bridge and only support it at each end. The curved bridge carries the transverse loads as tension or compression depending on the direction of the load. This is advantageous at crossings where the seabed is either deep or soft or a combination of both as this makes anchoring complicated. The principle is explained by Watanabe and Utsunomiya (2003): when the current is coming from the convex side, the bridge shape acts as a arch rib giving a much higher stiffness in the horizontal plane compared to a straight beam. In the other case, the bridge acts as a catenary cable. For the crossing of Bjørnafjorden both straight and curved alternatives have been considered (Nedrebø, 2016). Two of the concepts are described in Section 2.1.3.

2.1.2 Existing Floating Bridges

Even though the concept of floating bridges has been known for a long time, only about 20 long floating bridges used for traffic exist. In the following, the two Norwegian floating bridges, the Nordhordland Bridge and the Bergsøysund Bridge, will be described as well as some of the floating bridges found other places in the world.

(a) Nordhordlandsbrua consists of separated pontoons. The bridge is a combination of a floating bridge (left) and a cable-stayed bridge(right). Image from http://broer.no/bro/index.php?ID=43

(b) The floating bridge Bergsøysundbrua consists of separated pontoons. Image by Cato Edvardsen (Own work) [CC BY-SA 3.0 (http://creativecommons.org/licenses/by-sa/3.0)], via Wikimedia Commons.

Figure 2.1: Example of two floating bridges in Norway

The Bergsøysund Bridge

The Bergsøysund Bridge (Norwegian: Bergsøysundbrua) is a floating bridge in Norway located near Kristiansund and is a part of *Krifast*. The bridge has a length of 845 m for the floating part distributed over 7 pontoons as seen in Figure 2.2a (Watanabe & Utsunomiya, 2003). The total length of the bridge is 931 m.

The Bergsøysund Bridge does not have any mooring lines, meaning that the bridge is unconstrained in the lateral direction. The bridge is curved with a radius of

1300 m which, according to Watanabe and Utsunomiya (2003), increases the resistance to the rolling motion. The superstructure is created of steel pipe truss girders as seen in Figure 2.1b.

According to the Norwegian Public Roads Administration (2015c), the Bergsøysund Bridge is also used to determine the accuracy of different numerical methods used for dynamic analysis of bridges today. This is done by instrumentation of the bridge to monitor the actual response to different loads and then compare these results with those obtained from numerical methods. They are currently measuring wind, waves, position and structural response.

The Nordhordland Bridge

The Nordhordland Bridge (Norwegian: Nordhordlandsbrua) was finished in 1994 and connects Bergen to Nordhordland. The construction took 4 years with a total cost of 900 million NOK (in 1994) (Norwegian Public Roads Administration, 1994). The bridge is a combination of a floating bridge and a cable-stayed bridge as seen in Figure 2.1a. The floating section consist of a steel box girder which, as seen in Figure 2.2b, is supported by 10 pontoons (Aas-Jakobsen, n.d.). According to the main consultant, Aas-Jacobsen, the floating part of the bridge has the longest (1246 m) laterally unsupported span in the world. To achieve this, the bridge is constructed with a curvature as shown in Figure 2.2b. The unsupported solution is a result of the large water depth in the fjord, which is up to 500 m deep (Norwegian Public Roads Administration, 1994). The curvature of the box girder has a radius of 1700 m.

Figure 2.1a shows the cable-stayed bridge located at the southern end which creates a ship channel with a clearance of 32 m. This is similar to some suggestions for the crossing of the Bjørnafjord. The cable-stayed section is 369 m long giving the bridge a total length of 1615 m.

Typical span between the pontoons is 113.25 m with the steel girder on top (15.9 m in width and 5.5 m in height). The pontoon dimensions are 42 m long, 20.5 m wide and 7 m to 8.6 m high, with a draft of 4.3 m to 5.6 m. The pontoons are rounded in the horizontal plane for better hydrodynamic properties. According to the

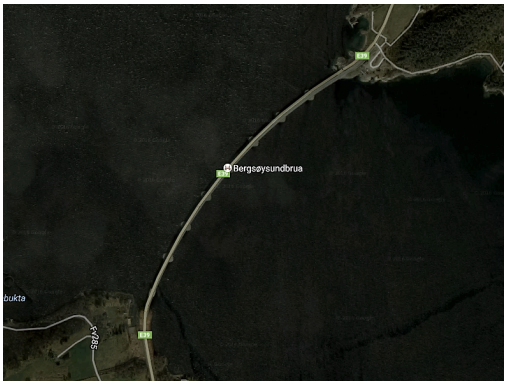

(a) Overview of Bergsøysund Bridge showing the 7 pontoons and the curvature of the bridge in the horizontal plane. Image from Google Maps, retrieved 07.11.2016.

(b) Overview of the Nordhordland Bridge showing the 10 pontoons and the curvature of the bridge in the horizontal plane. Image from Google Maps, retrieved 07.11.2016.

Figure 2.2: Overview of the Bergsøysund Bridge and the Nordhordland Bridge.

Norwegian Public Roads Administration (1994) the pontoons are divided into 9 separated cells inside for safety measures. This makes it possible in an accident to fill two neighbouring cells with water without endangering the bridge.

Floating Bridges Around the World

The longest floating bridge in the world, with 2350 m, is the Evergreen Point Floating Bridge, also known as the 520 Bridge located in Seattle, Washington, where it crosses Lake Washington (Lindblom, 2016). The bridge, which is also the worlds widest floating bridge measuring 35 m at the widest, opened in 2016 replacing a 40 m shorter bridge with the same name. According to Washington State Department of Transportation (n.d.-b), the bridge has as many as 77 pontoons with the biggest one as large as 8.5 m tall, 22.9 m wide, 109.7 m long and 11 000 t. Of the 77 pontoons, 21 are of the biggest type forming longitudinal pontoons where the traffic lane is placed, 54 are smaller supplementary pontoons which help to stabilize and support the floating bridge (Washington State Department of Transportation, n.d.-a). The bridge is almost straight and has as a consequence 58 anchoring lines to withstand lateral loads.

As opposed to the Norwegian bridges discussed, the pontoons on the Evergreen Point Bridge are continuous in addition to being box-shaped. This is possible due to relatively small waves and current on the lake. The bridge has a navigation channel located at the east end.

Washington is sometimes referred to as the *floating bridge capital* due to its many floating bridges (Gutierrez, 2012). Washington actually have five floating highway bridges. Which is a considerable amount considering that there is only about 20 floating traffic bridges around the world. But, the conditions differ from those found in the Norwegian fjords. Hence, other design methods are required in order to cross the norwegian fjords with floating bridges.

2.1.3 Suggested Floating Bridge Concepts

Two concepts suggested for the 4.5 km long crossing of Bjørnafjorden are developed by Aas-Jakobsen, COWI, Johs Holt, and Global Maritime on behalf of the Norwegian Public Roads Administration. The first is a curved floating bridge described in the report *Curved Bridge - Navigation Channel in South* ()2016a). The curved bridge is only anchored at the ends and consists of two parallel road beams 11.5 m above the sea level supported by 19 pontoons with an individual spacing of 197 m. The concept has no mooring lines connected to the sea bed.

The bridge girder has a curvature of 5000 m and the two box girders are 16 m wide and 5 m high. The navigation channel is located at the south end and consists of a cable stayed bridge with a span of 500 m.

The other concept is of the straight beam alternative. As described in Section 2.1.1, this requires additional lateral stiffness from mooring lines connected to the sea bed. This bridge concept is described in the report "Straight Bridge - Navigation Channel in South" (2016b). The bridge girder consists of only one beam which is supported by pontoons with 203 m spacing giving a total number of 18 pontoons.

Similar to the curved bridge alternative, the navigation channel is located at one of the ends spanned by a cable stayed bridge. Mooring lines are located at three different pontoons with three mooring lines in each direction, giving a total number

of 18 mooring lines. The mooring lines consist of bottom chain, wire and top chain.

These two floating bridge concepts and reports are used extensively in the work of this thesis.

Chapter 3

Theory

This chapter will present the basic concepts used to calculate the dynamic response of a floating bridge. Dynamic analysis varies from static analysis as the external loading varies with time and it has to include inertia, damping, reaction forces and the corresponding response.

An increased interest in Very Large Floating Structures (VLFS) the past two decades have brought new knowledge to the concept of floating bridges according to Wang and Tay (2011). As a consequence, there has been developed new innovative methods to minimize the hydroelastic motions, improve mooring systems and structural integrity. For VLFS there is a coupling between the structure deformation and the fluid motions.

3.1 Hydrodynamic Modelling

The following section will describe how the hydrodynamic effects can be included in the analysis. It will provide some basic information on waves and current needed to find loads on structures.

3.1.1 Free-Surface Fluid flow

The following equations and theories are described by Newman (2005), Pettersen (2014) and Faltinsen (1993).

The seawater is assumed to be inviscid and incompressible and the motion irrotational. It is then possible to describe the fluid velocity with a velocity potential, ϕ. The fluid velocity vector is given by $\boldsymbol{V}(x, y, z, t) = (u, v, w)$ at time t at the point $\boldsymbol{x} = (x, y, z)$. The potential, ϕ, has to satisfy certain requirements:

1. The Laplace equation,
$$\nabla^2\phi = 0 \tag{3.1}$$
has to be satisfied for the fluid to be incompressible. This gives us the following equation:
$$\frac{\partial^2\phi}{\partial x^2} + \frac{\partial^2\phi}{\partial y^2} + \frac{\partial^2\phi}{\partial z^2} = 0. \tag{3.2}$$
To find the velocity potential, the Laplace equation for irrotational flow is solved with different boundary conditions

2. The boundary condition at the bottom, given by Equation (3.3) where h is water depth, has to be fulfilled. The boundary condition states that the fluid has no downward velocity at the sea bottom.
$$\left(\frac{\partial\phi}{\partial z}\right)_{z=-h} = 0 \tag{3.3}$$

3. The dynamic free-surface condition is that the water pressure at the free surface is equal to the constant atmospheric pressure. By ignoring higher order terms, the dynamic condition can be written as Equation (3.4) where ζ is the wave elevation.
$$g\zeta + \left(\frac{\partial\phi}{\partial t}\right)_{z=\zeta} = 0 \tag{3.4}$$

4. The kinematic boundary condition at the surface states that wave particles on the surface stays on the surface. This is illustrated by Equation (3.5).

$$\frac{\partial \zeta}{\partial t} = \frac{\partial \phi}{\partial z} \tag{3.5}$$

Equation (3.7) shows the velocity potential for any water depth for a wave profile given by:

$$\zeta = \zeta_A \cos(kx - \omega t). \tag{3.6}$$

$$\phi = \frac{g\zeta_{\mathrm{A}}}{\omega} \frac{\cosh k(h+z)}{\cosh(kh)} \sin(kx - \omega t) \tag{3.7}$$

By combining the kinematic condition and the velocity potential, Equation (3.5), and Equation (3.7), it can be shown that the relation between wave frequency and wave length, the dispersion relation, is given as:

$$\omega^2 = kg \tanh kh. \tag{3.8}$$

For deep water, Equations (3.7) and (3.8) reduces to Equations (3.9) and (3.10) respectively.

$$\phi = \frac{\zeta_{\mathrm{A}} g}{\omega} e^{kz} \sin(kx - \omega t) \tag{3.9}$$

$$\omega^2 = kg \tag{3.10}$$

As a rule of thumb, deep water approximation can be used when $h > \lambda/2$. Meaning that the depth is larger than half the wave length, λ. For Bjørnafjorden, which

is approximately 500 m at the middle of the crossing, this corresponds to a wave length $\lambda < 1000$ m. Deep water assumption is therefore valid. But, close to the shore the depth reduces. It is therefore important to take this into account when considering the bridge ends. This effect is ignored in the analyses performed in this report.

For deep water, we can use the velocity potential, the surface profile and the dispersion relation (Equations (3.9), (3.6) and (3.10)) to find the dynamic pressure under the wave by using Bernoulli's principle. The dynamic pressure is given by:

$$p_{\text{dyn}} = -\rho \frac{\partial \phi}{\partial t} = \rho g \zeta_{\text{A}} e^{kz} \cos(kx - \omega t) \tag{3.11}$$

3.1.2 Hydrodynamic Forces

Incoming waves will be disturbed by the presence of the floating pontoons. The waves will be diffracted upon hitting the pontoon (the waves are reflected) and the pontoon will be set in motion. This will in turn generate outgoing waves from the pontoons. Within linear wave theory it is common to use superposition to separate these two sub-problems (Faltinsen, 1993).

1. Forces and moments on the pontoons from incident harmonically waves when it is restrained from oscillating. The hydrodynamic forces on the pontoons are called *wave excitation forces* and are composed of Frude-Kriloff and diffraction forces and moments.

2. Forces and moments on the pontoons when it is forced to oscillate with the same frequency as the incoming waves. In this case, there are no incident waves. The resulting hydrodynamic forces are called the fluid reactive forces. Often defined as *added mass*, *damping* and *restoring*.

Computation of Wave Loads

According to the "Sesam User Manual - Wadam" 2010b, the wave induced forces can be calculated in different ways depending on the type of model. For a Morison

model, both Morison's equation and the MacCamy-Fuchs formula can be applied. Potential theory is applied on panel models. Morison's equation is used on slender structures and Wadam uses first and second order 3D potential theory for large volume structures like the floating bridge pontoons.

Morison's Equation

For the slender mooring lines used on floating bridges Morison's equation can be used to calculate the wave loads. Morison's equation can be used on circular cylindrical members when viscous forces matter according to Faltinsen (1993). The horizontal force, $\mathrm{d}F$, acting on a strip of length $\mathrm{d}z$ can be written as

$$\mathrm{d}F = \rho \frac{\pi D^2}{4} \mathrm{d}z \, C_{\mathrm{M}} \, a_1 + \frac{\rho}{2} C_{\mathrm{D}} \, \mathrm{d}z \, |u| \, u \tag{3.12}$$

Where C_{M} and C_{D} is the mass and drag coefficients respectively. These have to be determines empirically.

3.1.3 Hydrodynamic Mass and Damping

To find the hydrodynamic coefficients is possible by using numerical programs as for example, WAMIT or Wadam. According to Langen (1981), it is also common to use coefficients calculated from two-dimensional flow in connection with strip theory for analysing ship motion. Since the pontoons are similar in shape, this method can be used to simplify the calculations.

With this assumption, the motion of a small section, $\mathrm{d}s$, reduces to a two-dimensional problem with the following DoF:

$$\boldsymbol{u}(t) = \begin{bmatrix} u_{\mathrm{y}}(t) & u_{\mathrm{z}}(t) & \phi_{\mathrm{x}} \end{bmatrix}^{\intercal}. \tag{3.13}$$

The terms represent local translation in y and z-direction and rotation about x-axis respectively. The axis system is illustrated in Figure 3.1. Translation in

x-direction corresponds to surge, translation in z-direction to heave and rotation about the y-axis to pitch as seen in Figure 3.1

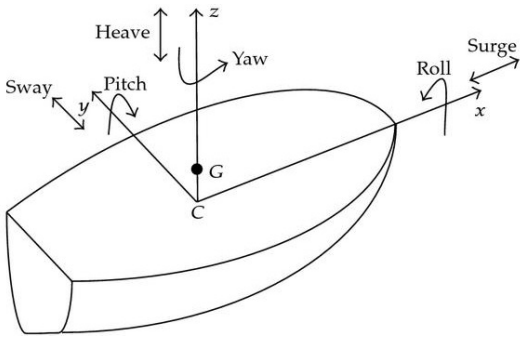

Figure 3.1: Ship with rigid-body motion modes. The names are used to describe the motion of the pontoons as well as the bridge itself. Image from Ibrahim and Grace (2010).

According to Langen (1981), the hydrodynamic matrices $\boldsymbol{m}^{(\mathrm{h})}$ and $\boldsymbol{c}^{(h)}$ (where $^{(h)}$ indicates hydrodynamic mass and hydrodynamic damping) for the two-dimensional section ds can be written as:

$$\boldsymbol{m}^{(h)}(\omega) = \begin{bmatrix} m_{yy}(\omega) & 0 & m_{y\phi}(\omega) \\ 0 & m_{zz}(\omega) & 0 \\ m_{y\phi}(\omega) & 0 & m_{\phi\phi}(\omega) \end{bmatrix} \tag{3.14}$$

$$\boldsymbol{c}^{(h)}(\omega) = \begin{bmatrix} c_{yy}(\omega) & 0 & c_{y\phi}(\omega) \\ 0 & c_{zz}(\omega) & 0 \\ c_{y\phi}(\omega) & 0 & c_{\phi\phi}(\omega) \end{bmatrix} \tag{3.15}$$

Vugts (1968) have estimated the hydrodynamic coefficients in Equations (3.14) and (3.15) for different types of cross sections using potential theory. The results have been published in *The Hydrodynamic Coefficients for Swaying, Heaving and Rolling Cylinders in a Free Surface* (1968). Figure 3.2 shows an example of the results obtained for a rectangular cross section.

These results can be used to calculate the added mass and damping matrices by adding up the contribution from each strip, dx, of the pontoon.

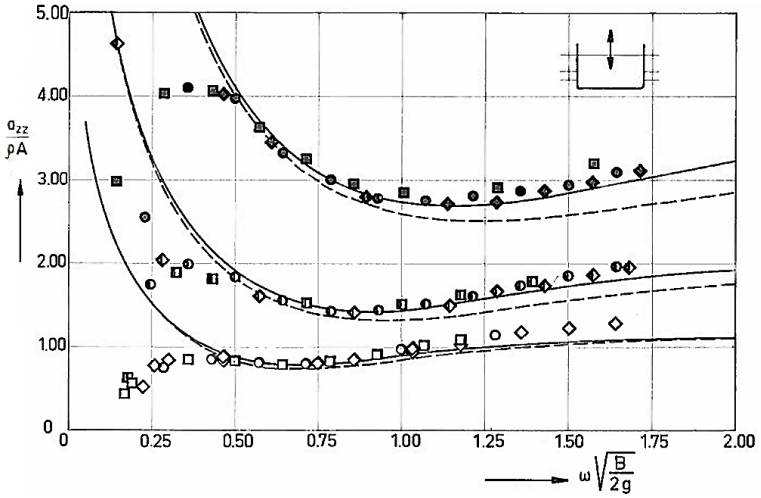

Figure 3.2: Frequency dependent added mass in heave for a two-dimensional cross section. The results vary with the ratio B/T, the largest ratio at the top. Image from Vugts (1968).

Today, with modern computer programs and relatively high computer power, commercial software is available to calculate these values numerically. These diffraction theory programs, such as WAMIT or Wadam, can be used to calculates the hydrodynamic forces. The method of performing a hydrodynamic analysis in Wadam is described in Section 6.1.3

Wave Exciting Forces

As for the hydrodynamic added mass and damping, a similar approach can be used to find the wave exciting forces. The book *The Hydrodynamic Coefficients for Swaying, Heaving and Rolling Cylinders in a Free Surface* (Vugts, 1968) also contains results from force measurements for different cross sections. These results can be used to estimate the wave exciting forces on structures with similar cross sections.

The wave exciting forces may also be obtained from computer software as Wadam. The method is described in Section 6.1.3.

3.2 Beam Theory

In general, what characterize a beam element is that it has a length several times longer than the other dimensions. Beams are described as one-dimensional elements and the cross sections are described by different scalar quantities (Damkilde, 2000). Beam theory is a simple way of performing initial design considerations and gives valuable insight in the structural behaviour (Bauchau & Craig, 2009).

As described by Damkilde (2000), beam theory is only a simplification of the three-dimensional continuum mechanics problem. Internal forces are transformed into stress distributions according to simplified methods. Hence, the results are only approximations of the real forces. The accuracy of the different beam theories depends on the assumptions and simplifications in each theory.

Euler-Bernoulli beam theory is one of the simplest theories and it assumes that a cross section of the beam is infinitely rigid in its own plane (Bauchau & Craig, 2009). In addition, the cross section is assumed to remain plane and normal to the deformed axis of the beam. According to Bauchau and Craig (2009), the Euler-Bernoulli theory is valid for long and slender solid elements.

Another, more accurate theory, is the Timoshenko beam theory. Timoshenko beam theory is an extension of the Euler Bernoulli beam theory and includes shear deformations (Haque, 2016). The assumption for Timoshenko beam theory that differs it from Euler-Bernoulli is that plane cross sections, which are initially normal to the longitudinal axis, will remain plane after deformation. Here, the cross section is no longer required to remain normal to the beam axis (Haque, 2016).

Both in Euler-Bernoulli and Timoshenko beam theory, torsion is treated separately (Damkilde, 2000). Torsion is described in Section 3.2.2.

The beam elements in RIFLEX are formulated using the concept of co-rotated ghost reference, meaning that the initial configuration translates and rotates as a rigid body located close to the actual deformed configuration (MARINTEK, 2016). The name used in "RIFLEX 4.8.1 Theory Manual", co-rotated ghost, is used as the reference frame follows the element like a "ghost".

Each node has 6 DoF at each node, 3 translational and 3 rotational degrees. Local x-axis is defined between the two nodes, local y-axis as the average principal y-axis at the two nodes while the z-axis is perpendicular to the xy-plane as shown in Figure 3.3.

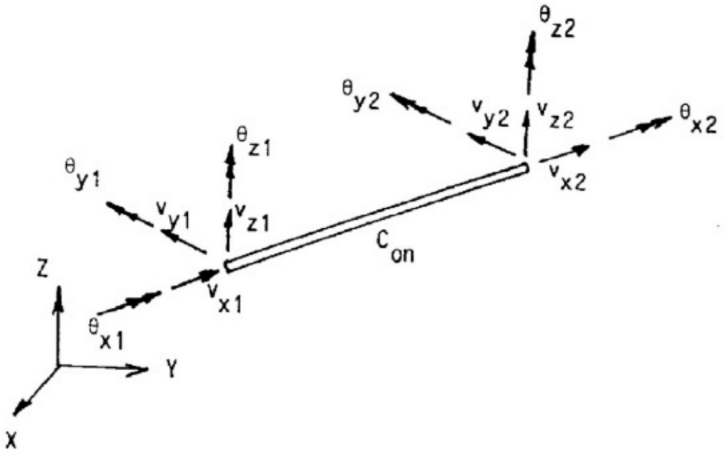

Figure 3.3: Nodal degrees of freedom for beam element. Image from MARINTEK (2016).

"RIFLEX 4.8.1 Theory Manual" lists the following assumptions which the beam theory used in the software is based on:

- A plane section of the beam initially normal to the x-axis, remains plane and normal to the x-axis during deformations.
- Lateral contraction caused by axial elongation is neglected.
- The strains are small.
- Shear deformations due to lateral loading are neglected, but St. Venant torsion is accounted for.
- Coupling effects between torsion and bending are neglected. Thus, warping resistance and torsional stability problems are not considered.

Torsion can be classified in two ways, uniform and non-uniform. St. Venant torsion is uniform torsion, where the member is allowed to warp freely and the torque is restricted entirely by torsional shear stress. For uniform torsion of a non-circular

cross section, transverse sections warp in thee axial direction. As long as the warping is taking place freely, the torsion moment is resisted by shearing stresses (Narayanan et al., 2011).

Stresses acting on a cross section can be divided into normal stresses and shear stresses (Damkilde, 2000). Normal stresses are caused by axial forces and bending moments. The normal stress can be calculated using Navier's formula (3.23) given in the following section.

Shear stresses are caused by shear forces and torsional moments. These are discussed in Section 3.2.2.

3.2.1 Bending Moment and Axial Force

As the plane sections remain plane, the normal strain is linearly distributed over the cross section. The normal strain is caused by axial elongation and curvature of the beam. Hooke's law gives the normal stress, σ_x, as

$$\sigma_x = E\varepsilon \tag{3.16}$$

Where E is the elastic modulus and ε is the strain. Axial force is given by

$$N = EA\varepsilon \tag{3.17}$$

And moment around the y and z-axis is given by Equations (3.18) and (3.19) respectively.

$$M_y = EI_{yy}\kappa_y \tag{3.18}$$

$$M_z = EI_{zz}\kappa_z \tag{3.19}$$

By combining Equations (3.17) through (3.19) with the strain distribution in Equation (3.20), the strain distribution can be rewritten as in Equation (3.21).

$$\varepsilon_x = \varepsilon_C - \kappa_y y + \kappa_z z \tag{3.20}$$

$$\varepsilon_x = \frac{N}{EA} - \frac{M_z}{EI_{zz}} y + \frac{M_y}{EI_{yy}} z \tag{3.21}$$

In Equation (3.20), κ is the curvature. Displacement i y-direction gives curvature κ_z. Curvature is defined as (Irgens, 1999b)

$$\kappa = \frac{\mathrm{d}^2 u}{\mathrm{d}x^2} = -\frac{M}{EI} \tag{3.22}$$

Equation (3.21) inserted into Hooks's law (3.16) gives Navier's formula as shown in Equation (3.23) (Irgens, 1999b). This is the axial stress due to axial force and bending moments.

$$\sigma = \frac{N}{A} + \frac{M_z}{I_z} y + \frac{M_y}{I_y} z \tag{3.23}$$

Bending Moment in Fixed Beam

Due to the symmetric loading on each side of the towers, the moment and stress distribution is close to the analytical solution for a fixed beam with equally distributed line load. For a fixed beam, the moment at ends and centre can be calculated by Equations (3.24) and (3.25) respectively.

$$M_{\text{end}} = \frac{ql^2}{12} \tag{3.24}$$

$$M_{\text{centre}} = \frac{ql^2}{12} \tag{3.25}$$

3.2.2 Shear Forces and Torsional Moment

Shear force in a structural member can be calculated as the change in moment over the distance as given in Equation (3.26) (Irgens, 1999b).

$$V = \frac{\mathrm{d}M}{\mathrm{d}x} \tag{3.26}$$

According to Damkilde (2000), the shear stress distribution due to shear force and torsional moment is a complicated problem and it exists analytical solutions only for a few cross sections. It is therefore necessary with numerical or approximate solutions.

For a thin walled, closed cross section the shear stress can be computed from Equation (3.27) (Leira, 2014) and according to Irgens (1999a), the accuracy is high for thin walled structures. The shear stress may also be assumed to be constant over the thickness as illustrated in Figure 3.4.

$$\tau = \frac{K}{t} = \frac{VS}{It} \tag{3.27}$$

Here, V is the shear force, S the first moment of area and I and t are the second moment of area and thickness respectively. The first area of moment, S, is calculated with Equation (3.28) (Irgens, 1999b).

$$S = \int_A y \,\mathrm{d}A = A\bar{y} \tag{3.28}$$

The first moment of area varies depending on where the section is cut, and the area, A, in Equation (3.28) is the area above the cut. The distance $\bar{y}$ is the perpendicular distance from the centroid of the above area to the neutral axis.

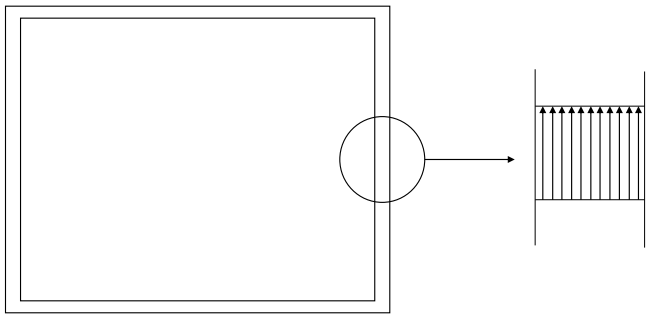

Figure 3.4: Shear force in a thin walled cross section due to torsion

For a closed box cross section, as shown in Figure 3.5, with a vertical shear force, the shear stress is zero at point A, increases linearly towards the corners and towards maximum at point D. As both area and arm varies from the corner towards point D, the increase is no longer linear.

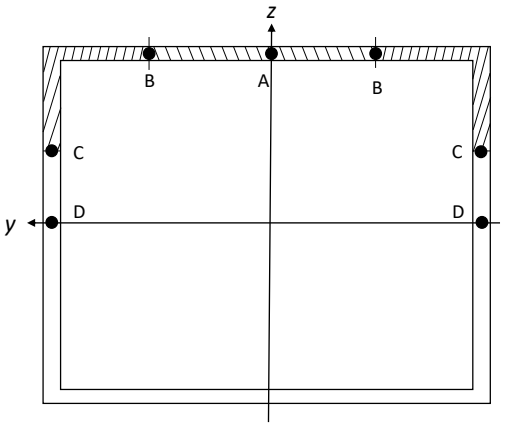

Figure 3.5: Typical rectangular box cross section.

According to Damkilde (2000) and Irgens (1999a), the results for shear stresses due to torsion is generally very accurate for thin walled cross sections. Torsional resistance is much higher for closed cross sections compared to open and the maximum shear stresses much lower.

The bridge girder consists of a closed cross section. For closed cross sections, the shear stress is constant over the thickness, as shown in Figure 3.4, and creates a shear flow around the cross section (Damkilde, 2000). The resulting torsional

moment is proportional to enclosed area and the torsional moment of inertia is given as Equation (3.29) (Amdahl, 2005) where A_C is the enclosed area. The integral of t^-1 defines the average thickness along the contour, C.

$$I_t = \frac{4A_c^2}{\int_C \frac{\mathrm{d}s}{t}} \tag{3.29}$$

The maximum shear stress in a closed cross section is given by Equation 3.30 where T is the torsional moment.

$$\tau_{\max} = \frac{T}{2A_C t_{\min}} \tag{3.30}$$

3.2.3 von Mises Yield Criterion

von Mises yield criterion is used to identify a yield limit for metals. The von Mises yield criterion is formulated by the *von Mises stress*, also referred to as *equivalent tensile stress*, σ_v. According to the yield criterion, yield occurs when the equivalent stress equals the yield stress, $\sigma_v = \sigma_Y$. The equivalent stress is calculated according to Equation (3.31) for plane stress (Irgens, 1999b).

$$\sigma_v = \sqrt{\sigma_x^2 + \sigma_y^2 - \sigma_x\sigma_y + 3\tau_{xy}^2} \tag{3.31}$$

Plane stress is assumed as the thickness of the outer plates are small compared to the overall dimensions of the cross section.

3.2.4 Velocity and Acceleration

Velocity and acceleration can be calculated for a body point if the time-dependent displacement vector is known. Given a vector with displacements, $r(t)$, velocity

in each direction can be calculated according to Equation (3.32) where you can substitute the variable x with y and z to find the velocity in each direction. In the equation, $\mathrm{d}x$ represents the change in position between each time step, whilce $\mathrm{d}t$ is the duration of each time step.

$$V = \frac{\mathrm{d}x}{\mathrm{d}t} \tag{3.32}$$

Accelerations are found by differentiating the displacement once more as shown in Equation (3.33)

$$a = \frac{\mathrm{d}V}{\mathrm{d}t} = \frac{\mathrm{d}^2x}{\mathrm{d}t^2} \tag{3.33}$$

3.3 Cable Forces

Cables are structural members only capable of carrying axial forces in tension. Therefore, the only force component present in a cable is axial force, N. This makes it easy to calculate the stresses. The stress is calculated with Equation (3.34) where A is the cross section area of the cable.

$$\sigma = \frac{F}{A} \tag{3.34}$$

3.4 Static Analysis

According to "RIFLEX 4.8.1 Theory Manual" (MARINTEK, 2016), the purpose of a static analysis is to find the nodal displacement vector so that the system is in equilibrium. The static equilibrium configuration is given as the solution of the following system:

$$\boldsymbol{R}^S(\boldsymbol{r}) = \boldsymbol{R}^E(\boldsymbol{r}) \tag{3.35}$$

where $\boldsymbol{r}$ represents the nodal displacements, $\boldsymbol{R}^S$ is the internal structural reaction forces and $\boldsymbol{R}^E$ is the external force vector. Generally, both the internal and external vectors will be non-linear (MARINTEK, 2016). The solution is hence found by application of incremental-iterative procedure. Different procedures are outlined in the book *Dynamisk analyse av konstruksjoner [Dynamic analysis of structures]* (1979) by Langen and Sigbjørnsson.

3.4.1 Restoring Forces

According to Faltinsen (1993), for a freely floating body restoring forces will follow from hydrostatic and mass considerations. For a body with symmetry in all planes, only heave, roll and pitch will have restoring forces. The restoring force and moments may be written as

$$F_k = -C_{kj}\eta_j \tag{3.36}$$

which defines the restoring coefficient C_{kj} representing the restoring force in k-direction due to motion in j-direction. The restoring coefficients for heave, roll and pitch are given by Equations (3.37a), (3.37b) and (3.37c) respectively.

$$C_{33} = \rho g A_{\mathrm{WP}} \tag{3.37a}$$

$$C_{44} = \rho g V z_B - m g z_G + \rho g \iint_{A_{\mathrm{WP}}} y^2 \,\mathrm{d}s = \rho g V \overline{\mathrm{GM}}_{\mathrm{T}} \tag{3.37b}$$

$$C_{55} = \rho g V z_B - m g z_G + \rho g \iint_{A_{\mathrm{WP}}} x^2 \,\mathrm{d}s = \rho g V \overline{\mathrm{GM}}_{\mathrm{L}} \tag{3.37c}$$

Buoyancy Compensation Force

This section is based on Marit Irene Kvittem's PhD thesis on "Modelling and response analysis for fatigue design of a semi-submersible wind turbine" (2014)

and an unpublished note by Thomas Viuff, PhD Candidate at the Department of Marine Technology at the Norwegian University of Science and Technology (NTNU).

The coupled analysis in SIMA includes both a RIFLEX-part for beam elements (bridge) and SIMO-part for floating bodies (pontoons). In SIMO, the assumption is that the floating body is neutrally buoyant without the RIFLEX elements (Marit Irene Kvittem, 2014). But, for a floating bridge structure, the neutrally buoyant position includes the RIFLEX elements (the bridge girder). The effect of gravity and buoyancy in the Equation of Motion (EoM) is assumed to be taken into account in the restoring matrix in SIMO, while it is assumed to be included as nodal forces in the Finite Element Method (FEM) in RIFLEX. To account for this inconsistency, a *buoyancy compensating force*, acting at Centre of Buoyancy (CoB), is applied on the floating SIMO bodies.

This way of including a buoyancy compencating force is, according to Marit Irene Kvittem, suitable when the weight is applied symmetrically and much smaller than the pontoon weight. As indicated by Viuff, the validity of this assumption is questionable as the weight of the RIFLEX element for a floating bridge is much larger than for a floating wind turbine as described in Marit Irene Kvittem's PhD thesis.

Only the pontoons are modelled in Wadam, and the restoring forces are calculated according to Equations (3.37a) through (3.37c) for each pontoon. To avoid including the buoyancy force twice due to the different ways SIMO and RIFLEX includes it, the following procedure are described by Thomas Viuff (and is included here since the note is unpublished).

1. Calculate the mass matrix for the pontoon alone for use in Wadam.
2. Import the mass matrix to Wadam and do the hydrodynamic panel method analysis for the pontoon alone.
3. Import Wadam output to SIMA.
4. In SIMA add a specified force equal to the weight of the pontoon at the Centre of Gravity (CoG). Alternatively, specify *include gravity* for the floating

bodies.

5. In SIMA, add a specified force equal to the buoyancy force of the body in the centre of buoyancy.

6. In SIMA, change the hydrostatic matrix, so the buoyancy-, and mass terms in Equations (3.37a), (3.37b) and (3.37c) are gone. The updated elements of the restoring matrix are found by Equations (3.38a) and (3.38b)

$$C_{44}^{new} = C_{44} - \rho g V z_B + m g z_G = \rho g \iint_{A_{\mathrm{WP}}} y^2 \, \mathrm{d}s \tag{3.38a}$$

$$C_{55}^{new} = C_{55} - \rho g V z_B + m g z_G = \rho g \iint_{A_{\mathrm{WP}}} x^2 \, \mathrm{d} \tag{3.38b}$$

The first order motion transfer functions calculated in Wadam are dependent on the stiffness properties and will therefore not be correct when using the described method. But, the results needed from Wadam in SIMA is the added mass, potential damping and the first order wave excitation force transfer functions. These results are not affected by the method described above.

3.5 Dynamic Analysis

In a dynamic analysis the all components in the equilibrium equation is time dependent. This section explains some aspects of the dynamic analysis of structures.

3.5.1 Dynamic Time Domain Analysis

As described in *Bruprosjektering - Prosjektering av bruer, ferjekaier og andre bærende konstruksjoner [Bridge Design - Design of Bridges, ferry quays, and other load-bearing constructions]* (Norwegian Public Roads Administration, 2015a), use of non-linear FEM is used in the time domain. Also, for slender systems, formulations for large deformations should be used. This supports the use of nonlinear

methods in the time domain. Time domain analysis is used in RIFLEX to analyse the structure. To do a dynamic analysis, the basic approach is to solve the EoM

$$\boldsymbol{M}\ddot{\boldsymbol{r}}(t) + \boldsymbol{C}\dot{\boldsymbol{r}}(t) + \boldsymbol{K}\boldsymbol{r}(t) = \boldsymbol{F}(t) \tag{3.39}$$

where $\boldsymbol{M}$, $\boldsymbol{C}$ and $\boldsymbol{K}$ are the $n \times n$ mass, damping and stiffness matrices respectively and $\boldsymbol{F}$ is the external loading on the system. The $n \times 1$ vector $\boldsymbol{r}$, $\dot{\boldsymbol{r}}$ and $\ddot{\boldsymbol{r}}$ represent the position, velocity and acceleration of the system.

In "RIFLEX 4.8.1 Theory Manual" (2016) the dynamic equilibrium equation of a spatially discretized finite element system is given by Equation (3.40).

$$\boldsymbol{R}^I(\boldsymbol{r}, \ddot{\boldsymbol{r}}, t) + \boldsymbol{R}^D(\boldsymbol{r}, \dot{\boldsymbol{r}}, t) + \boldsymbol{R}^D(\boldsymbol{r}, t) = \boldsymbol{R}^E(\boldsymbol{r}, \dot{\boldsymbol{r}}, t) \tag{3.40}$$

Here, $\boldsymbol{R}^I$ is the inertia force vector, $\boldsymbol{R}^D$ is the damping force vector, $\boldsymbol{R}^S$ is the internal structural reaction force vector, $\boldsymbol{R}^E$ is the external force vector and $\boldsymbol{r}$, $\dot{\boldsymbol{r}}$ and $\ddot{\boldsymbol{r}}$ is the structural displacement, velocity and acceleration vectors respectively.

The inertia force vector, $\boldsymbol{R}^I$ is a function of the structural mass matrix, structural mass matrix accounting for internal fluid flow and displacement dependent hydrodynamic mass matrix accounting for the structural acceleration terms in the Morison equation (MARINTEK, 2016). But, as all RIFLEX elements are above the waterline with no internal water chambers, it is only the first term that is included.

The damping force vector, $\boldsymbol{R}^D$, includes internal structural damping, hydrodynamic damping and specified dampers (MARINTEK, 2016). Only structural damping is relevant for the analysis performed in this thesis. Structural damping is explained in more in Section 3.7.1.

The "RIFLEX 4.8.1 Theory Manual" (2016) lists the most important nonlinear effects in dynamic analysis for slender structures:

- Geometric stiffness, i.e. contribution from axial force to transverse stiffness.

- Nonlinear material properties.
- Hydrodynamic loading according to the generalized Morison equation expressed by relative velocities.
- Integration of loading to actual surface elevation.
- Contact problems, e.g. bottom contact, riser collision, vessel/riser, pipe/stinger and contact.

Not all items are relevant for a floating bridge analysis, e.g., all material properties in the model is given as linear. How the nonlinearities are treated in the analysis of finite element analysis is either as nonlinear or linearised.

Nonlinear Time Domain Analysis

A nonlinear analysis can including all the mentioned nonlinearities. This is done by a step-by-step numerical integration if the incremental dynamic equilibrium equations (MARINTEK, 2016). A Newton-Raphson iteration method is frequently used.

Linearised Time Domain Analysis

The dynamic equation, Equation (3.39), is solved step by step with linearised mass, damping and stiffness matrices. This means that the matrices are kept constant during the analysis (MARINTEK, 2016). Non-linear effects like changing the stiffness matrix due to changes in the geometry is neglected. The only non-linear affect accounted for is the hydrodynamic loading. According to "RIFLEX 4.8.1 Theory Manual", this reduces the computational time significantly compared to a complete non-linear approach, and is a reasonable assumption when the hydrodynamic loading is the dominating non-linear effect.

3.5.2 Numerical Integration of the Equation of Motion

Solution of the dynamic equilibrium equation for a on-degree-of-freedom-system

$$m\ddot{u} + c\dot{u} + ku = Q(t) \tag{3.41}$$

is an initial value problem where solution is determined from initial values (Langen & Sigbjørnsson, 1979). By dividing the time interval where a solution is needed, into several time steps, we can solve the equation for each step by using the information about previous step. The solution at the wanted step can be found by assuming certain variation of the motion during the time step. According to Langen and Sigbjørnsson (1979), the accuracy of this method is dependent on the time steps. Smaller time steps will give a more accurate solution, but it will come with a cost of higher computational time. Langen and Sigbjørnsson (1979) describes two main groups of methods: *the difference formulation* and *numerical integration.*

Difference Formulation

The difference formulation replaces the derivatives in Equation (3.41) with a difference expression. These can be found by Newton's equidistant intarpolation folmulation with backwards integration (Langen & Sigbjørnsson, 1979). Figure 3.6 shows how the derivatives can be represented with the approximated parabola.

The second derivative can be represented as

$$\ddot{u}_k = \frac{u_{k+1} - 2u_k + u_{k-1}}{h^2} \tag{3.42}$$

and the first as

$$\dot{u} = \frac{u_{k+1} - u_{k-1}}{2h}. \tag{3.43}$$

Equations (3.42) and (3.43) are inserted into Equation (3.41). This makes it possible to solve for u_{k+1} when u_k and u_{k-1}. Here k represents the step number.

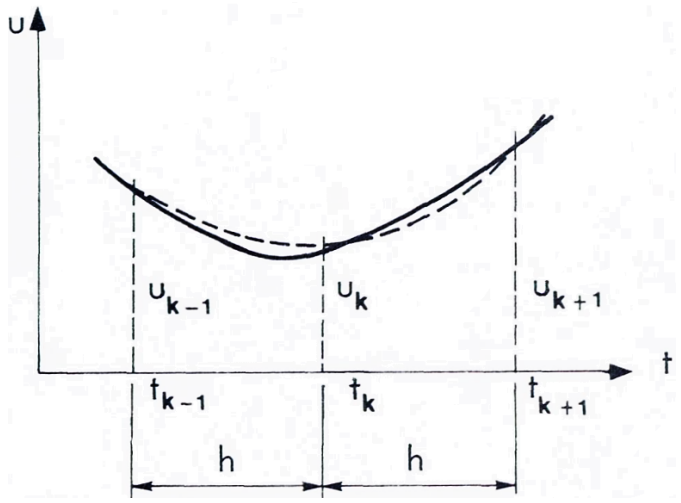

Figure 3.6: The continuous line repsresents the actual velocity as a function of time, while the dotted line represents a fitted parabola through three points. Image: Langen and Sigbjørnsson (1979).

Numerical Integration

Numerical integration is the other method described in *Dynamisk analyse av konstruksjoner [Dynamic analysis of structures]* (1979), and is the method used in RIFLEX. By integration of the acceleration, the velocity and displacement are found by the following equations

$$\dot{u}_{k+1} = \dot{u}_k + \int_0^h \ddot{u}(t)\,\mathrm{d}t \tag{3.44}$$

$$u_{k+1} = u_k + \int_0^h \dot{u}(t)\,\mathrm{d}t \tag{3.45}$$

where h is the time step length and velocity is defined as

$$\dot{u}(t) = \frac{1}{m}(Q(t) - c\dot{u}(t) - ku(t)). \tag{3.46}$$

By assuming how the acceleration varies over the interval it is possible to solve Equations (3.44) and (3.45). Different assumptions leads to different methods. These methods include, among others, *constant initial acceleration*, where acceleration is assumed to be constant and equal to the start value, *Constant average acceleration* and *linear acceleration*.

Newmark's β-family

Newmark's β-family are according to Langen and Sigbjørnsson (1979), the staring point for the above methods which can be considered as special cases of Newmark's general integral equations

$$\begin{aligned} \dot{u}_{k+1} &= \dot{u}_k + (1-\gamma)h\ddot{u}_k + \gamma h\ddot{u}_{k+1} \\ u_{k+1} &= u_k + h\dot{u}_k + (1/2-\beta)h^2\ddot{u}_k + \beta h^2\ddot{u}_{k+1} \end{aligned} \tag{3.47}$$

The β and γ terms are determined from stability and accuracy requirements. According to Langen and Sigbjørnsson (1979), the solution is unconditionally stable when

$$\gamma \geq \frac{1}{2} \tag{3.48}$$

$$\beta \geq \frac{1}{4}\left(\gamma + \frac{1}{2}\right)^2 \tag{3.49}$$

By changing the value of γ, one can introduce artificial damping in the system.

$$\begin{aligned} \gamma > \frac{1}{2} &\quad \text{positive artificial (numerical) damping} \\ \gamma < \frac{1}{2} &\quad \text{negative artificial (numerical) damping} \\ \gamma = \frac{1}{2} &\quad \text{no artificial (numerical) damping} \end{aligned} \tag{3.50}$$

According to "RIFLEX 4.8.1 Theory Manual" (2016), $\gamma = 1/2$ is normally used to obtain second order accuracy.

The method is based on a constant time step throughout the analysis and can be applied for both non-linear as well as linearized analysis (MARINTEK, 2016). See Section 5.4 for a discussion about the parameter values used for the analysis of the X-Bridge.

Accuracy

Accuracy of the integration methods depends on the dynamic loading, time step and the physical properties of the system.

According to Langen and Sigbjørnsson (1979), the integration is accurate for $h/T < 0.01$ for all methods. The parameters correspond to time step length and load period. For a given sea state it is therefore important to identify how small periods you are required to take into consideration in order to capture all loads.

As Langen and Sigbjørnsson (1979) describes, the step length is chosen to achieve the required accuracy in the most important mode shapes (usually the lowest ones, i.e., the longest periods).

3.6 Eigenvalue Analysis

For structures like floating bridges with wave loads, it is important to identify the eigenvalues and eigenmodes of the structure. By identifying eigenperiods and corresponding eigenmodes, one is able to investigate if any of the modes are triggered by the dynamic loads. The eigenperiod is given by the following equation

$$T_0 = \frac{2\pi}{\omega} = 2\pi\sqrt{\frac{\boldsymbol{M} + \boldsymbol{A_{ii}}}{\boldsymbol{K}}} \tag{3.51}$$

where $\boldsymbol{M} + \boldsymbol{A_{ii}}$ corresponds to the total mass of the system plus the added mass in the direction considered. For large floating structures as the pontoons suggested for the floating bridge, the added mass represents a significant addition in heave due to the large area. $\boldsymbol{K}$ represents the stiffness.

Eigenperiods are important to consider in comparison with the load period. If a structure has an eigenperiod that coincide with the load period, resonance can occur. This could lead to large displacements of the structure. As Equation (3.51) shows, the eigenperiod can be adjusted by modifying the added mass. This is suggested in the report "Straight Bridge - Navigation Channel in South" (2016b) where extra flanges are mounted on the pontoon in order to move the eigenperiod range away from the most critical wave periods.

3.6.1 Eigenvalue Problem

In the book *Dynamisk analyse av konstruksjoner [Dynamic analysis of structures]* by Langen and Sigbjørnsson (1979), the eigenvalue problem is described as follows.

The dynamic equilibrium is expressed as

$$\boldsymbol{M}\ddot{\boldsymbol{r}} + \boldsymbol{C}\dot{\boldsymbol{r}} + \boldsymbol{K}\boldsymbol{r} = \boldsymbol{Q}(t) \tag{3.52}$$

where $\boldsymbol{M}$, $\boldsymbol{K}$ and $\boldsymbol{C}$ corresponds to mass matrix, stiffness matrix and damping matrix respectively. The vector $\boldsymbol{r}$ represents displacement, velocity and acceleration. External loads are given by $\boldsymbol{Q}$.

For free undamped vibration, we have $\boldsymbol{C} = 0$ and $\boldsymbol{Q}(t) = 0$. Equation (3.52) reduces to

$$\boldsymbol{M}\ddot{\boldsymbol{r}} + \boldsymbol{K}\boldsymbol{r} = 0. \tag{3.53}$$

Harmonic vibrations where $\boldsymbol{r} = \boldsymbol{\phi}\sin(\omega t)$, the solution to (3.53) becomes

$$\left(\boldsymbol{K} - \boldsymbol{\omega}^2 \boldsymbol{M}\right) \boldsymbol{\phi} = 0. \tag{3.54}$$

This is described as the *eigenvalue problem on general form*. The *special eigenvalue problem* (the eigenvalue problem on standard form) is given by

$$(\boldsymbol{A} - \boldsymbol{\lambda I})\boldsymbol{x} = 0 \tag{3.55}$$

where $\boldsymbol{A}$ is a quadratic matrix of dimension n and has a non-trivial solution, $\boldsymbol{x} \neq \boldsymbol{0}$, when

$$p(\lambda) = \det |\boldsymbol{A} - \lambda \boldsymbol{I}| = 0. \tag{3.56}$$

The characteristic equation, Equation (3.56), of the eigenvalue problem has n solutions, $\lambda_1, \lambda_2 ... \lambda_\mathrm{n}$ which are the eigenvalues of $\boldsymbol{A}$.

As described in *Dynamisk analyse av konstruksjoner [Dynamic analysis of structures]*, each eigenvalue, λ_i has a corresponding eigenvector $\boldsymbol{x}_i$ which is found by solving Equation (3.55) for all λ_i.

Accoring to Langen and Sigbjørnsson (1979), the matrix

$$(\boldsymbol{A} - \boldsymbol{\lambda I}) \tag{3.57}$$

becomes singular. Due to this, intermediate, characteristic parameters have to be introduced into $\boldsymbol{x}$. As a consequence, Equation (3.54), does not give any information about the magnitude of the vibrations. It only gives information about the shape of the vibrations.

3.6.2 Solution Algorithm

There exist several solutions algorithms to the eigenvalue problem, in SIMA, the Lanczos method is applied. According to Bostic (1991), the Lanczos method has

proven to be efficient for solving large-scale problems. The eigenvalue problem on standard form, as described in Equation (3.55), is solved by a recursion formula (an iterative procedure).

A detailed desctiption of the Lanczos methos is described in "Lanczos Eigensolution Method for High-Performance Computers" 1991.

3.7 Damping

Damping will always be present in a real system, so that motion of the system will decrease if no external load is present. This damping can be difficult to calculate accurately for a complex system. Different simplified methods are therefore used Langen and Sigbjørnsson (1979). Some of the different models are

- Linear and nonlinear viscous damping (velocity dependent damping)
- Structural damping (displacement dependent damping)
- Coulomb damping (constant damping)

3.7.1 Structural Damping

Structural damping comes from the internal friction in the material. The damping can be described by a hysteresis curve, as seen in Figue 3.7. For a perfectly linear elastic material, the stress-strain curve would become a straight line, but for real materials, we get a curve on the form shown in Figure 3.7. The area within the curve represents the loss of energy per volume unit of the material per single stress cycle (Witoś & Stefaniuk, 2011).

According to MARINTEK (2016), internal structural damping has to be included in the dynamic analysis in the Riflex analysis in order to account for the energy dissipation in the structure itself. The damping is also related to the cross section properties of the structure (MARINTEK, 2016).

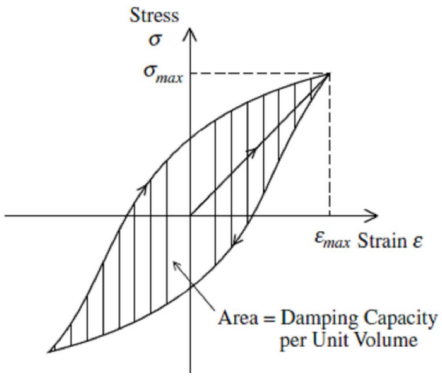

Figure 3.7: Hysteresis loop for mechanical damping for a typical metal. Image: Witoś and Stefaniuk (2011)

3.7.2 Modal Damping

According to Langen and Sigbjørnsson (1979), the data information we have on structural damping is usually on modal form, meaning that the damping is related to a certain mode shape. The damping ratio can be found by exciting the structure in resonance.

Proportional Damping

For structural damping, it is difficult to decide all terms in the damping matrix, $\boldsymbol{C}$. It is therefore in many cases expressed as a linear combination of the mass matrix, $\boldsymbol{M}$, and the stiffness matrix, $\boldsymbol{K}$, or decided from modal damping data (Langen & Sigbjørnsson, 1979).

By assuming that the damping force is proportional to the velocity of each mass point, $\boldsymbol{C}$ gets proportional with $\boldsymbol{M}$ as seen in Equation (3.58). Damping proportional to strain velocity gives proportionality to $\boldsymbol{K}$ as shown in Equation (3.59).

$$\boldsymbol{C} = \alpha_1 \boldsymbol{M} \tag{3.58}$$

$$\boldsymbol{C} = \alpha_2 \boldsymbol{K} \tag{3.59}$$

By combining of Equations (3.58) and (3.59), the damping can be expressed as in Equation (3.60) (Langen & Sigbjørnsson, 1979).

$$\boldsymbol{C} = \alpha_1 \boldsymbol{M} + \alpha_2 \boldsymbol{K} \tag{3.60}$$

This damping is called *Proportional damping* or *Rayleigh-damping*. It is now seen that $\boldsymbol{C}$ has the same orthogonality as $\boldsymbol{M}$ and $\boldsymbol{K}$, and the damping ratio, λ_i, for each mode, can be expressed as (Langen & Sigbjørnsson, 1979)

$$\lambda_i = \frac{\bar{c}_i}{2\bar{m}_i\omega_i} = \frac{1}{2}\left(\frac{\alpha_1}{\omega_i} + \alpha_2\omega_i\right) \tag{3.61}$$

where α_1 damps out the lower mode shapes and α_2 the higher. It is possible to calculate α_1 and α_2 if the damping ratio for two response frequencies are known by (Langen & Sigbjørnsson, 1979)

$$\alpha_1 = \frac{2\omega_1\omega_2}{\omega_2^2 - \omega_1^2}\left(\lambda_1\omega_2 - \lambda_2\omega_1\right) \tag{3.62a}$$

$$\alpha_1 = \frac{2\left(\omega_2\lambda_2 - \omega_1\lambda_1\right)}{\omega_2^2 - \omega_1^2} \tag{3.62b}$$

See Section 5.4 for the discussion on how this is included in the dynamic analysis.

3.8 SIMA/RIFLEX

The analysis in this paper is done using the software SIMA. SIMA is developed as a Joint Industry Project by Norwegian Marine Technology Research Institute

(Marintek) (now SINTEF Ocean) and Statoil. The software is developed to create a simple and user-friendly method of creating models to be used in various analyses. This is done in a 3D Graphical User Interface (GUI) which gives you instant validation of all changes, and then Sima writes the input files and feeds them into the physics engines. Riflex is one of these physics engines that are included in Sima. It is used to analyse slender systems, e.g., a riser system. According to MARINTEK (2016) Riflex was developed to analyse risers, but it is also well suited for any type of slender structures, such as floating bridges.

MARINTEK (2016) describes the characteristics for the slender systems adequate for Riflex analyses as:

- Small bending stiffness
- Large deflection
- Large upper end motion excitation
- Nonlinear cross section properties
- Complex cross section structure

The complex cross section is not modelled in Sima, rather a global cross section is applied (MARINTEK, 2016). This means that cross section properties such as axial-, bending-, and torsional stiffness must be specified as input. Riflex is based on nonlinear finite element formulation and includes both static and dynamic analysis. This includes eigenvalue analysis, natural frequencies, mode shapes and response to harmonic and irregular excitation (loading).

Chapter 4

The X-bridge Concept

The following chapter focuses on the concept and idea behind the X-Bridge. The concept is developed by Rune Risnes in Risnes Innovation.

4.1 Concept Idea

The overall goal of the X-Bridge concept is to utilise well-known construction methods to build a floating bridge at a significant lower cost than other concepts presented as part of the ongoing project on E39. To achieve this, the idea is to avoid using large bridge towers and mooring systems which include expensive subsea operations. The concept is based on a modular design which also is intended to reduce costs further.

The X-Bridge concept consists of two bridge girders in a X-shape seen from above, this is illustrated in Figure 4.1. The two girders are shaped as arcs in a concave shape (both arcs curves towards each other). A curved bridge will carry lateral loads as tension or compression depending on the direction of load as described previously in Section 2.1.1. This eliminate the need for lateral support by mooring lines and is advantageous at crossings where the seabed is either deep, soft or a combination of both as this makes anchoring complicated. The principle is explained by Watanabe and Utsunomiya (2003): when the current is coming from

the convex side, the bridge shape acts as an arch rib giving a much higher stiffness in the horizontal plane compared to a straight beam. In the other case, the bridge acts as a catenary cable.

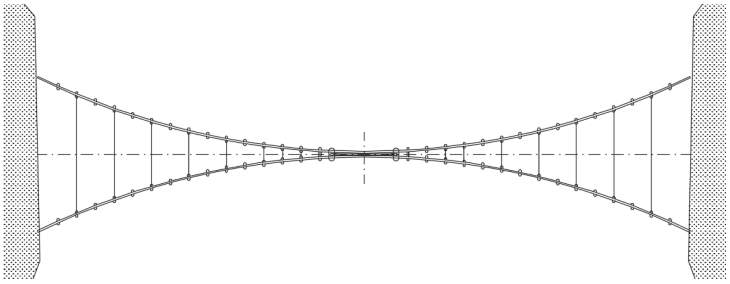

Figure 4.1: Principal sketch of the X-Bridge concept, top view. Image: Rune Risnes.

A problem whit the arch design is when the loading comes from the convex side, it creates compression forces in the arch. With high loads this could lead to buckling of the arch which will reduce the strength of it. Some concepts have solved this problem by adding mooring lines on the convex side. Instead of arch compression, forces will be transferred as tension to the mooring lines. But, as mentioned, the X-bridge concepts is avoiding mooring lines to reduce costs.

In order to reduce the compressive forces in the arch experiencing loading from its convex side, the idea is to transfer some of these forces to the other arch which will carry these as tension forces. To achieve this, the arches are connected along the whole span with cables, see Figure 4.1.

The idea is that by letting the bridge being able to expand and move towards land at the abutments, it will reduce its capability to be able to take compressive forces. This movement will cause the connective cables to transfer tension forces to the other arch. One possible way of introducing this, both in a computer model and for an actual construction, is by connecting one of the ends to a nonlinear spring. A nonlinear spring should have a low stiffness for motion towards land, and a high stiffness restraining it from moving any closer than a specified point for motions towards the fjord.

Due to numerical instability in the model created for the analysis, it is decided, in agreement with supervisor, to exclude this functionality from the model.

4.2 Model Description

The model is created after the principal sketches shown in Figures 4.1 and 4.2. Since the concept is in an early stage at this point, no detailed drawings apart from Figures 4.1 and 4.2 are available.

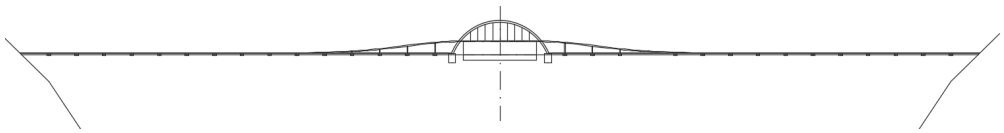

Figure 4.2: Principal sketch of the X-Bridge concept, side view. Image: Rune Risnes

The elevated midsection, as shown in Figure 4.2 is a navigation channel for ships to pass below the bridge structure. Dimensions of the channel is dependent on where the bridge is intended to be placed as the ship traffic and sizes of ships vary. To reach its intended height, the bridge will be inclined towards the midpoint. According to the rules in "NA-rundskriv 2015/2 - Fartsgrenser og motorveger - Ny dimensjoneringsklasse for motorveg med fartsgrense 110 km/t [Speed limits and motorway - New dimensioning class for motorway with speed limit 110 km/h]" (2015b), the maximum allowed incline on the road is 5 % for roads with speed limits up to 110 km/h.

In addition, the handbook *Bruprosjektering - Prosjektering av bruer, ferjekaier og andre bærende konstruksjoner [Bridge Design - Design of Bridges, ferry quays, and other load-bearing constructions]* (2015a) specifies some extra requirements for floating bridges. At mean water level, the maximum incline should be 0.5 % lower than the allowed incline for the road class described in "NA-rundskriv 2015/2 - Fartsgrenser og motorveger - Ny dimensjoneringsklasse for motorveg med fartsgrense 110 km/t [Speed limits and motorway - New dimensioning class for motorway with speed limit 110 km/h]" (2015b). The highest expected tide with a return period of 1 year should not cause the incline to exceed 1 % unit allowed for the road class. These requirements are for simplicity ignored here. The handbook also set the requirement for maximum "abrupt" changes in the incline, but these changes are assumed to be smooth and not included in the model. The horizontal

view of the bridge with the mentioned requirements for a navigation channel is illustrated in Figure 4.3

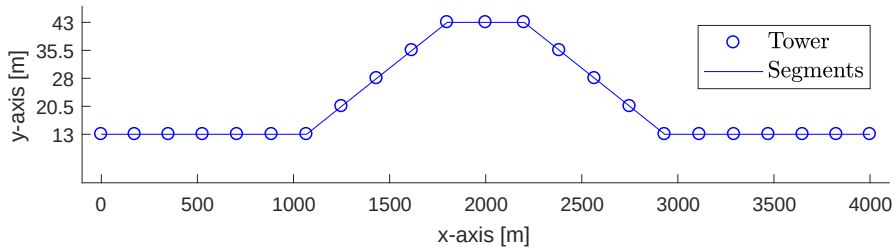

Figure 4.3: Sideview of the segment layout and the location of the tower/bridge girder connection.

Inclined segments are slightly longer, but the extra length is $< 1\,\%$ and therefore ignored and not discussed any further.

Navigation channel dimensions are set to fulfil the requirements found in the report *Design Basis* (2016). This report sets the design requirements for the crossing of Bjørnafjorden. The dimensions of the navigation

4.3 Initial Design Dimensions

In this section, the initial overall design dimensions and how they are chosen described. How more specific dimensions are decided are given in Section 5.1.

4.3.1 Overall Dimensions

As the model is intended to give some information about the concepts potential for the Coastal Highway Route E39, the main dimensions are set relatively large in order to allow for large fjord crossings found along the Western coast of Norway. The crossing distance for the model is set to 4000 m. As an initial curvature radius for the bridge girder, a radius of 6000 m are chosen. Distance and curvature are set to these values as suggested by Rune Risnes. According to Øderud and Nordahl

(2006), the normal distance from a straight line spanning from one end of the arch to the other for suspension bridge cable is around 10 % of the length. This distance is sometimes referred to as "crown height". Initial crossing length and radius corresponds to a crown height of approximately 350 m. By choosing this radius, the goal is to achieve some of the principles used for the tension cables in suspension bridges.

Segment length have been suggested by Rune Risnes not to be any longer than 200 m. This length limit is a result of discussions between Risnes and a potential manufacturer of the bridge girder segments. To find the length of each segment, the remaining distance to cover after subtracting the length of the navigation channel is divided into equal segments. An element length of 184 m corresponds to the lowest number of element without exceeding the limit of 200 m and is set as the segment length for the model.

An overview of the bridge segments with locations for towers and pontoons are illustrated in Figure 4.4. The curvature is set to 6000 m and, as the figure shows, the crossing length is 4000 m.

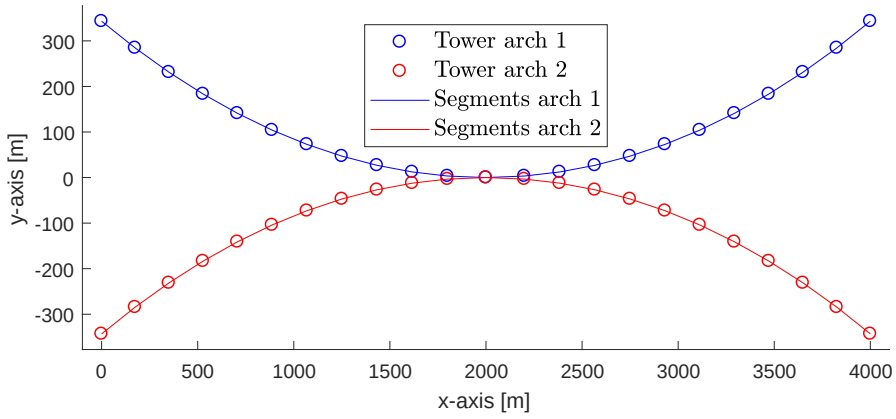

Figure 4.4: Overview of the segment layout and location of pontoons. Pontoons are marked as circles on the plot, girders are represented by the solid lines between pontoon locations.

4.3.2 Bridge Girder

The bridge girder is a combination of the two different girders described in the reports *Curved Bridge - Navigation Channel in South* (2016a) and "Straight Bridge - Navigation Channel in South" (2016b). These are also discussed in Section 2.1.3.

The girder has overall dimensions according to one of the two parallel girders used in the curved bridge, as each girder are designed to have two driving lanes. But, each bridge girder is designed as a single bridge girder like the one described for the straight bridge alternative.

4.3.3 Pontoons

It is decided to use three different pontoon sizes in the model. For the low bridge, where each pontoon carries the weight equivalent of one girder segment (plus the tower), a small pontoon is used. For the middle section, where the two girders are connected, a one-pontoon solution is chosen. The sections with standard segment length is carried by a medium pontoon and the navigation channel, with a larger span, is carried by a large pontoon.

Deciding the pontoon size and optimize this is a comprehensive task, the method described here is therefore simplified in many aspects. As a starting point, the pontoons described in "Straight Bridge - Navigation Channel in South" are used. These are designed to carry a girder with approximately twice the self-weigh of one girder in the X-Bridge concept. This pontoon size is therefore used for the large pontoons at each side of the navigation channel where both arches are supported by the same pontoon. For the two other pontoons, the initial size was decided by reducing the water plane area and mass.

Chapter 5

Method

5.1 Deciding Dimensions

As this report is written in the early stage of the X-Bridge, few details for the bridge is known. It is therefore necessary to decide initial values for the main parameters for the bridge. In the following sections the procedure for several fundamental values are described

5.1.1 Bridge Girders

The bridge girder cross section is shown in Figure 5.1 and is suggested by Rune Risnes in Risnes Innovation. The main dimensions of the cross section are summarised in Table 7.1 in Section 7.1.1 of the results.

To simplify the calculation of the global properties of the cross section, an equivalent plate thickness has been used instead of including longitudinal stiffeners in the calculations. The equivalent plate thicknesses are also shown in Table 7.1.1.

Results from "Straight Bridge - Navigation Channel in South" (2016b) and *Curved Bridge - Navigation Channel in South* (2016a) are used to compare hand calculations done for the cross section shown in Figure 5.1. These results are for similar

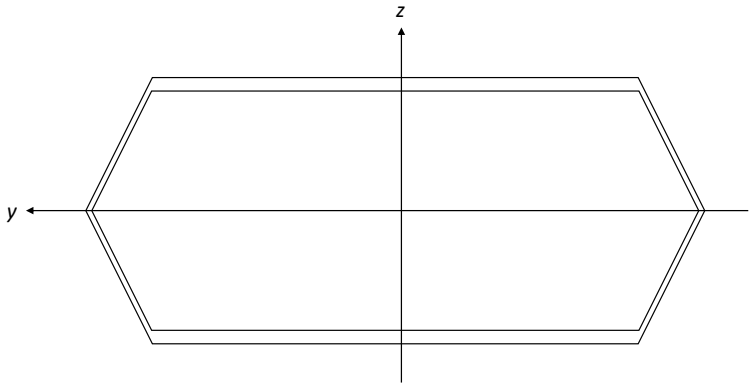

Figure 5.1: Bridge girder cross section

cross sections and calculation methods are validated by performing the hand calculations for both cross sections. The comparison of the results in the report and results obtained by hand calculations can be found in Appendix E. Calculations for the cross section used in the X-Bridge concept are also found in Appendix E. A summary of the cross section properties can be found in Section 7.1.1 with the most important values summarised in Table 7.2.

To calculate the steel weight of transverse stiffeners, a conservative approximation is done by comparing relative weight. By comparing weight of steel skin and longitudinal stiffeners and the weight of the transverse stiffeners for the cross sections in the previously mentioned reports, a relative weight is found. This weight is set to 16 % of the steel skin including longitudinal stiffeners. This is done to find the total steel weight of the bridge girder.

Table 5.1 shows the steel properties used in the calculations. Yield strength is set to 460 MPa according to *DNV-RP-C208* (2013).

Table 5.1: Steel properties used in calculations.

Parameter	Unit	Value
E	[Pa]	2.1×10^{11}
G	[Pa]	8.08×10^{10}
ν	[-]	0.3

5.1.2 Navigation Channel

In order to allow for ship traffic, the suggested design includes a navigation channel at the midsection where the two arches are connected. In the model, the functional design requirements for Bjørnafjorden are used (Larssen, Larsen, Strømsem, & Sørby, 2016). The required vertical clearance, defined as the distance from the water surface to the bridge deck soffit, is set to 45 m. This height should include deflection form traffic in the serviceability limit state *frequently occurring* (Larssen et al., 2016). Horizontal clearance in the navigation channel is set to 400 m.

Due to the long horizontal span, an increased bending stiffness about the horizontal axis is required for the navigation channel. As illustrated in Figure 4.2, one way of doing this is to build a tied-arch bridge for the long span. This is not included in this report. Instead, the bending stiffness for the long span is set as $EI_{y,nav.girder} = EI_{y,girder} \cdot 10$ for simplicity.

The navigation channel girder is modelled as two separate girders connected to the same node at the centre of the channel, as seen in Figure 5.2.

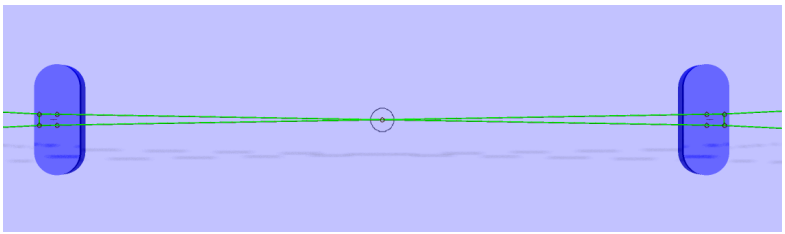

Figure 5.2: Navigation channel bridge layout. Arches are connected at the supernode in the middle.

5.1.3 Towers

Dimensioning of the towers, going from the pontoons to the bridge girder, are done in the same way. The diameter of the tower is set to 8 m with a plate thickness of 40 mm. Main dimensions are summarised in Table 7.3 in Section 7.1.2 and calculated cross section properties are shown in Table 7.4 in the same section.

In SIMA, all elements on the bridge superstructure is modelled as slender beam elements. These elements are modelled along the neutral axis of each structural part. To place the neutral axis of bridge girder at the correct height, one has to consider the height of the bridge girder itself. To simplify the modelling, the tower height is increased to give the bridge girder the correct height of its own neutral axis. To avoid the extra mass added by increasing the tower height, the mass is reduced so that the total mass equals the total mass of a tower with correct height.

This increases the tower height and potentially increases the tower response. Due to the relatively short tower height, compared to the bridge span, this response is assumed to be small.

5.1.4 Cable

Steel cables used for cable supported bridges are usually made out of steel wires with a diameter between 3 and 7 mm with a considerably larger tensile strength than that of ordinary structural steel (Gimsing & Georgakis, 2012). A cable is made up of several wires, often combined in a strand consisting of a core wire surrounded with wires in a helical pattern, which in turn is combined to a cable as illustrated in Figure 5.3. This reduces the modulus of elasticity, and for a seven-wire strand it usually lies around 190 MPa (Gimsing & Georgakis, 2012).

Figure 5.3: Seven strand cable with one core wire surrounded by six wires in a helical pattern. Image from Gimsing and Georgakis (2012)

As it exists few similar structures as the X-Bridge, it is decided to use cables with the same stiffness as the mooring lines used in the straight bridge concept described in the report “Straight Bridge - Navigation Channel in South”. These are after all designed to carry some of the vertical forces on the bridge and the number of cables and mooring lines are about the same for the two concepts.

5.1.5 Pontoons

As the bridge is constructed with separate girders for the part closest to land, but a single girder at the navigation channel, the weight carried by each pontoon varies along the bridge. As a consequence, it is decided to use different pontoon sizes. The design is done with the pontoon taken from *Curved Bridge - Navigation Channel in South* (2016a) as a starting point. The size of the pontoons is decided depending on the weight of the superstructure each pontoon carries. It is assumed that each pontoon carries the weight of half the girder span on each side, the tower and its self-weight, as seen in Equation (5.1).

$$m = m_t + m_g + m_p \tag{5.1}$$

For the pontoons at each end of the navigation channel, the total loading includes the weight of both girders with the extended navigation channel span. The weight is therefore close to the girder weight described in *Curved Bridge - Navigation Channel in South* (2016a). Hence, the same pontoon size is used for the pontoons at the navigation channel. The main dimensions are shown in Table 7.5 in Section 7.1.3 of the Result Section.

As Figure 5.4 shows, the two bridge arches are carried by one pontoon also for the two sections closest to the navigation channel. This is due to the short distance between the arches towards the midsection.

These pontoons carry less weight than the navigation channel pontoons and are reduced in size. The water plane area and the mass is reduced to 80 % of the navigation channel pontoons. Length, breadth and radius are kept at the same relative sizes and are calculated to ensure the wanted water plane area.

The height of the pontoons is calculated to give the wanted weight. See Section 6.1.1 for a thorough description of how the pontoons are built.

For the low bridge, where each arch is carried by separate pontoons, the pontoons are reduced further in size. The water plane area as well as the mass are for these pontoons set to 50 % of the navigation channel pontoons. The weight carried by

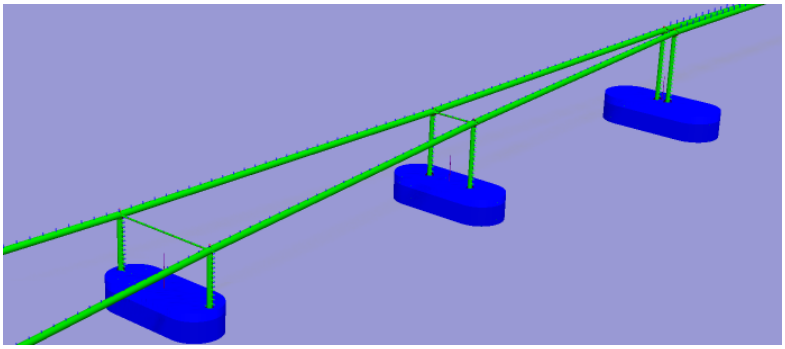

Figure 5.4: Bridge layout at midsection. Each pontoon carries the weight of both bridge girders. The rightmost pontoon is large while the two others are medium.

the small pontoons are less than 50 % of the navigation channel pontoons, but 50 % is used as a conservative estimate to ensure enough hydrostatic stiffness.

The chosen water plane stiffness is checked according to the method described in Section 5.1.5 to ensure that the vertical stiffness acceptable.

For future references, these three pontoon sizes will be referred to as large, medium and small, respectively.

The pontoon described in *Curved Bridge - Navigation Channel in South* (2016a), is designed with a flange at the bottom as seen on Figure 5.5. This is installed to increase the added mass in heave in order to alter the eigenperiod of the pontoon in heave motion. This flange is not used in the design for the pontoons in the model for the X-Bridge.

The internal layout of the pontoons is shown in Figure 5.6. The cross section is divided into 21 watertight compartments. The subdivision of the cross section is done to ensure sufficient strength, but most importantly to reduce the consequence of damage to the pontoons. Damaged conditions are not evaluated in the analysis, but the cross section layout is used to create the mass model of the pontoons as described in Sectio 6.1.1.

The layout shown in Figure 5.6 is used for the largest of the pontoons at the navigation channel. The strengthening of the pontoon walls at the rounded part is not included in the model. The large wall thickness at the rounded walls is to

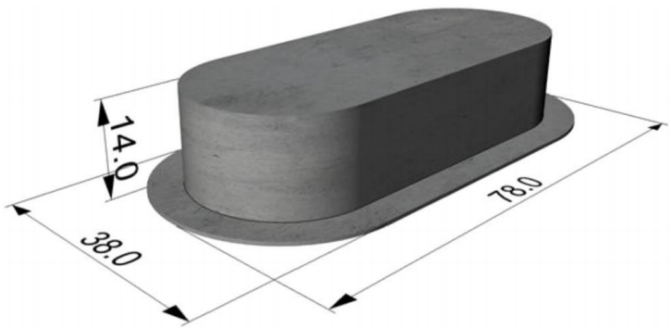

Figure 5.5: Pontoon used in *Curved Bridge - Navigation Channel in South* (2016a) with bottom flanges and main dimensions. Figure by Aas-Jakobsen, COWI, Johs Holt, and Global Maritime (2016a).

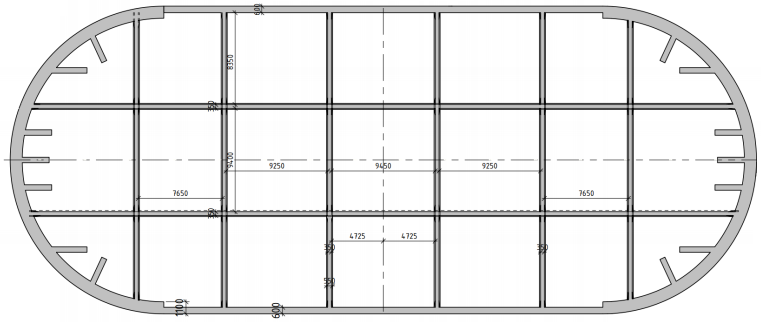

Figure 5.6: Layout of the pontoon cross section showing relative wall thickness and compartments. Figure by Aas-Jakobsen, COWI, Johs Holt, and Global Maritime (2016a)

withstand ship impacts (Aas-Jakobsen et al., 2016a). For the large and medium pontoon, the same dimensions as shown in Figure 5.6 are used. For the small pontoon, the thickness is reduced. The different thicknesses are summarised in Table 7.6 in the result section.

As the largest pontoon has the same outer dimensions as the pontoon used as a staring point, the inner compartment layout is kept. For the medium and small pontoons, the number of inner compartments are kept and the relative size is set to the same as for the large pontoon.

When the outer dimensions on the medium and small pontoon are kept at the

same relative size as for the large pontoon and the top and bottom thickness as well as internal layout is set, it is possible to calculate the required height in order to obtain the wanted mass.

This section shows that there are a lot of parameters to vary in order to obtain a reasonable pontoon design, the method described here is only a simplified method to come up with a potential design. The method described here includes some trial and error in order to come up with reasonable dimensions since all parameters affects each other. As a consequence, some parameters have to be set according to comparable pontoons.

Pontoon Draft

In order to calculate the correct properties in Wadam, the pontoons have to be analysed at correct draft. Initially, the draft for each pontoon size is estimated by calculating the total weight (including self-weight) and the water plane stiffness, C33, as shown in Equation (5.2) The estimated draft can also be found by solving Equation (5.3) for the draft, d.

$$\text{Draft [m]} = \frac{\text{Total weight [N]}}{\text{Water plane stiffness [N/m]}} \tag{5.2}$$

$$\rho V(d) = m_p + m_t + m_g \tag{5.3}$$

Here, mp, m_t and m_t are the mass of the pontoon, tower and girder respectively. The girder mass is estimated by assuming that each pontoon carries their own section of the bridge.

The estimated draft is used to analyse the pontoons in Wadam to obtain the hydrostatic stiffness matrices and later the added mass, potential damping and the first order wave excitation force transfer functions. The hydrostatic stiffness matrices are used on the model created in SIMA as input to the SIMO bodies. By

doing a static analysis of the entire model with the hydrostatic stiffness obtained from Wadam, the draft at static equilibrium is found. In order to find the exact draft, it is necessary with several iterations. A static analysis in SIMA gives the vertical equilibrium position of each pontoon based on the total mass, buoyancy force and water plane stiffness. The change in draft from initial position to static equilibrium position is used to update the draft. For each draft, new hydrostatic matrices and buoyancy forces are calculated for the pontoons. This process is continued until the difference in initial position and static equilibrium position is sufficiently small enough. Results are found in Section 7.1.3.

Water Plane Stiffness

In the report *Curved Bridge - Navigation Channel in South* (2016a), there is set a requirement to the water plane stiffness. Vertical deflection due to traffic is limited to $< 1\,\text{m}$ for a load corresponding to $0.7 \times$ traffic loading. To calculate the traffic loading, rules found in Eurocode (Norsk Standard, 2003) are used. The applied traffic load is governed by the number of notional lanes. The number of notional lanes are set according to the regulations given in the Eurocode. For each notional lane, the equivalent line load ([N/m]) is calculated giving the total equivalent line load for each bridge girder. This line load is then used to calculate to estimate the loading on each pontoon by multiplying it with the bridge girder length carried by the respective pontoon. The vertical deflection of each pontoon is estimated with this load and the water plane stiffness, *C33*, to verify that the stiffness is sufficient. Results from the calculations are shown in Section 7.1.3.

5.2 Linear Model

In a linear model, there will be a linear relationship between the wave height and the measured response in the model. In order to verify whether the model is linear or non-linear, the model is analysed with a regular wave with wave period corresponding to the peak period, $T_p = 6\,\text{s}$, for Bjørnafjorden. The analysis is done with different wave height in order to compare the response. Wave heights are set

to 1 m to 11 m. To check the linearity, the moment response at the low bridge is checked. See Section 7.5.1 for results.

Simulation duration is set to 300 s, but only results after 200 s are used, this is to avoid transient effects on the measured data as it takes some time for the waves to reach all pontoons.

5.3 Dynamic Response

Initial dynamic calculations turned out to be extremely time consuming with the chosen number of elements in the model. As the model contains two parallel bridge girders as well as several cables, the number of elements is large. One 3 h analysis takes several days to finish.

Due to the long analysis time, it is, in agreement with supervisor, decided to only run analyses with regular waves. With regular waves, it is possible to investigate the response for certain wave height and wave period combinations in a much shorter time. For the regular wave analysis, it is sufficient to run the analysis for a considerably shorter time. For the analyses conducted, 300 s is found to be sufficient to obtain steady state in the response, avoiding transient effects. By reducing the simulation length from 10 800 s (3 h) to 300 s, each analysis is possible to run in a day.

5.4 Damping

As explained in Section 3.5.2, there are different solution algorithms for solving the EoM. When using the Newmarks's β-family algorithm, artificial numerical damping is introduced for $\gamma > 1/2$. Since early versions of the bride model shows some instability regarding displacements getting too large for the solution to converge, and fails to complete some runs, it is decided to introduce some numerical damping in order to obtain a more stable model.

The Newark parameters are set to the values below. These values correspond to those suggested as *simulator default* in SIMA.

$\gamma = 0.505$ positive artificial (numerical) damping

$\beta = \frac{1}{3.9}$

Section 3.7 discusses physical damping of the system. According to Wilson (1999), a typical way of estimating the proportionality factors is by setting the two critical damping ratios equal for the two frequencies, $\lambda_i = \lambda_j = \lambda$, and then proportionality coefficients may be calculated according to Equation (5.4). This ensures the damping to be at a minimum level of what is given for the two frequencies. For frequencies in-between, the damping will be smaller.

$$\begin{aligned} \alpha_2 &= \frac{2\lambda}{\omega_i + \omega_j} \\ \alpha_1 &= \omega_i \omega_j \alpha_2 \end{aligned} \tag{5.4}$$

The specified damping is set to 3 % in order to obtain a more stable model. In Figure 5.7, the damping as function of frequency is given. The specified damping, marked as red crosses on the figure, is set for frequencies corresponding to periods covering most of the relevant wave periods from 2 s to 10 s.

The proportional damping coefficients then becomes

$\alpha_2 = 0.0159$ Stiffness proportional damping

$\alpha_1 = 0.0314$ Mass proportional damping

5.5 Bridge Girder Stresses

As described in Section 3.2, stresses in the bridge girders arises from the axial force, N, bending moments, M, and shear forces, V.

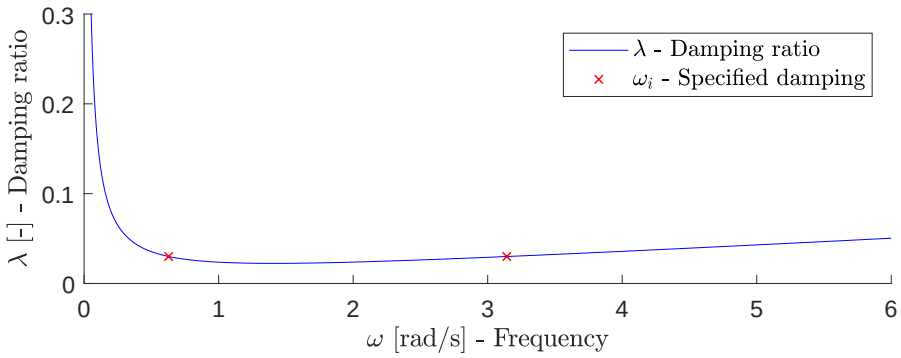

Figure 5.7: Damping as a function of eigenfreguency for proportional damping.

The points of interest when analysing the bridge girder stresses are marked with numbers 1 through 6 in Figure 5.8.

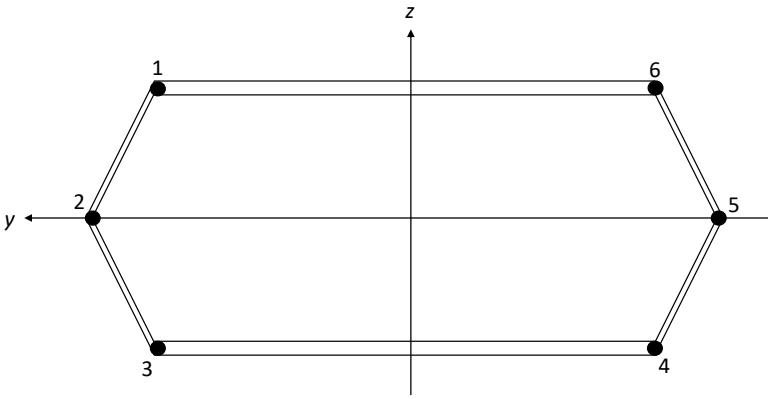

Figure 5.8: Bridge girder cross section with locations for stress calculations.

5.5.1 Axial Stress

Axial stresses are induced by both axial forces and bending moments. These are calculated as described in Section 3.2.1 according to Navier's formula as given in Equation (3.23).

Stress due to axial force is constant over the cross section, while the stress due to moment varies linearly over the cross section with its maximum points at maximum y and z values. The points marked in Figure 5.8 covers these.

5.5.2 Shear Stress

Stresses due to shear are calculated with background in the procedure described in Section 3.2.2. As the cross section is symmetric around two axes, it is only necessary to calculate the shear stress for one quarter of the section. Due to the thick top and bottom plates, the shear stress is assumed to be of most interest at the vertical plates which are much thinner. The shear stress is therefore calculated for the corner, corresponding to points 1, 3, 4 and 6 in Figure 5.8 and the intersection between the two inclined webs, corresponding to points 2 and 4 in Figure 5.8.

Since the shear stress distribution over the cross section is of no interest, Equation (3.27) is used to calculate expressions for the shear stress as a function of the shear force only, this is done by inserting numerical values for the second moment of area, thickness and first moment of area for the points of interest. The calculated values are listed in Tables 5.2 and 5.3 for vertical and horizontal shear stress respectively. The last value listed in the tables, τ/V, is used to calculate the shear stress for the point of interest with the shear forces obtained from the analysis in Sima.

As seen from the tables, τ/V for horizontal shear force are small compared to the vertical. In Section 7.3.3 it is discussed how small the horizontal shear forces are.

Table 5.2: Calculation of shear stress due to vertical shear force for point 1 and 2 which covers all points 1 through 6 on Figure 5.8.

Vertical shear		Corner, point 1	Side, point 2
A	[m^2]	0.300	0.411
I_y	[m^4]	5.654	5.654
I_z	[m^4]	20.773	20.773
t	[m]	0.006	0.006
$\bar{y}$	[m]	3.000	2.394
S	[m^3]	0.900	0.983
τ/V	[m^{-2}]	26.528	28.973

Share forces due to torsional moments are calculated according to Section 3.2.2 with the torsional moment obtained from the results from Simo.

Table 5.3: Calculation of shear stress due to horizontal shear force for point 1 and midpoint of top/bottom plate.

Horizontal shear		Corner, point 1	Top
A	[m^2]	0.111	0.411
I_y	[m^4]	5.654	5.654
I_z	[m^4]	20.773	20.773
t	[m]	0.006	0.020
$\bar{y}$	[m]	9.250	4.606
S	[m^3]	1.023	1.892
τ/V	[m^{-2}]	0.009	0.016

Chapter 6

Modelling

This Chapter describes the different steps that are used to create the complete model of the floating bridge system of the X-Bridge. This chapter is intended to give the reader a clearer picture of how the model is made and analysed. See Section 5.1 for a description of how the different dimensions are decided.

6.1 Hydrodynamic Analysis

Hydrodynamic calculations are done in order to obtain hydrodynamic properties for the pontoons. The procedure is the same for all three pontoons, only the dimensions, as described in Section 5.1.5 are different. The hydrodynamic analysis is conducted using software developed by DNV GL. The software used is part of the Sesam software package delivered by DNV GL. Software used is GeniE, HydroD and Wadam.

6.1.1 Mass Model

In order to get the correct hydrostatic coefficients, a mass model has to be created. The mass model is generated in the software GeniE according to the dimensions

described in Section 5.1.5. The different main dimensions are also summarised in Table 7.5 in Section 7.1.3.

Figure 6.1 shows how the model is made in GeniE. The blue lines on top of the pontoon indicates how the model is created by modelling only one quarter and then mirror it around both axes in the xy-plane. The mass model also contains the different compartment walls. These are important to include in order to get both the total mass and the correct centre of gravity and radius of gyration.

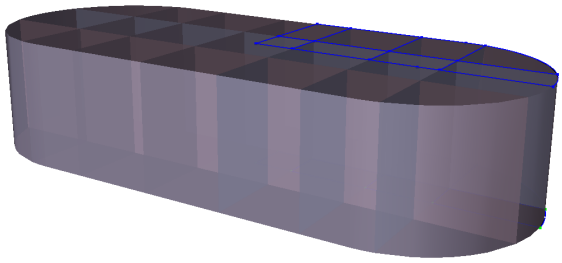

Figure 6.1: Mass model generated in GeniE. The model shows how tho pontoon is divided into several compartments. The blue lines on the top indicates how the pontoon is modelled.

The mass model is exported from GeniE as a finite element model file (.FEM).

6.1.2 Panel Model

The panel model used in HydroD is created in GeniE. Panel models are used in stability and hydrodynamic analyses in HydroD. The panel model describes the wetted surfaces for a model and contains only the outer hull of the pontoons. Figures 6.2a shows the outer structure of the pontoon which is modelled for only a quarter of the total model. This is to reduce the number of panels to be analysed in HydroD as the software is capable of utilizing the double symmetry.

In order for the software to know which panels to calculate to properties for, a dummy load case has to be defined on the panel model. This load case is illustrated in Figure 6.2b as the orange field at the outside of the pontoon.

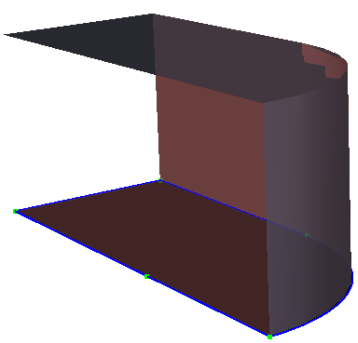

(a) Pontoon structure created of plates with wet surfaces.

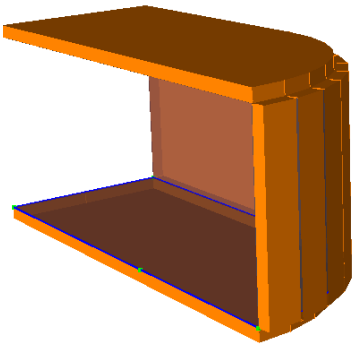

(b) Pontoon with dummy hydrostatic pressure around the model.

Figure 6.2: Pontoon with wet surface and with dummy hydrostatic pressure.

The mesh size on the panel model are initially set according to the recommendations given by DNV in "Recommended Practice, DNV-RP-F205"(2010a).

- diagonal length in panel model $< 1/6$ of smallest wave length analysed.
- fine panel mesh to be applied in areas with abrupt changes in geometry (edges, corners).
- finer panel mesh towards water-line in order to calculate accurate wave drift excitation forces.

After running the first analysis, the mesh size is reduced to achive the maxium number of panels on the model. This is done to achieve more accurate results, and the time spent on analysing each pontoon is still within a few hours.

The panel model is exported from GeniE as a finite element model file (.FEM).

6.1.3 Wadam Analysis in HydroD

The software HydroD is used to analyse the mass and panel model created in GeniE. Both finite element models are imported into HydroD and assembeled into a hydromodel.

The analysis of the hydromodel is done in Wadam which is an analysis program

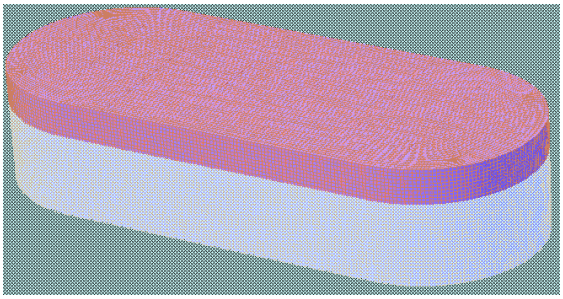

Figure 6.3: Hydromodel in HydroD. The model is located with the water surface at the desired draft.

for calculation of wave-structure interaction. Wadam is started from the GUI of HydroD. Wadam is a powerful tool and can find many properties, among those are wave excitation forces, hydrodynamic added mass and damping, rigid body motions and so on. If a structural model is created in addition to the panel model described earlier, Wadam can transfer the loads on the panel model to the structural model (DNV, 2010b). Wadam calculates loads using (DNV, 2010b):

- Morison's equation for slender structures.
- First and second order 3D potential theory for large volume structures.
- Morison's equation and potential theory when the structure comprises of both slender and large volume parts. The forces at the slender part may optionally be calculated using the diffracted wave kinematics calculated from the presence of the large volume part of the structure.

In this analysis, the pontoon is considered as a large volume structure, so potential theory is used to calculate the loads.

In HydroD, a Wadam run is set up by using the built-in Wadam wizard. The wizard guides the user through the necessary steps to set up a specific analysis. The analysis is set to frequency domain. A direction set for the waves are set from 0° to 90° (due to double symmetry) with a step interval of 5°. The frequency is set to a range from 0.006 28 rad/s to 18.849 55 rad/s, corresponding to periods from 0.333 s to 1000 s. At the short periods, the spacing is small in order to capture all effects. The spacing becomes more and more coarse for longer periods as the

functions approach constant values for long periods. There is a limit on number of frequencies allowed in the analysis so the number of frequencies used is 54.

The mass and panel model are located with the desired draft (see Section 7.1.3 for the discussion on how to estimate the draft). Wadam has an option of removing irregular frequencies from the radiation diffraction solution (DNV, 2010b). The analysis is done with the option activated.

The results from the Wadam analysis are exported from HydroD as a Hydrodynamic Results Interface File (DNV, 2010b) containing transfer functions for rigid body responses together with transfer functions for off-body kinematics and the rigid body matrices. As mentioned in the discussion in Section 3.4.1, the motions transfer functions are not valid.

6.2 Coupled Model in SIMA

The bridge model is created in the software SIMA developed by SINTEF Ocean (former MARINTEK). The SIMA software is a platform for several other programs like RIFLEX and SIMO as well as a post processor.

6.2.1 RIFLEX Model

The software RIFLEX is developed to do static and dynamic analyses on slender marine structures, with a special focus on slender riser applications. The floating bridge is represented as a series of slender elements by defining a cross section with the properties shown in Table 7.2 in Section 7.1.1.

Supernodes are located at each land connection and at each bridge girder segment. The supernodes are used to connect the bridge girder segments together with each other as well as connecting them to the towers. The towers are in turn connected to a supernode located at the top of each pontoon. This is illustrated in Figure 6.4 together with the general names used in the model.

Figure 6.4 shows an element between the two nodes *n2ponttop* and *n2pontloc*. This

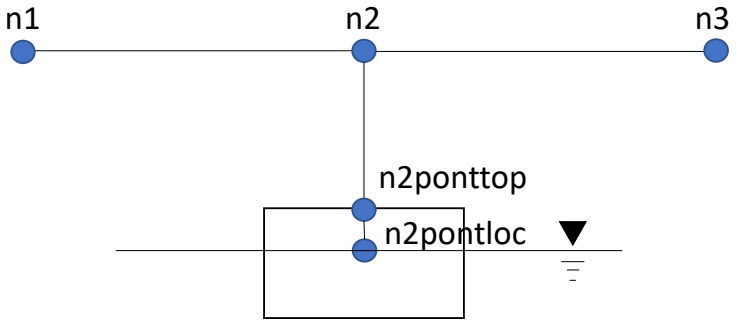

Figure 6.4: Supernode configuration with general names used in the model

element is used to connect the pontoon location node to the bottom of the tower element. The pontoon location node works as a connection between the RIFLEX model and the SIMO body. The element between is a "dummy" element, meaning it has no physical properties. The mass is set to zero and the stiffness is set very large in order to make the element work as a rigid connection between the tower and pontoon.

Cables

Initially, the cables connecting the two bridge girders are modelled as *simple wire coupling*, but this method does not work. See Appendix C for a closer description of the problem.

To represent the cables, it is decided in agreement with supervisor, to use ordinary RIFLEX bar elements. These elements have the same properties as a pre-stressed cable. The axial force carried by a bar element represents the net reduction in tension force for an equivalent cable. The effect lost with this configuration is the pre-tension of the bridge girder itself. In order to avoid too large deflections of the cables, the mass has to be placed at the ends (at the bridge) as point masses.

6.2.2 SIMO Model

The pontoons are represented as floating SIMO bodies. These are connected to the *n2pontloc* supernode as described in previous section. The hydrodynamic properties fond in HydroD, as described in Section 6.1.3, are imported to each pontoon. For each pontoon, the buoyancy compencating force is applied as well as mass included. This is discussed closer in Section 3.4.1.

6.2.3 Program Flow

For the dynamic analysis, the SIMO module generates the wave time series initially. This means that the programs assume small displacements of the body. The results are imported into the RIFLEX module as nodal forces varying in time. RIFLEX then solves the EoM for the entire system in time domain. The program calculates displacement for all nodes and forces for all elements. In order to obtain the results, the user has to specify which nodes and elements to store the information about. In order to capture the moments and shear forces acting on each segment, the results from five elements, two at the end, one in the middle ant two in between are stored. The same is done for the node displacement.

All results are exported using the post processor. Then the results are imported into MATLAB in order to generate the desired plots and perform different calculations.

Chapter 7

Results

This chapter contains the result of the initial bridge design and the model analysis results. Discussions regarding the results are done consecutively.

7.1 Bridge Design

The first sections summarise the main dimensions decided for the bridge design.

7.1.1 Bridge Girder

The main dimensions of the bridge girder are suggested by Rune Risnes in Risnes Innovation and are summarised in Table 7.1. The resulting cross section properties are shown in Table 7.2.

7.1.2 Towers

Main dimensions for the towers are listed in Table 7.3 and the most important tower properties are shown in Table 7.4.

Table 7.1: Main dimensions of the bridge girders

General dimension	[m]	Equivalent plate thickness	[m]
Total width	22.0	Top	0.020
Cross section height	6.0	Upper inclined	0.006
Height upper inclined web	3.0	Lower inclined	0.006
Height lower inclined web	3.0	Bottom	0.020
Width upper inclined web	3.5		
Width lower inclined web	3.5		

Table 7.2: Cross section properties of girder used in analysis.

Cross section property	Unit	Value
Area	[m^2]	0.71
I_y weak axis	[m^4]	5.65
I_z strong axis	[m^4]	20.77
I_t Torsional moment of inertia	[m^4]	16.18
Radius of gyration about local x-axis	[m]	4.01
Axial stiffness (EA)	[N]	1.49×10^{11}
Bending stiffness y, weak axis	[Nm^2]	1.19×10^{12}
Bending stiffness z, strong axis	[Nm^2]	4.36×10^{12}
Torsional stiffness	[Nm^2/rad]	9.25×10^{11}
Steel skin (including longitudinal stiffeners)	[kg/m]	5578.48
Transverse stiffeners[1]	[kg/m]	892.56
Total steel weight	[kg/m]	6471.04
Total steel weigh	[kN/m]	63.48
Asphalt, railings etc[2]	[kN/m]	30.62
Total permanent load (self-weight)	[kN/m]	94.10
Total permanent load (self-weight)	[kg/m]	9592.37

[1] 16 % of longitudinal weight as described in Section 5.1.1.

[2] (Weight corresponds to the same weight as used in *Curved Bridge - Navigation Channel in South* (2016a))

Table 7.3: Tower dimensions.

General dimension	[m]
Diameter	8.000
Plate thickness	0.040
Effective thickness vertical	0.048
Effective thickness total[1]	0.055

[1] Total effective thickness is an estimate based on similar cross section in *Curved Bridge - Navigation Channel in South* (2016a).

Table 7.4: Cross section properties for tower used in analysis.

Property	Unit	Value
Area	[m^2]	1.21
I (bending)	[m^4]	9.65
I (torsion)	[m^4]	19.30
Radius of gyration about x-axis	[m]	4.00
Axial stiffness	[N]	1.01×10^{10}
Bending stiffness	[Nm^2]	2.03×10^{12}
Torsional stiffness	[Nm^2/rad]	1.56×10^{12}
Self-weight	[kg/m]	10 769.82
Self-weight	[kN/m]	105.65

7.1.3 Pontoon Design

Results from initial pontoon dimensions are shown in Table 7.5 for outer dimensions and the different thicknesses are shown in Table 7.6. The method of deciding the dimensions are described in Section 5.1.5. The dimensions are used for the first hydrostatic analyses.

Table 7.5: Main dimensions for the three pontoon sizes.

Main pontoon parameters		Large	Medium	Small
Length	[m]	68.00	60.82	48.08
Breadth	[m]	28.00	25.04	19.80
Radius	[m]	14.00	12.52	9.90
Height	[m]	14.50	13.09	12.85
Draft	[m]	9.78	8.70	8.74
Water plane area	[m^2]	1735.75	1388.60	867.88
Displaced volume	[m^3]	16 967.63	12 085.25	7654.75
Mass	[kg]	1.14×10^7	9.19×10^6	5.77×10^6

Table 7.6: Thickness of pontoon walls, bottom and top.

	Large [m]	Medium [m]	Small [m]
Top	0.60	0.60	0.50
Bottom	0.60	0.60	0.50
Straight walls	0.60	0.60	0.55
Circular walls	1.10	1.10	1.00
Longitudinal inner wall	0.35	0.35	0.30
Transverse inner wall	0.35	0.35	0.30

Draft Iteration Process

In Wadam, the initial draft is used to calculate the hydrostatic stiffness matrix needed for the static analysis of the actual draft. Since the initial drafts are based

on simplified hand calculations, the actual draft differs slightly as the pontoons carries more or less weight than estimated. Figure 7.1 shows how large the deflection of the pontoons are compared to the assumed initial draft.

Figure 7.1 shows only the deflection for half of the pontoons along arch 1, but due to symmetry, the deflections are equal for the second half as well as for the other arch.

The first iteration, as seen in Figure 7.1, shows that the small pontoons (number 2 through 8) are deflected upwards, meaning that the initial displaced volume is too large. The draft is hence reduced with 0.2 m. For the medium and large pontoon, the initial displacement is too small, and the draft is adjusted with 0.7 m and 0.4 m, respectively. Already after the second iteration, marked with blue circles in Figure7.1, the largest deflection is less than 0.13 m. This corresponds to about 1 % error compared to the total draft.

The cable connecting the two bridges have a relatively small mass compared to the bridge girder and the pontoons. In Figure 7.1, the red circles show the deflection after adding the mass of the cable (initial dimensions). As seen, the draft is almost unchanged, the cable mass is therefore not to have any particular influence on the pontoon draft.

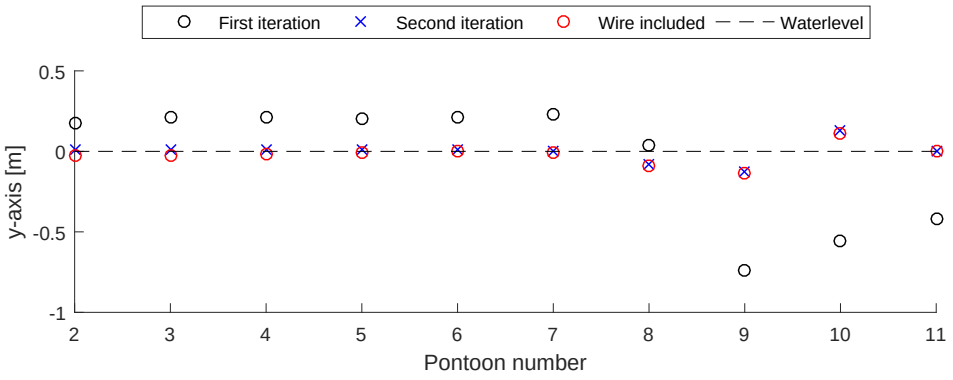

Figure 7.1: Deflection of pontoons in static analysis for each iteration of draft. Note that the pontoons are numbered according to their Supernode connection. Pontoon number 2 through 8 are small, pontoon number 9 and 10 are medium and pontoon number 11 is large.

Table 7.7 summarises the adjustment on the pontoon draft compared to the initial calculations. The new drafts in Table 7.7 are used for the hydrodynamic analyses in Wadam. The results for pontoon number 9, where the displacement used in the analysis is too small, may be a bit on the non-conservative side as the hydrodynamic forces acting on the pontoon is dependent on the submerged volume.

But, as mentioned, the relative error in draft is small and it is assumed that the difference in forces will be close to values corresponding to the exact draft.

Table 7.7: Summary of pontoon draft calculations. Negative adjustment corresponds to reduction in draft.

	Small [m]	Medium [m]	Large [m]
Pontoon height	12.85	13.10	14.50
Initial draft	8.74	8.70	9.78
Initial freeboard	4.11	4.4	4.72
Adjustment	−0.20	0.70	0.40
New draft	8.54	9.4	10.18
New freeboard	4.31	3.70	4.32

Water Plane Stiffness

The water plane stiffness is checked according to the method described in Section 5.1.5. Table 7.8 shows how the carriageway is divided into notional lanes and Table 7.9 shows how the equivalent line load for each notional are calculated. It also includes the total line load for the bridge girder.

The results in Tables 7.8 and 7.9 are for each bridge girder. The calculated total load on the midsection of the bridge, where the two girders are carried by one pontoon is therefore multiplied with two.

In Table 7.10 the total loading on each pontoon is shown. The small pontoon carries the traffic load on one bridge girder, while the medium and large pontoon carries the loading from both girders. All three pontoons satisfy the minimum requirement for vertical stiffness. As seen in the table, the utilisation is relatively

Table 7.8: Number and width of notional lanes.

Description	[m]/[-]
Carriageway width, w	10
Width of notional lane, w_l	3
Number of notional lanes, n	3
Width of remaining area	1
Pedestrian width	3

Table 7.9: Calculation of equivalent line loads for the uniformly distributed traffic loads.

Placement	Axial loads [kN]	Uniformly distributed load [kN/m^2]	Equivalent line loads [kN/m]
Notional lane 1	300	9	16.2 [1]
Notional lane 2	200	2.5	7.5
Notional lane 3	100	2.5	7.5
Rest area	0	2.5	2.5
Pedestrian	0	2.5	7.5
Total			41.2

[1] a load factor of 0.6 is used (Larssen, Larsen, Strømsem, & Sørby, 2016)

high for the large pontoon, this is due to the long span between the large pontoons at the navigation channel.

Table 7.10: Water plane stiffness requirement.

		Small	Medium	Large
Traffic load	[kN]	5304	10 607	16 840
C33	[kN/m]	8727	13 963	17 453
Allowed deflection	[m]	1.00	1.00	1.00
Deflection	[m]	0.61	0.76	0.96
Requirement		OK	OK	OK

7.2 Hydrodynamic Analysis of Pontoons

The software HydroD is used to run the hydrodynamic solver Wadam, as described in Section 6.1.3. In the following section, hydrostatic results from the Wadam analysis is shown. See Appendix E for information regarding the hydrodynamic result files.

7.2.1 Hydrostatic Stiffness Matrix

The first results found in Wadam are the hydrostatic stiffness matrices for the three pontoons. As described in Section 3.4.1, the hydrostatic stiffness matrices have to be corrected due to the buoyancy compensation force. Table 7.11 shows the stiffness matrix for the small pontoon as given by the results from the Wadam analysis for the small pontoon. Symmetry and no mooring lines gives restoring forces for only heave, roll and pitch motions, corresponding to *C33*, *C44* and *C55*. For readability of the table, the force units are summarised in Table 7.14.

In Table 7.12, the values are corrected according to the method described in Section 3.4.1. As seen, the heave stiffness, *C33,* is unchanged as it is only dependent on the water plane area which remains the same. Roll, *C44*, and pitch, *C55*, stiffness

Table 7.11: Hydrostatic stiffness matrix from Wadam analysis for the small pontoon.

	1, Surge	2, Sway	3, Heave	4, Roll	5, Pitch	6, Yaw
1, Surge	0	0	0	0	0	0
2, Sway	0	0	0	0	0	0
3, Heave	0	0	8.73×10^6	0	0	0
4, Roll	0	0	0	6.12×10^7	0	0
5, Pitch	0	0	0	0	1.24×10^9	0
6, Yaw	0	0	0	0	0	0

are increased to account for the buoyancy compensating force. Results for all three pontoons are summarised in Table 7.13.

The initial hydrostatic stiffness matrix from Wadam also contains numerical noise for some of the coupling terms. As the pontoons are symmetric, all coupling terms are removed from the matrices and set to zero manually.

Table 7.12: Hydrostatic stiffness matrix corrected for buoyancy compensation force for the small pontoon.

	1, Surge	2, Sway	3, Heave	4, Roll	5, Pitch	6, Yaw
1, Surge	0	0	0	0	0	0
2, Sway	0	0	0	0	0	0
3, Heave	0	0	8.73×10^6	0	0	0
4, Roll	0	0	0	2.60×10^8	0	0
5, Pitch	0	0	0	0	1.44×10^9	0
6, Yaw	0	0	0	0	0	0

Table 7.13: Summary of corrected hydrostatic stiffness components due to buoyancy compensation force.

		Small	Medium	Large
C44	Wadam	6.12×10^7	3.02×10^8	4.62×10^8
	Corrected	2.60×10^8	6.59×10^8	1.04×10^9
C55	Wadam	1.24×10^9	3.28×10^9	5.18×10^9
	Corrected	1.44×10^9	3.63×10^9	5.75×10^9

Table 7.14: Units for restoring forces summarised for better readability of the stiffness matrices.

Units for restoring forces	
C33	[N/m]
C44	[N m]
C55	[N m]

7.3 Static Analysis

This Section summarises the static results from Wadam as well as SIMA.

7.3.1 Bending Moments

The structure carries most of the loading as bending moments. Most importantly are the bending moment in the bridge girder, but the moments in the tower are also included.

Bridge Girder

Figure 7.2 shows the static bending moment of the bridge girder for one of the arches. The bending moment is a result of the structures self-weight as there are no external loads. Due to symmetry, the moment is equal for the other arch. The largest bending moment occurs at the midspan of the navigation channel due to the long span.

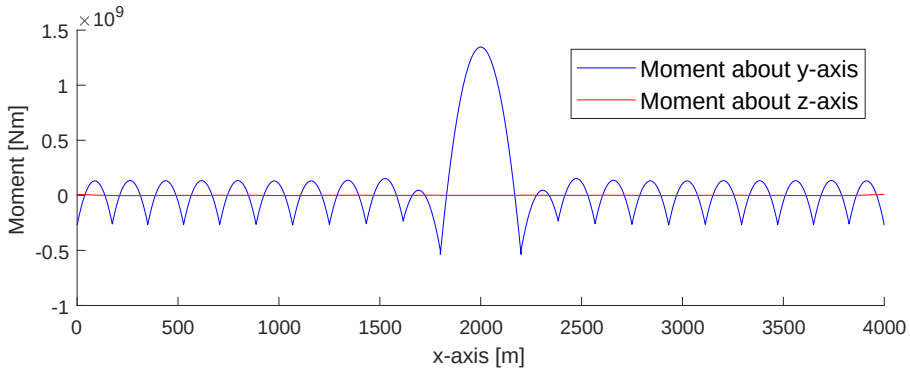

Figure 7.2: Static bending moment of the bridge girder. Due to symmetry, only bending moment for one girder is shown.

For the low bridge, the largest moment is observed at the tower connections. The symmetric loading around the tower connections gives a moment distribution close to the distribution for a fixed beam with uniform distributed load, as explained in

Section 3.2.1. A comparison of the results from SIMA with analytical values are shown in Table 7.15. As the calculations shows, the results obtained from SIMA agrees with the calculated values.

Table 7.15: Comparison of analytical bending moment for a beam with fixed ends and results from SIMA

Location	Analytical [N m]	SIMA [N m]	Difference [%]
M_{end}	2.65×10^8	2.70×10^8	-1.73
M_{centre}	1.33×10^8	1.31×10^8	1.21

For the tower connection at the navigation channel, the loading asymmetrical, and as a consequence, the moment distribution is closer to the moment distribution for a beam with free ends due to the large loading at one side of the towers.

As there are no external forces in transverse direction of the bridge, there is no considerable bending moment of about the vertical z-axis. The value of the static bending moment about z-axis are compared to the bending moment about the y-axis in Figure 7.2 as the red line, and shows that the value is insignificant. In addition, the z-axis is the strong bending axis.

Towers

Bending moment in the towers are summarised in Table 7.16 on page 81. Notice that for towers, local y-axis is along negative global y-axis and local z-axis is along global x-axis The largest bending moments are located at the intersection between the tower and the bridge girder.

The tower names correspond to those used in the model and follows a logical pattern. The name *nXXaXtow* is generated according to the supernode connection in the bridge girder. Tower *n02a1tow* is connected to node number 2 in arch number 1. The last part *tow* is added to indicate that the element is a tower element. When the input files to RIFLEX and SIMA are generated outside SIMO, SIMO has a limit in variable and element names on six to eight characters depending on what type it is.

Table 7.16: Tower heigh, maximum moment and stress about y- and z-axis and location for maximum for arch 1. Local y-axis is along negative global y-axis and local z-axis is along global x-axis.

Tower	Height [m]	$M_{y\max}$ [N m]	$\sigma_{y\max}$ [MPa]	Location [m]	$M_{z\max}$ [N m]	$\sigma_{z\max}$ [MPa]	Location [m]
n02a1tow	8.67	-8.02×10^5	0.3	8.67	3.60×10^6	1.5	8.67
n03a1tow	8.67	-7.37×10^5	0.3	8.67	5.72×10^6	2.4	8.67
n04a1tow	8.67	-7.85×10^5	0.3	8.67	6.63×10^6	2.7	8.67
n05a1tow	8.67	-7.15×10^5	0.3	8.67	6.92×10^6	2.9	8.67
n06a1tow	8.67	-5.34×10^5	0.2	8.67	6.69×10^6	2.8	8.67
n07a1tow	8.67	-7.61×10^5	0.3	8.67	5.67×10^6	2.4	8.67
n08a1tow	16.16	-1.18×10^6	0.5	16.16	4.18×10^6	1.7	16.16
n09a1tow	24.25	7.92×10^4	0.0	24.25	1.57×10^6	0.7	24.25
n10a1tow	31.74	6.49×10^6	2.7	31.74	4.96×10^6	2.1	31.74
n11a1tow	38.56	-3.66×10^7	15.2	38.56	2.01×10^6	0.8	38.56
n13a1tow	38.56	3.66×10^7	15.2	38.56	2.01×10^6	0.8	38.56
n14a1tow	31.74	-6.49×10^6	2.7	31.74	4.96×10^6	2.1	31.74
n15a1tow	24.25	-7.91×10^4	0.0	24.25	1.57×10^6	0.7	24.25
n16a1tow	16.16	1.18×10^6	0.5	16.16	4.18×10^6	1.7	16.16
n17a1tow	8.67	7.61×10^5	0.3	8.67	5.67×10^6	2.4	8.67
n18a1tow	8.67	5.34×10^5	0.2	8.67	6.69×10^6	2.8	8.67
n19a1tow	8.67	7.15×10^5	0.3	8.67	6.92×10^6	2.9	8.67
n20a1tow	8.67	7.85×10^5	0.3	8.67	6.63×10^6	2.7	8.67
n21a1tow	8.67	7.37×10^5	0.3	8.67	5.72×10^6	2.4	8.67
n22a1tow	8.67	8.02×10^5	0.3	8.67	3.60×10^6	1.5	8.67

The table shows values only for arch 1, but due to symmetry, the bending moment and stress about local y-axis is the same. Around local z-axis, the bending moment are in the opposite direction, but of the same magnitude. The complete list of bending moments and stresses for arch 2 is shown in Table B.5 in Appendix B.2.

The largest moments are observed in *n11a1tow* and *n13a1tow*, which are the two towers at each end of the navigation channel. The bending moment about local y-axis in the tower connections are caused by the asymmetric loading of the towers closest to the navigation channel. This asymmetry may become even larger when a complete model containing a tied-arch bridge is included as will add weight to the structure.

Since the bending moments are relatively small, the shear stress will not be considered for the towers. By looking at the maximum stress observed in the towers, found in the fourth and seventh column of Table 7.16, it is noted that the stresses due to bending moments are small and insignificant. The only exception is for the two navigation channel towers as mentioned.

7.3.2 Torsional Moment in the Bridge Girder

Static torsional moment in the bridge girder is shown in Figure 7.3 together with the corresponding shear stresses. The shear stress is calculated with Equation (3.30) in Section 3.2.2. As the figure shows, the static shear stress due to torsional moment is less than 10 MPa for all segments. This value is small compared to the shear stress due to bending moment as described later in Section 7.3.5. The contribution from static torsional moment is therefore not included in the equivalent stress calculations at the end of Section 7.3.5.

7.3.3 Shear Forces in the Bridge Girder

The static shear force is calculated according to the method described in Section 3.2.2. Figure 7.4 shows the static vertical shear force in the bridge girders. The largest shear forces in the girder are observed at the tower locations. The shear force diagram shown looks like what you would expected for a beam with uniform

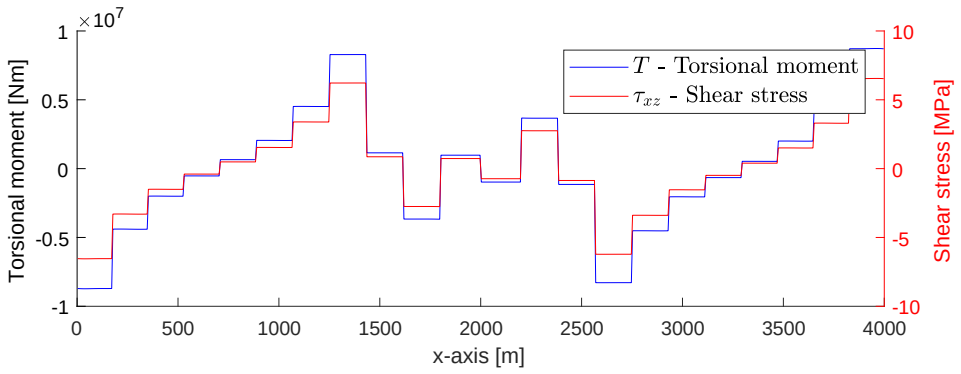

Figure 7.3: Static torsional moment and shear stress in bridge girder

distributed load (self-weight). Hand calculations also show that the peaks at the tower connections agree with the values calculated by Equation (7.1) where q is the uniformly distributed load corresponding to the self-weight of the bridge girder and L is the length between each tower.

$$V = \frac{qL}{2} \tag{7.1}$$

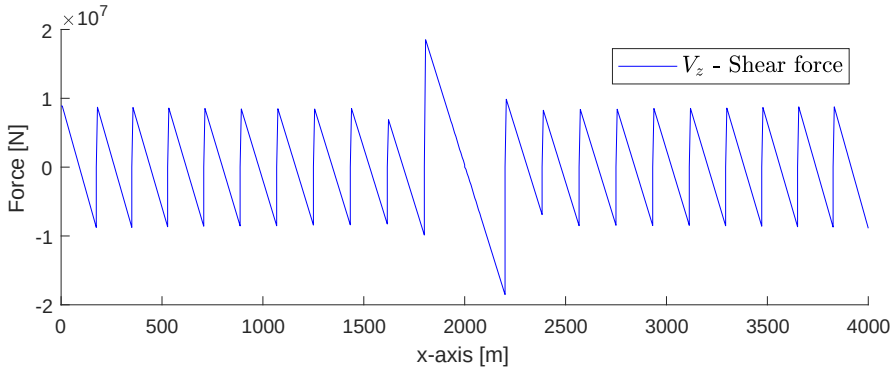

Figure 7.4: Static shear force in bridge girder calculated from the static bending moment.

As expected when looking at Figure 7.2, which shows the static bending moment about the two axes, the horizontal shear force is insignificant.

Stresses due to the shear force are calculated in Section 7.3.5.

7.3.4 Effective Tension and Compression Forces

Static tension and compression forces are relatively small in the bridge girder, as it carries most of the load as bending moment. The towers on the other hand, carries the loading as axial loads.

Bridge Girder

The tension forces in the bridge girder is relatively small as most of the loading is taken as bending moment. This is illustrated in Figure 7.8 which shows that the normal stress, σ_A, due to tension forces is close to 0 compared to the stress due to bending moment.

The largest measured tension along the bridge girder is approximately 1 MN. With a cross section area of $0.71\,\mathrm{m}^2$, as seen in Table 7.2, this corresponds to less than 1.5 MPa stress due to axial forces. The static axial force will therefore note be considered any further for the bridge.

Cables

The tension force in static equilibrium for the cables are not correct since they are modelled with wrong self-weight as described in 6.2.1. But, the static tension force in the cables are used to identify the dynamic part of the axial force when looking at dynamic results for the cables. The stresses are shown in Figure 7.5. The figure only shows the tension for the first seven cables, as the cables on the other side of the navigation channel has the same force distribution.

Since the cables are modelled as fixed bar elements, the idea is that they behave as a cable with pretension as described. The interesting results from the cables are therefore the dynamic part. See Section 7.5.3 for dynamic axial force results.

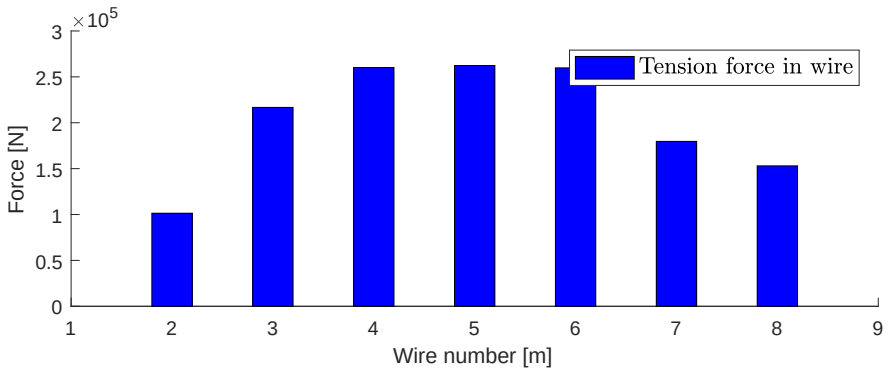

Figure 7.5: Relative static force in cables. Values are not physically correct, as the self-weight used is not correct. Values are used to calculate the dynamic change.

Towers

The static compressive force in the towers are shown in Figure 7.6 together with the stress for one arch at one side of the navigation channel. The loading is symmetric, and equal for corresponding towers. Hand calculations shows that the compressive force corresponds the weight of the superstructure carried by the tower. As seen in Figure 7.6, this gives a larger compressive force in the towers closest to the navigation channel. Static stresses are well within the yield limit.

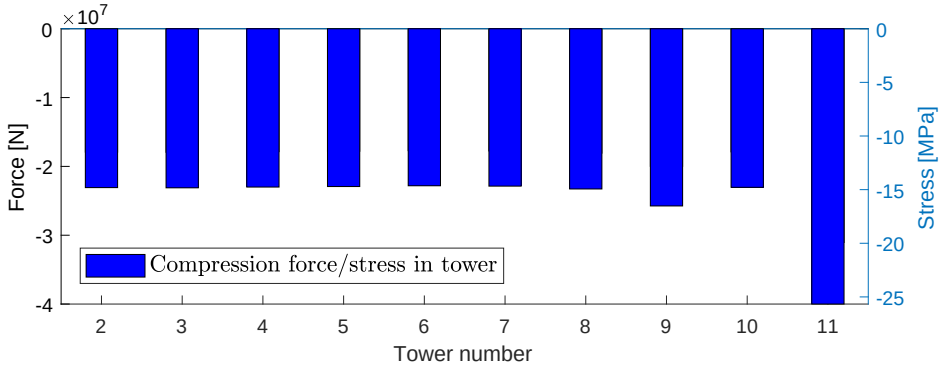

Figure 7.6: Static compression forces and stresses in towers.

7.3.5 Stresses

For the bridge girder, the dominating stress is due to the static bending moment about the y-axis. For the cables, the stress arises from tension forces and the towers are dominated by compressive forces.

Bridge Girder

Initially, the bending stiffness about the weak y-axis was set to the same value along the whole bridge, including the long span at the navigation channel. As seen in Figure 7.7, the stress about y-axis gets too large for the navigation channel, as the steel used has a yield capacity of 460 MPa. The bending stiffness is therefore increased for this section. As described in Section 5.1.1, the second moment of area about y-axis, I_y, is multiplied with the power of 10. This increase is just a simple approximation of the added strength a cable strayed bridge, or similar, has to add for the navigation channel.

The stress is calculated at the bottom of the cross section, at $z = -3\,\text{m}$. At this point the girder is tension, while at the top, where $z = 3\,\text{m}$, it is in compression. Due to the symmetry about the y-axis, the magnitude of the stress is the same at the top where $z = 3\,\text{m}$.

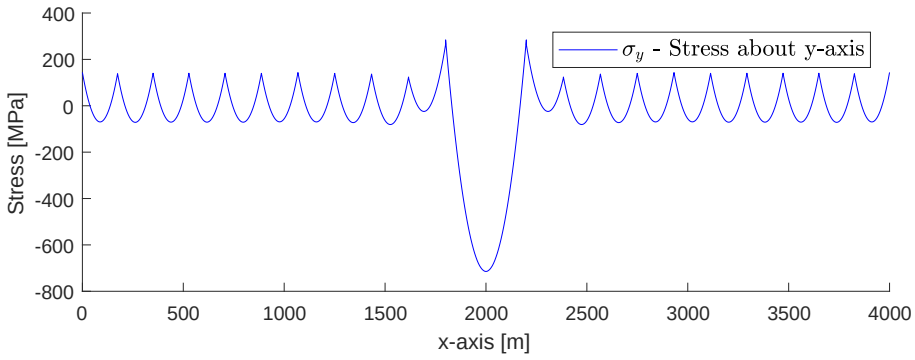

Figure 7.7: Stress about y-axis before adjusting the second moment of area, I_y, for the navigation channel.

After the bending stiffness at the navigation channel is increased, the bending

stress is reduced for that section. The results are shown in Figure 7.8. The stress is measured at the bottom of the bridge girder. The largest stress occurs at the transition from ordinary girder to the girder used for the navigation channel. At this point, the moment is large, as seen on Figure 7.2, while the bending stiffness is the same as for rest of the ordinary girder. As there will be a transition between the ordinary girder and the navigation channel, the focus will be on the stresses in the ordinary girder. The added bending stiffness about the y-axis is just an indication on how strong the navigation channel bridge has to be.

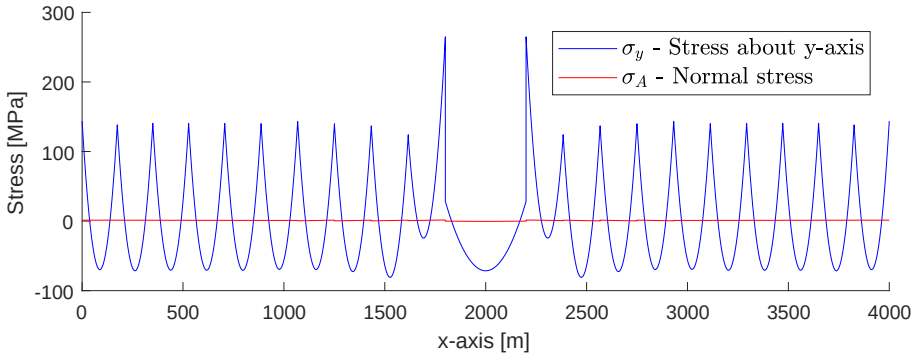

Figure 7.8: Static bending stress and normal stress in bride girder after adjusting bending stiffness for the midsection.

For the low part of the bridge, the largest stress peaks occur at the tower locations. At these locations, the bridge girder deck is in tension while the bottom of the girder is in compression. Between each pontoon, where the other local maxima occurs, it is opposite.

The values at the tower locations are approximately 143 MPa and 71 MPa at the middle of the span. Both values are well within the limits of the yield stress of 460 MPa.

Stresses due to shear forces are calculated according to Section 5.5.2 for the corner point (1) and side (2) as seen in Figure 5.8 on page 59.

Figure 7.9 shows the result for the calculated shear stress at the points of interest. The blue line is for the corner point between the top plate and the side plate, and the red line is for the midpoint on the bridge girder walls. The shear stresses are

relatively equal for the two points.

As the figure clearly shows, there are large shear stresses in the bridge girder at static equilibrium. As the midsection is modelled as an ordinary section, the result here will not be focused on. For the low bridge section the maximum value of shear stress occurs at the bridge tower. The maximum values are at approximately 230 MPa and 255 MPa for point 1 and 2 respectively.

These high shear stresses are caused by the large bending moment about the y-axis in combination with the thin plate thickness for the bridge girder sides. This plate thickness is only 6 mm. As mentioned previously, the bridge girder dimensions are based on suggested values from Risnes Innovation who came up with the concept. The stress values are still below the yield criteria which is 460 MPa (without any safety factor), but have to be checked in combination with other stresses according to the yield criteria described in Section 3.2.3.

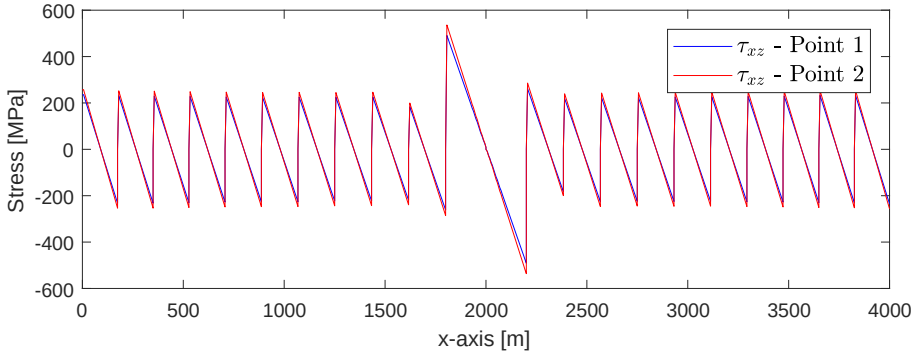

Figure 7.9: Static shear stress in bridge girder due to self-weight. High stresses are caused by the thin walls in the girder.

Towers

Stresses in the towers along arch 1 are summarised in Table 7.16 on page 81. The largest stresses along each tower are located at the intersection between the bridge girder and the tower. The largest value is observed at the towers closest to the navigation channel, where the bending stress about the y-axis is 15.2 MPa. But, overall all stresses are small for the static equilibrium compared to the yield

strength of 460 MPa. Stresses for arch 2 are found in Table B.5 in Section B.2. As explained for the bending moment, the values for arch 2 are of the same magnitude as for arch 1.

von Mises Stress in the Bridge Girder

In Section 7.3.5 it is shown that the largest bending stress occurs at the largest values of z, furthest away from the neutral axis. This point corresponds to points 1, 3, 4 and 6 in Figure 5.8 on page 59. The upper points, 1 and 6 are in compression while the two others are in tension due to the static bending moment about the y-axis between the towers and opposite at the towers. For these points, the static shear stress is also calculated.

As described in Section 3.2.3, the equivalent stress can be calculated for stress combinations. It is sufficient to look at the four mentioned points, as the shear stress is just slightly larger at the neutral axis, and here the bending stress is zero. Only stresses due to bending moment and shear forces are considered as these are the ones of significant magnitude.

By combing the two stress components according to Equation (3.31) in Section 3.2.3, the equivalent stress, σ_v, along the bridge girder is calculated. The equivalent stress in the bridge girder is shown in Figure 7.10.

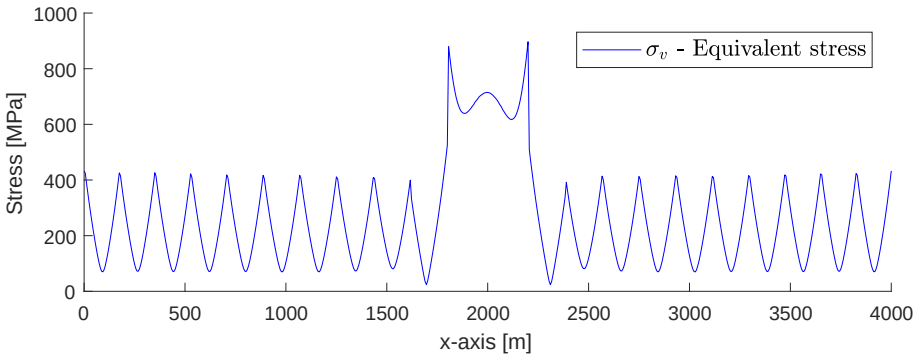

Figure 7.10: Static equivalent stress in bridge girder when bending moment and shear stress due to bending are accounted for.

As seen in the figure, the equivalent stress is at its largest at each side of the navigation channel. The equivalent stress is more than 900 MPa and a definite reason to include some sort of extra reinforcement at the navigation channel. The local peak at the middle of the navigation channel is where the shear stress equal zero and the bending moment has its maximum as seen in Figures 7.9 and 7.2 respectively.

The largest equivalent stress in the low bridge is located at each tower connection. As seen in Figures 7.2 and 7.9, this is where both the bending moment and the shear stress have their maximum value. In combination, the equivalent stress reaches 425 MPa. The requirement, according to Section 3.2.3, is still within the von Mises yield criterion, but there is not much capacity left for dynamic loads. See Section 7.5.2 for results with dynamic loading.

7.4 Eigenvalue Analysis

Dynamic analysis in SIMA is used to perform an eigenvalue analysis of the bridge structure. As described in Section 3.6, the eigenvalue analysis does not give any information about the relative amplitude between the modes, only the shape. In the following figures, the 10 first mode shapes are shown. The mode shapes are plotted in both xy-plane (seen from above) and xz-plane (seen from the side) in order to better visualise the relative motion of the bridge girders. The two girders are also plotted in two different colours to better distinguish their relative motion. In addition, the static configuration is shown with a dotted line.

As Figures 7.11 through 7.18 on the following pages shows, the first 8 modes are dominated by horizontal motions. These modes have eigenperiods ranging from 77.52 s down to 13.64 s. The first mode shape dominated by vertical motion is mode 9 with an eigenperiod of 11.89 s.

The first mode has an eigenperiod of 77.52 s for horizontal motion. In comparison, the straight bridge alternative described in “Straight Bridge - Navigation Channel in South” (2016b) has a eigenperiod of 78.25 s while the curved bridge described in *Curved Bridge - Navigation Channel in South* (2016a) has a period of 56.72 s

As seen in Figure 7.11a, the first mode shape consists of 3 half waves. In the straight bridge concept, the first mode consists of only one half wave. The curved concept has two half waves for the first mode shape.

All three concepts are dominated by horizontal mode shapes for the first 5 to 9 mode shapes. These mode shapes are important modes for response from wind, as the wind and eigenperiods are long. Analyses with wind loads are not performed on the model, but this should be included in further work. The modes dominated by wind are slowly varying with virtually no damping and can therefore cause large displacements.

The important modes for wind driven sea are those with a period close to the waves. As the peak period in Bjørnafjorden is $T_p = 6\,\mathrm{s}$, the most important modes will be in this range. Especially vertical modes will be of importance since these causes bending about the weak axis of the bridge. In Appendix D.2 two examples of mode shapes in this range is shown. Appendix D.1 contains a table with all eigenmode frequencies and periods. AppendixD.2 contains more mode shape plots.

Some mode shapes have a rotational motion of the global bridge girder. Some are also combinations of one or several types.

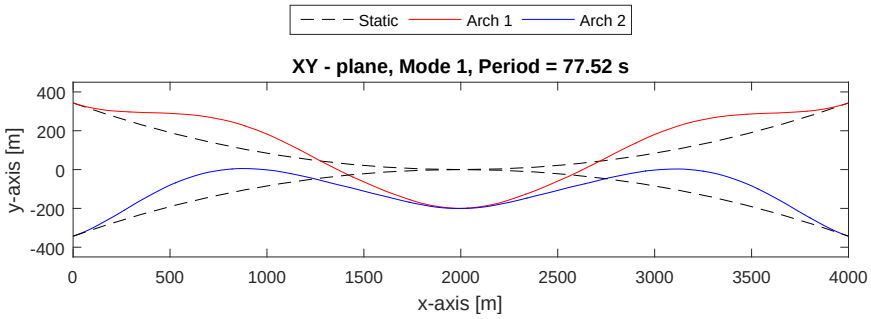

(a) Horizontal

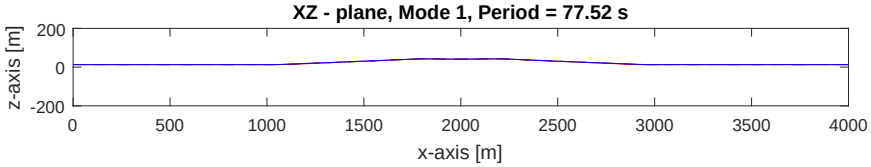

(b) Vertical

Figure 7.11: Mode 1 dominated by horizontal motions.

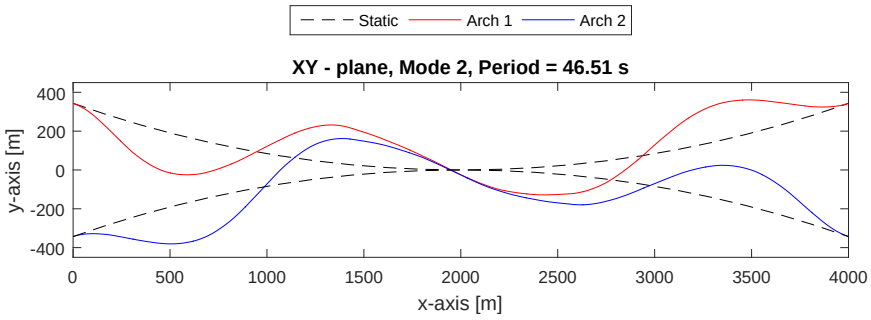

(a) Horizontal

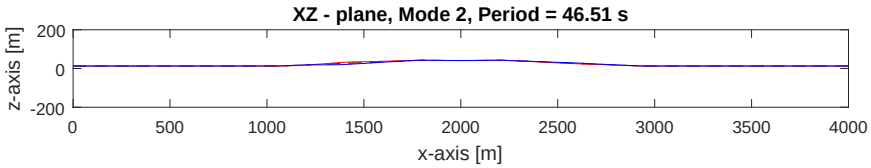

(b) Vertical

Figure 7.12: Mode 2 dominated by horizontal motions.

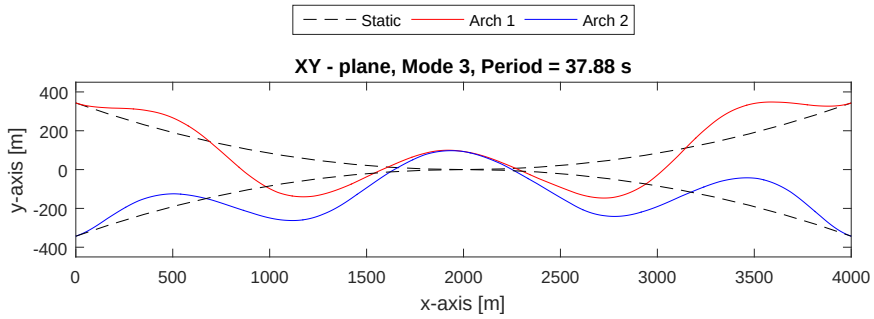

(a) Horizontal

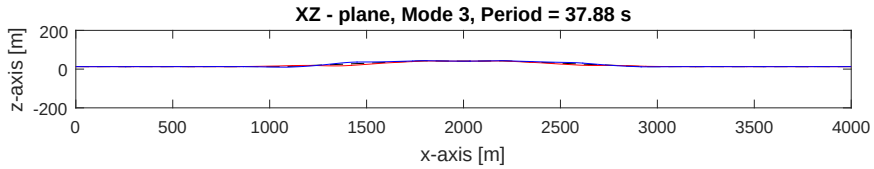

(b) Vertical

Figure 7.13: Mode 3 dominated by horizontal motions.

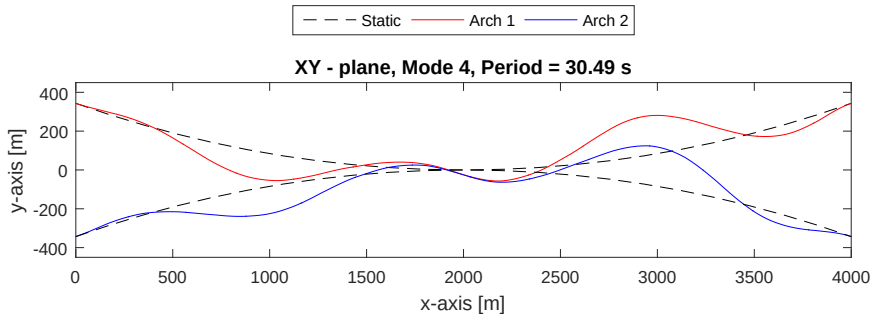

(a) Horizontal

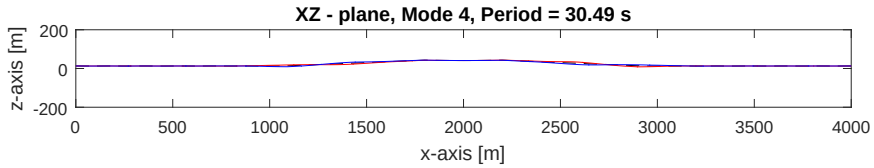

(b) Vertical

Figure 7.14: Mode 4 dominated by horizontal motions.

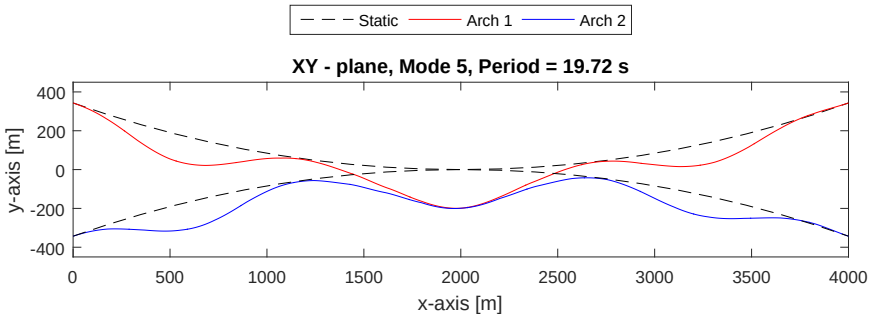

(a) Horizontal

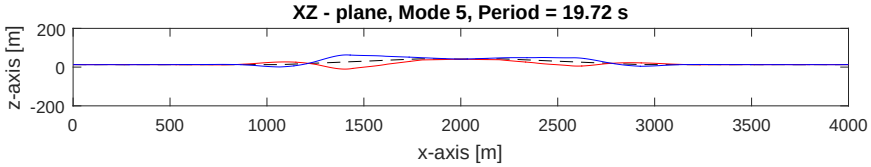

(b) Vertical

Figure 7.15: Mode 5 dominated by horizontal motions

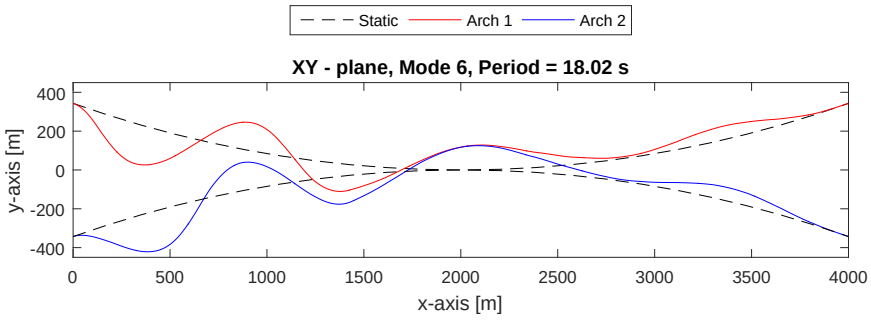

(a) Horizontal

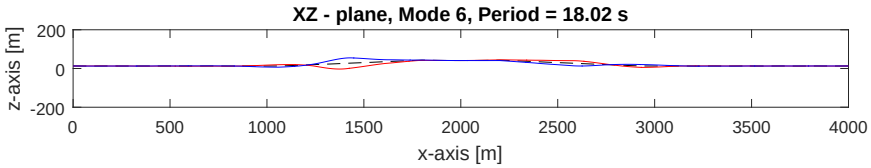

(b) Vertical

Figure 7.16: Mode 6 dominated by horizontal motions.

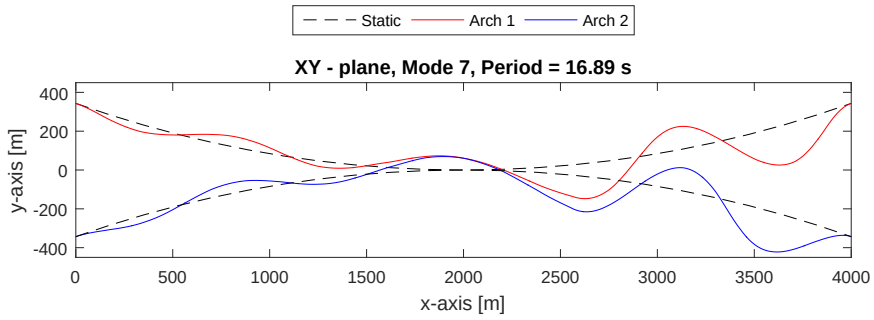

(a) Horizontal

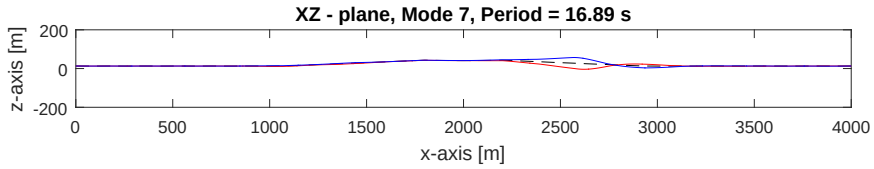

(b) Vertical

Figure 7.17: Mode 7 dominated by horizontal motions.

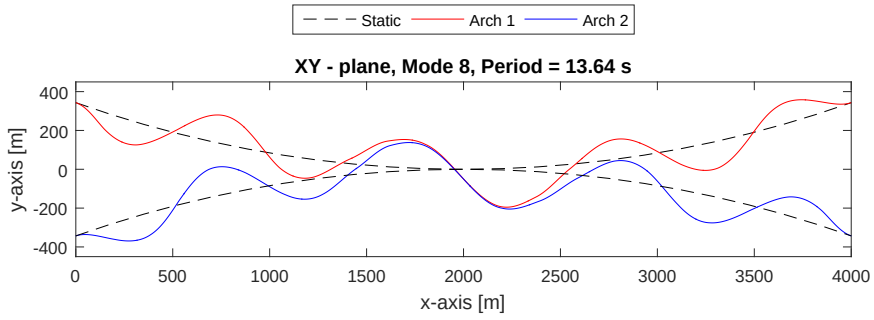

(a) Horizontal

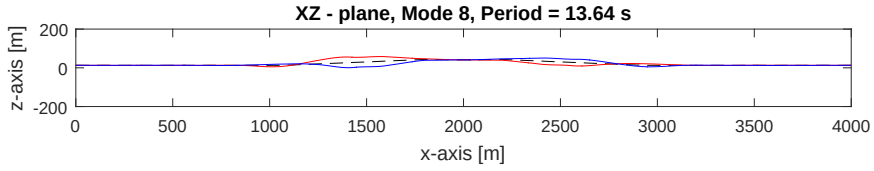

(b) Vertical

Figure 7.18: Mode 8 dominated by horizontal motions. Also some rotational motion.

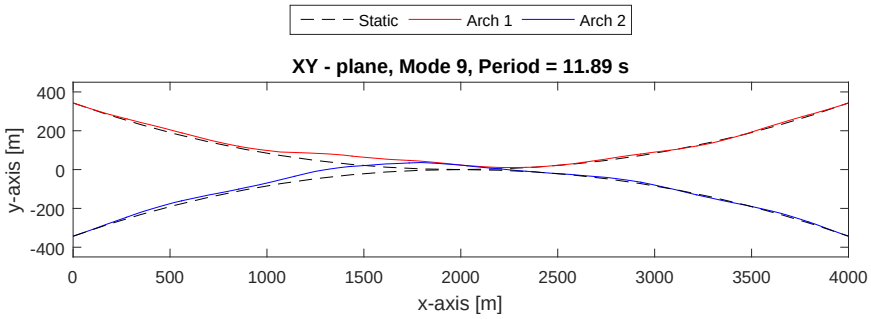

(a) Horizontal

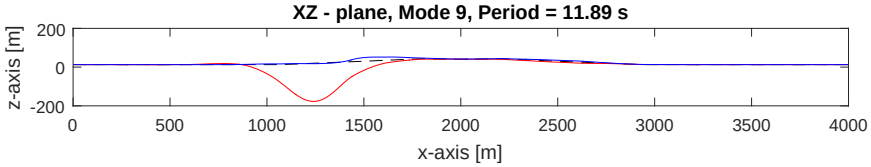

(b) Vertical

Figure 7.19: Mode 9 dominated by vertical motions.

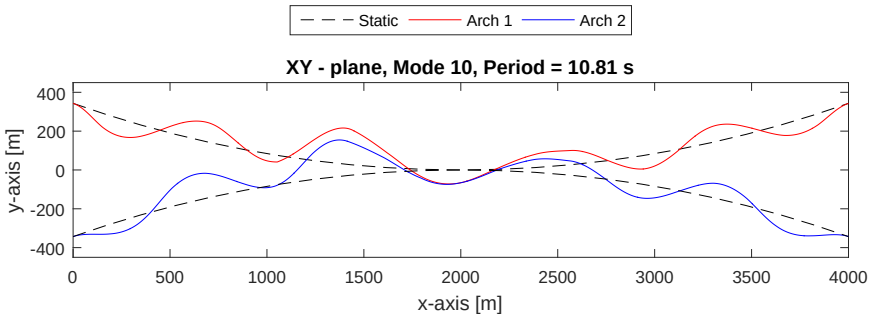

(a) Horizontal

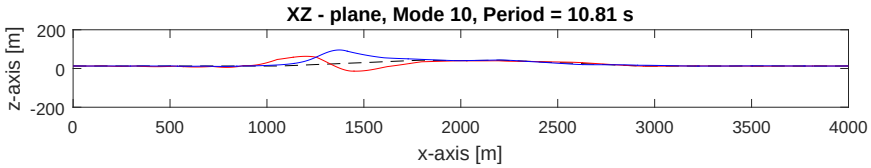

(b) Vertical

Figure 7.20: Mode 10 dominated by horizontal motions. Some global rotation.

7.5 Dynamic Response in Regular Waves

The following section contains results where the model is exposed to regular waves. All waves used are with wave height, H, from 1 m to 11 m and wave period from 2 s to 15 s. These values reflect the significant wave height and peak period for Bjørnafjorden, which is $H_s = 3$ m and $T_p = 6$ s.

As described in Section 7.5.1, the model behaves linearly for the investigated responses, meaning the results for one wave height can be used to calculate the response for another wave height.

Some results will show that there is a difference between the response in each bridge girder. But, in order to investigate various parameters, several of the results focus on only one bridge girder.

7.5.1 Linear or Nonlinear Response

As suggested in Section 5.2, the response is measured for a range of wave heights from 1 m to 11 m. To check if the response is linear, the bending moment at one of the bride girders are measured. Figures 7.21a and 7.21b shows the maximum, mean and minimum bending for two segments. As the figure shows, the bending moment follows the same pattern for both wave heights indicating that there is a linear relationship between the wave height and the response.

In Figures 7.22a and 7.22b the dynamic response, difference between maximum and minimum bending moment, are plotted against the wave height. Section 7.5.3 also contains a study of the linearity of the axial forces occurring in the cables.

7.5.2 Response in Regular Waves

Initially, the model is tested with an extreme regular wave with a height of 5 m and a period of 51 s. The wave period corresponds to a wave length approximately as long as the crossing of 4000 m. The extreme regular wave is intended to verify that the model behaves in the intended way.

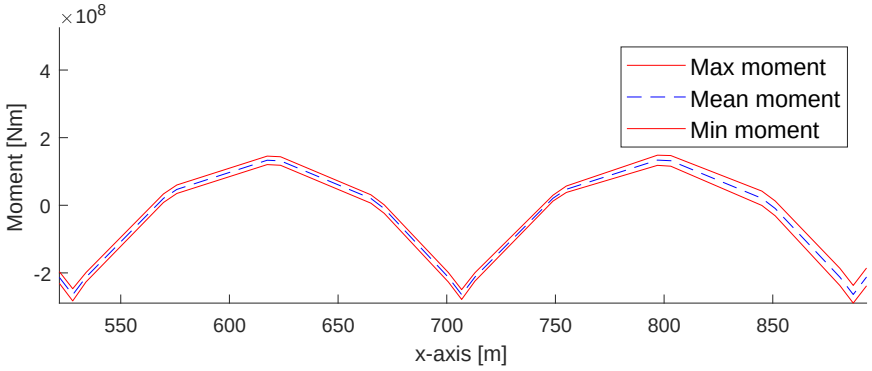

(a) $H = 1\,\mathrm{m}$ and $T = 6\,\mathrm{s}$.

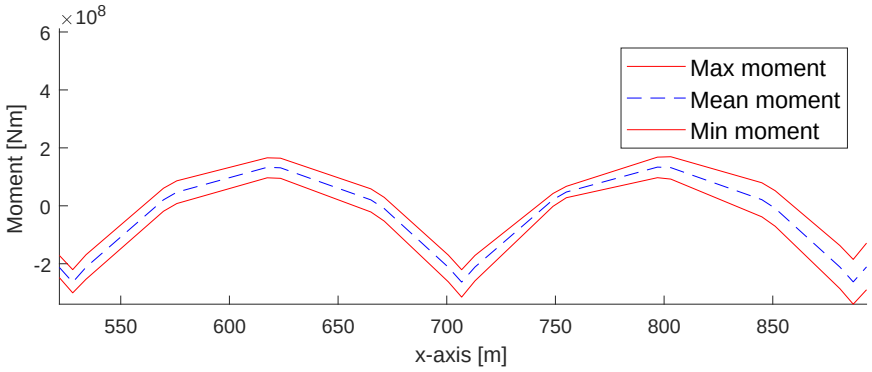

(b) $H = 3\,\mathrm{m}$ and $T = 6\,\mathrm{s}$.

Figure 7.21: Dynamic bending moment about the y-axis for the same section of the low bridge with different wave heights

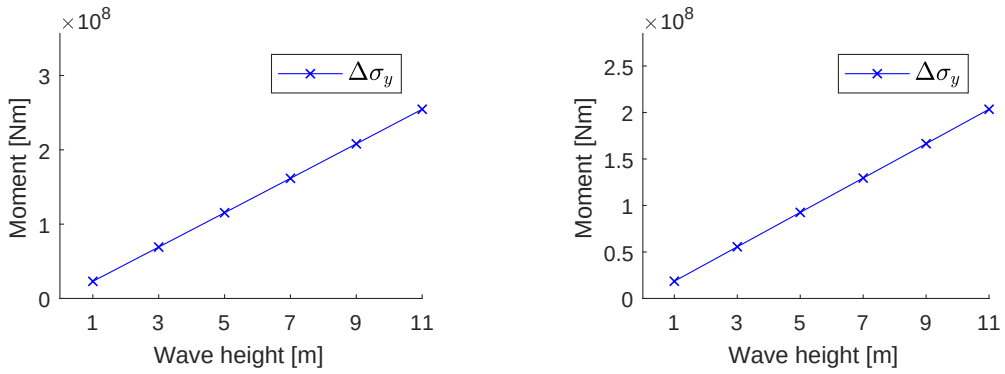

(a) Tower (b) Midspan

Figure 7.22: Difference between maximum and minimum moment, Dynamic moment, for a section at the low bridge.

Figure 7.23 shows a snapshot of the dynamic analysis with the extreme regular wave. The wave direction is along the bridge just for illustration purposes. Similar results are obtained with a wave perpendicular to the crossing. As the figure shows, the pontoons follow the wave elevation as expected for long wave periods.

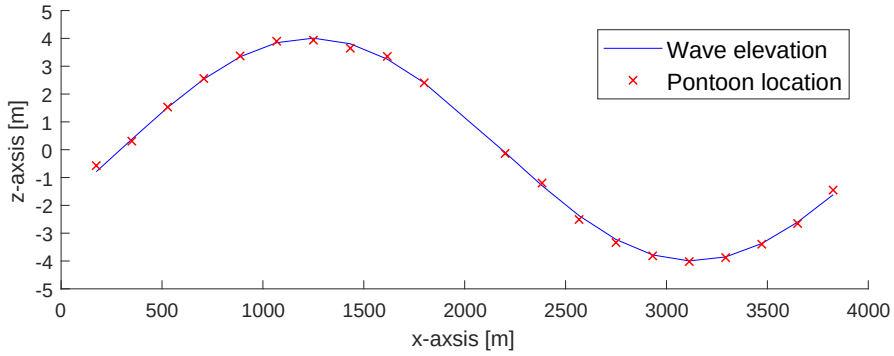

Figure 7.23: Pontoon motion in an extreme regular wave with a period of 51 s.

For regular wave analysis, the typical response pattern is shown in Figure 7.24. As the figure illustrates, the dynamic response is in a transient state initially. After some time, the response reaches steady state with the same period as the applied wave, which is 6 s for this case.

When analysing the response results, it is the regular part that is of interest. Responses are therefore taken as the average value from 200 s to 300 s. Most of the plots in this section are envelope plots. An envelope plot shows the maximum and minimum response of a value varying over time. Information about period, relative phase to wave and number of peaks all disappear in an envelope curve, only information about the extreme value is visualized.

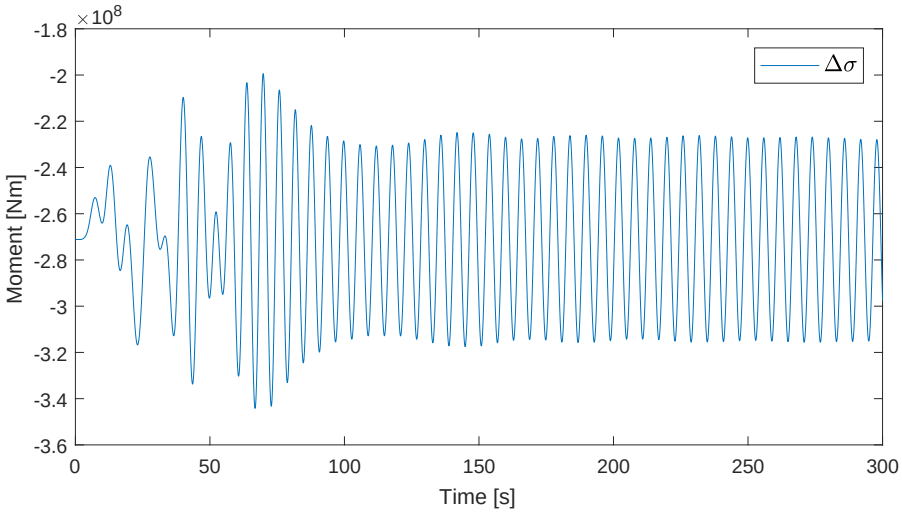

Figure 7.24: Typical response pattern for regular wave analysis shows how the result is in a transient state initially before reaching steady sate.

Response at Significant Wave Height and Peak Period

Results for a regular wave with $H = 3\,\text{m}$ and $T = 6\,\text{s}$, corresponding to the significant wave height, H_s, and peak period, T_p, for Bjørnafjorden, are shown in the following sections.

Motion of Pontoons

Figures 7.25a and 7.25b shows the extreme values for pontoon motion in the vertical direction. Notice that there is a difference in displacement between two corresponding pontoons at each arch.

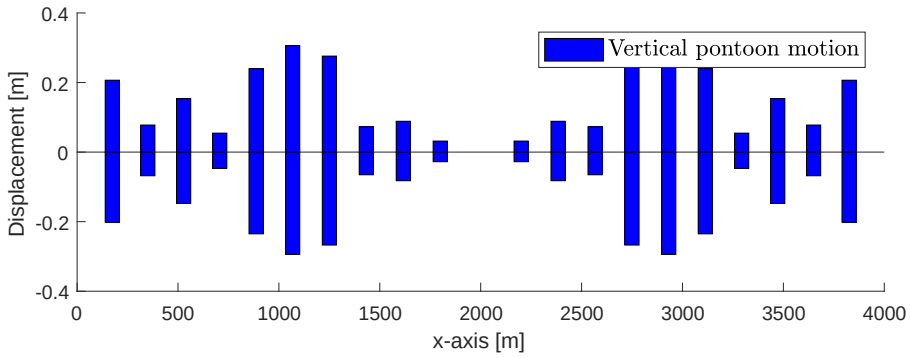

(a) Arch 1

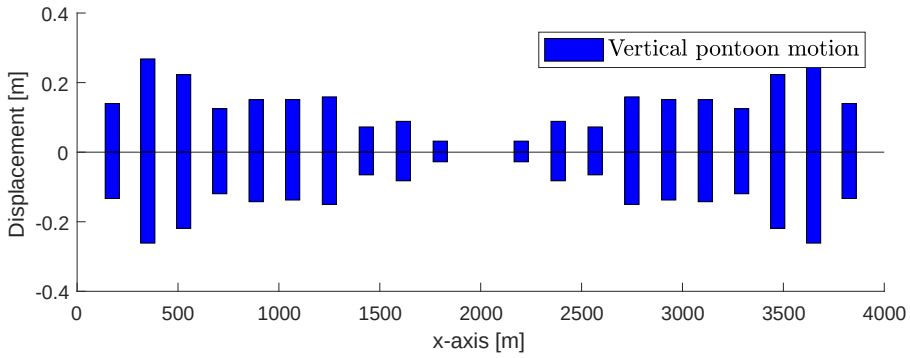

(b) Arch2

Figure 7.25: Vertical motion of pontoons for $H = 3\,\mathrm{m}$ and $T = 6\,\mathrm{s}$

To ensure that these results are correct, the time history of the second pontoon for both arches is plotted in Figure 7.26. The plot in this figure is from raw data from SIMA and has not been treated in any way contrary to the result in Figure 7.25. This shows that the data in Figure 7.25 is treated correctly.

The difference in displacement must therefore come from the model. As the pontoons are analysed in Wadam without including the effect of adjacent bodies, the wave experienced by each pontoon is exactly the same. This implies that forces with equal magnitude are acting on each pontoon, as the first order wave force transfer functions are the same for both pontoons.

All other parameters are also the same for the two pontoons corresponding to each other on each arch. The only difference between them is the direction of bridge girder curvature.

To investigate this phenomenon further, the analysis is run with opposite wave heading. The results show the same behaviour, with larger motions on one of the pontoons. For opposite direction, it is the pontoon at arch 1 that has the largest displacement of the two pontoons considered as opposed to results from the initial run shown in Figure 7.27. This shows that the two arches are equal and indicates that the wave direction affects the girder stiffness.

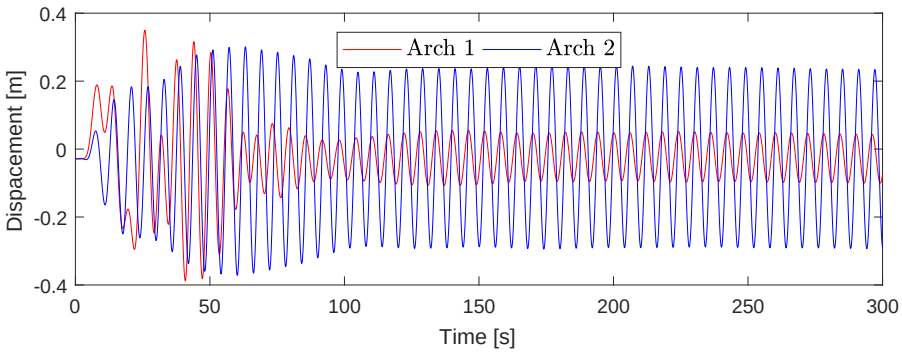

Figure 7.26: Verification of vertical pontoon motion shows how the displacement for the second pontoon (from land) is larger for the pontoon at arch 2.

Similar results are obtained for the horizontal pontoon motions along the y-axis. By comparing the horizontal motion in Figures 7.27a and 7.27b with the vertical

motions in Figures 7.25a and 7.25b, it is observed that the relative motions between the pontoons are the same for the vertical and the horizontal motions. The horizontal motions are larger than the vertical.

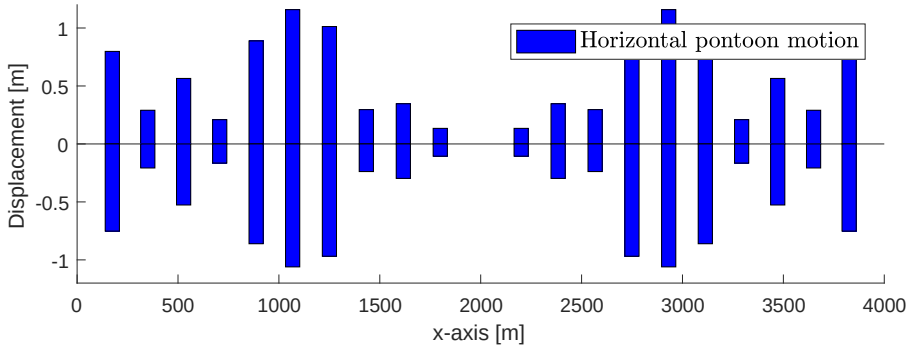

(a) Arch 1

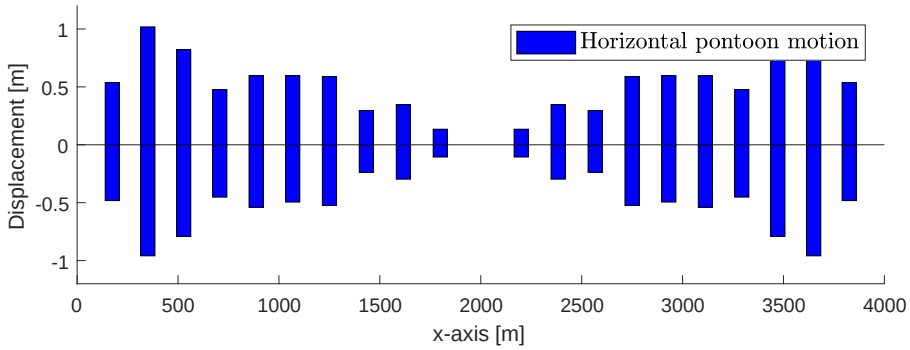

(b) Arch2

Figure 7.27: Horizontal motion of pontoons for $H = 3\,\text{m}$ and $T = 6\,\text{s}$

An explanation to why the displacements are different in each arch depending on wave direction could be found by looking at the axial force in the bride girders. Depending on the wave direction, the two girders will experience a difference in tension and compression. With waves propagating along positive global y-axis, arch number 2 curves away from the waves, and will therefore experience higher tension forces. Arch 1 has its curvature toward the incoming waves and will hence experience higher compression forces. This is illustrated in Figure 7.28.

The dynamic axial force is discussed later, but the result for arch 1 can be seen in

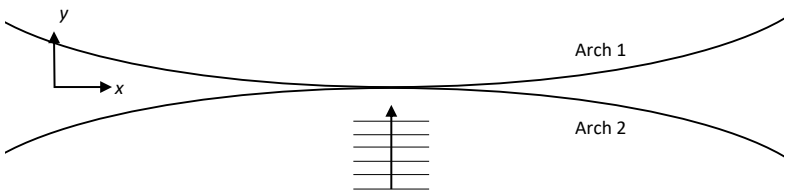

Figure 7.28: Wave direction gives larger tension forces in arch 2 and compresison in arch 1.

Figure 7.36. It is observed that the magnitude of the compressive force is larger than the tensile force is this arch. This changes the geometric stiffness of the girder. This agrees with the previous statement. Stating that the girder stiffness is dependent on wave direction.

Another explanation could be due to the pontoon pitch motion at each bridge girder being out of phase. This can lead to different forces acting at different times on each arch relative to the wave forces. Also, by studying the mode shapes with a period around 6 s, it is observed that for some of the modes, the amplitudes are of different magnitude.

Acceleration

Since the largest displacements are observed for horizontal motion of the sixth pontoon along arch number one, the acceleration for this pontoon is calculated.

Acceleration for the sixth pontoon along arch one is calculated by Equation (3.33) in Section 3.5.1. The acceleration is shown in Figure 7.29. As seen, the highest observed acceleration in regular waves with $H = 3\,\mathrm{m}$ and $T = 6\,\mathrm{s}$ is $0.2\,\mathrm{m/s^2}$.

In the reports *Curved Bridge - Navigation Channel in South* (2016a) and "Straight Bridge - Navigation Channel in South" (2016b) by Aas-Jakobsen et al. the horizontal acceleration is limited to $0.5\,\mathrm{m/s^2}$ and $0.3\,\mathrm{m/s^2}$ respectively. These values are for a one-year storm, but serves to give a quantitative value on acceptable accelerations.

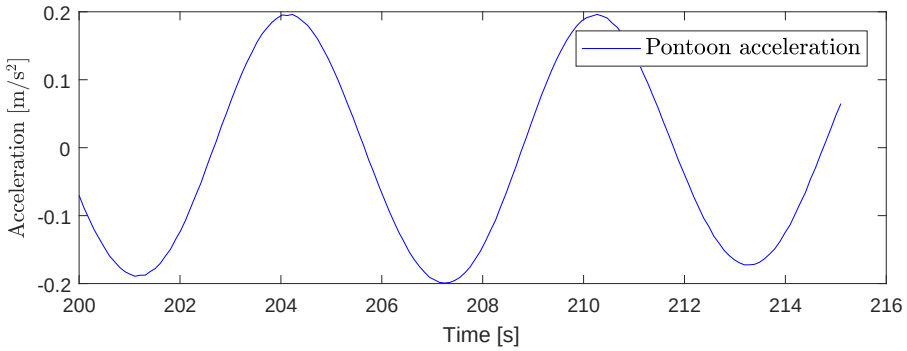

Figure 7.29: Horizontal pontoon acceleration for the sixth pontoon from land with $H = 3\,\text{m}$ and $T = 6\,\text{s}$.

Dynamic Bending Moment in Bridge Girder

Figures 7.21a and 7.21b shows that the difference between the static moment and dynamic moment is relatively small. For readability, the plots in Figures 7.30 and 7.31 shows the difference in maximum and minimum bending moment about y-axis. This value is either added or subtracted to the static bending moment shown in Figure 7.2.

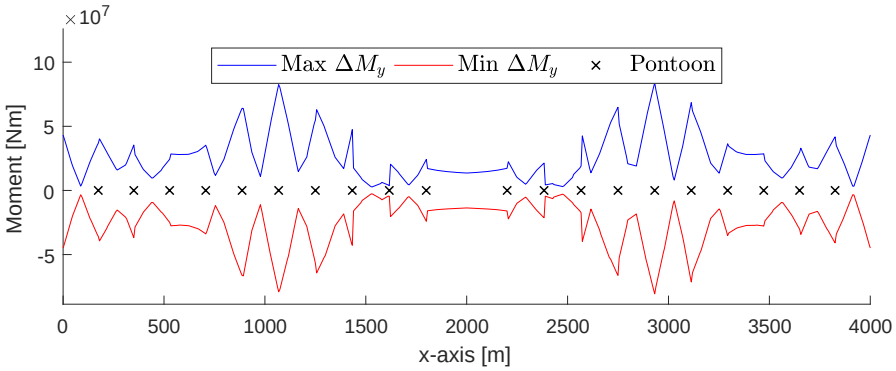

Figure 7.30: Dynamic bending moment about the y-axis for regular waves with $H = 3\,\text{m}$ and $T = 6\,\text{s}$ for arch 1.

As discussed for the pontoon motion, and seen in Figure 7.25, there is a difference in response between the two arches. The same is, as expected, observed in the

bending moment as this is dependent on the deformation of the beams.

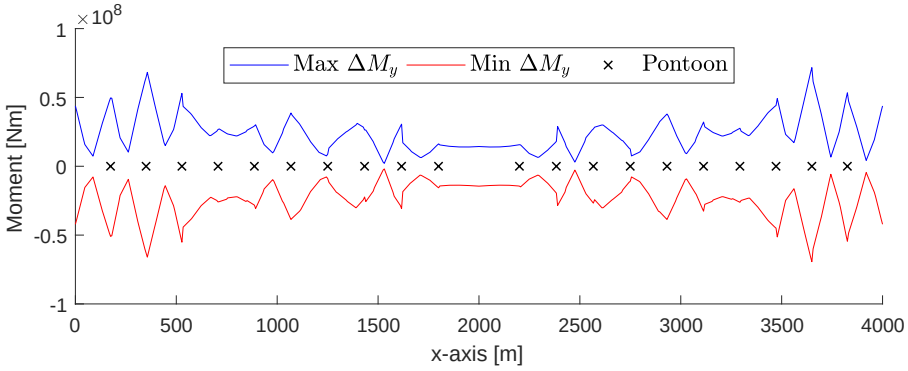

Figure 7.31: Dynamic bending moment about the y-axis for regular waves with $H = 3\,\text{m}$ and $T = 6\,\text{s}$ for arch 2.

It can also be observed that for arch 1, the largest dynamic moment is found around 1000 m, halfway between land and the navigation channel. For arch 2, the largest dynamic moment is around 350 m. Looking back at the pontoon displacement for each of the corresponding arches in Section 7.5.2, the largest moments coincide with the pontoons with the largest relative displacement in vertical direction.

This shows that the dynamic bending moment about the y-axis is dependent on the vertical motion of the pontoons.

In Figures 7.32 and 7.33the dynamic bending moment about the z-axis is shown. Since the static bending moment in that direction is close to zero, the figure also illustrates the total dynamic bending moment. The dynamic bending moment is in the same order of magnitude as about the y-axis. With the second moment of area, found in Table 7.2, and the y value for the points of interest (Figure 5.8) ranging from 7.5 m to 11 m, the bending stress calculated according to Equation (3.23) is in the same order of magnitude as the dynamic stress due to dynamic bending about the y-axis.

It is worth noticing that the maximum dynamic bending moment about the z-axis is in the same area as for the dynamic bending moment about the y-axis. The largest value is found at the sixth pontoon from land, around 1100 m from land. Looking back at the static equivalent stress due to bending and shear forces, Figure

7.10, the peaks are located at the pontoons. The total dynamic stress should therefore be further investigated for the peak values located around the mentioned pontoon.

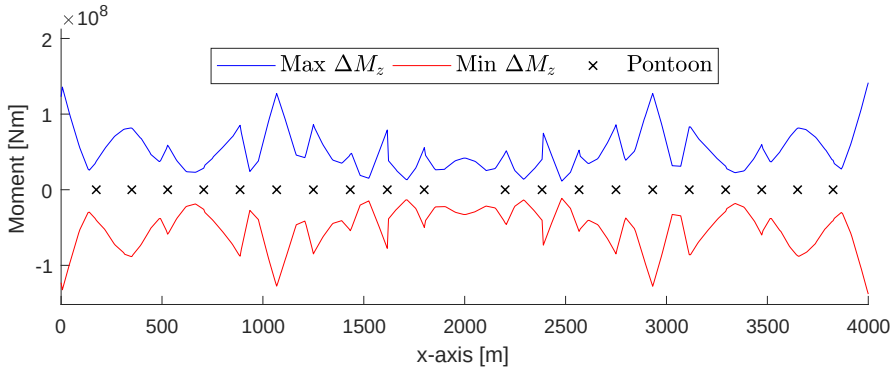

Figure 7.32: Dynamic bending moment about z-axis for the bridge girder in arch 1. Equals also total bending moment about the z-axis as the static bending moment is close to zero.

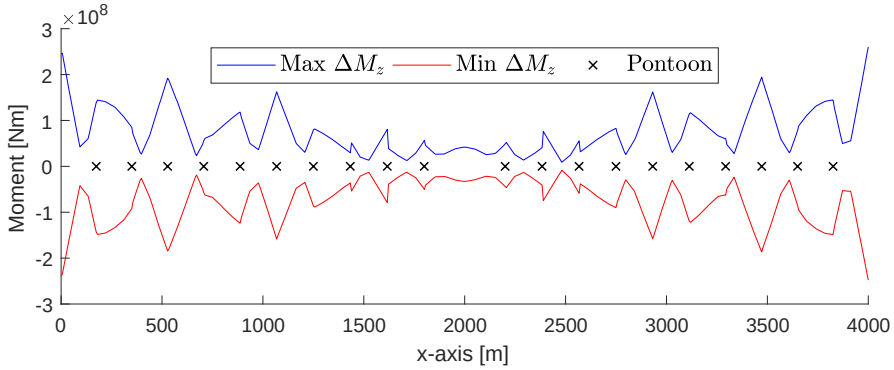

Figure 7.33: Dynamic bending moment about z-axis for the bridge girder in arch 2. Equals also total bending moment about the z-axis as the static bending moment is close to zero.

Dynamic Shear Force in Bridge Girder

Dynamic shear force for regular waves with $H = 3\,\text{m}$ and $T = 6\,\text{s}$ are shown in Figures 7.34a and 7.34b for horizontal and vertical shear force respectively. The

figures show the difference in shear force compared to the mean shear stress. As mentioned, the static shear force in horizontal direction is close to zero, Figure 7.34a is therefore also representative for the total horizontal shear force in the bridge girder. The value in Figure 7.34b has to be added or subtracted to the static shear force in order to find the total shear force with dynamic loading.

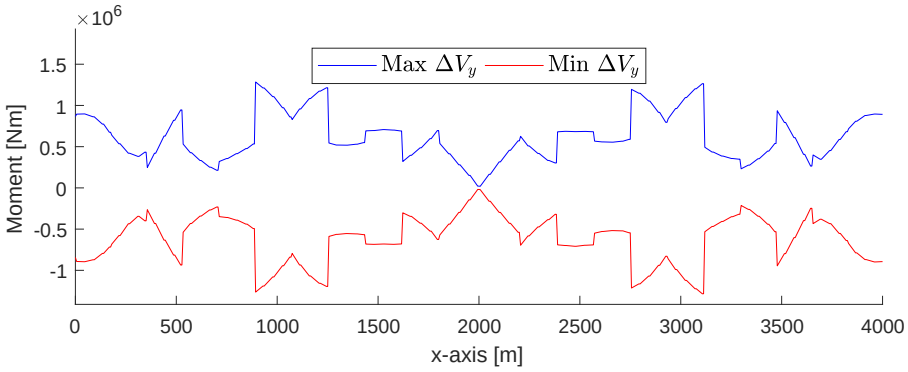

(a) Shear force in horizontal direction.

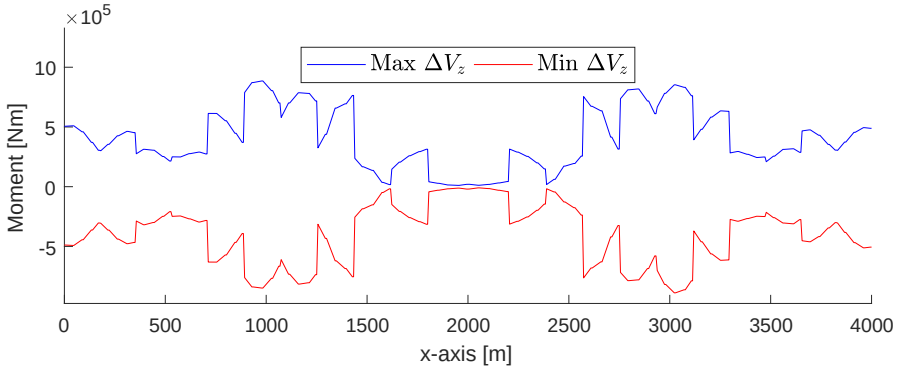

(b) Shear force in vertical direction.

Figure 7.34: Dynamic shear force at $H = 3\,\text{m}$ and $T = 6\,\text{s}$ for arch 1

As both Figures 7.34a and 7.34b show, the largest dynamic shear stresses occur around 1100 m from land. This coincide with the location where the largest displacement and dynamic bending moment is observed. Which is reasonable, since the shear force is dependent on the change in bending moment.

Dynamic Torsional Moment in Bridge Girder

The dynamic torsional moment in the bridge girder for arch 1 is shown in Figure 7.35 for a regular wave with $H = 3\,\text{m}$ and $T = 6\,\text{s}$. The dynamic torsional moment is much larger than the static torsional moment in Figure 7.3, and it is therefore close to the total.

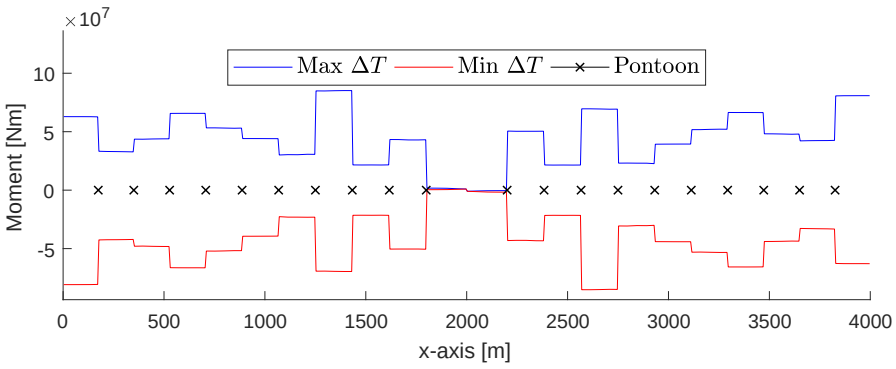

Figure 7.35: Dynamic torsional moment in bridge girder for regular waves with $H = 3\,\text{m}$ and $T = 6\,\text{s}$ for arch 1.

Dynamic Axial Force in Bridge Girder

The dynamic axial force in the bridge girder for arch 1 is shown in Figure 7.36 for a regular wave with $H = 3\,\text{m}$ and $T = 6\,\text{s}$. Both the static and dynamic axial forces are relatively small, but only the largest, the dynamic, is considered in the equivalent stress calculation.

Dynamic von Mises Stress in Bridge Girder

Dynamic equivalent stress is calculated for point 3 and 4 (maximum stress will alternate between the two points) shown in Figure 5.8, corresponding to the corner between the vertical wall and the bottom plate. At this point, the girder is in tension due to bending moment about the y-axis. This point is also in tension due to dynamic bending moment about the z-axis. According to the results in

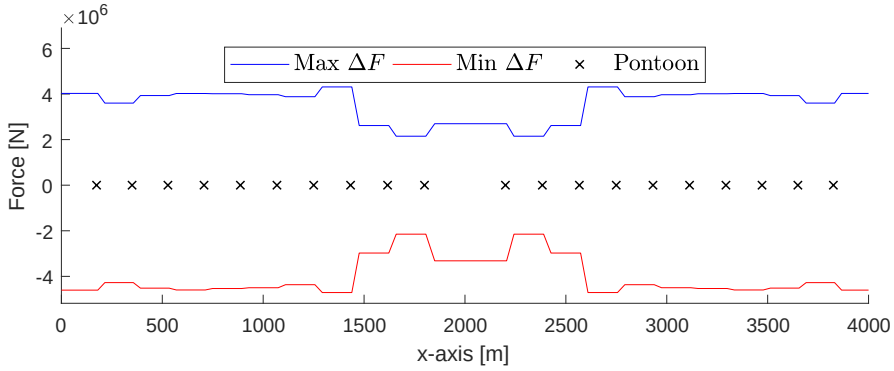

Figure 7.36: Dynamic axial force in bridge girder for regular waves with $H = 3\,\mathrm{m}$ and $T = 6\,\mathrm{s}$ for arch 1.

previous section for the dynamic axial force, this point also experience stresses due to tension in the bridge girder. All these components contribute to the total axial stress, σ_x according to Navier's Formula as seen in Equation (3.23). The axial force and bending moment about the z-axis fluctuates around zero, meaning they vary on contributing or reducing the total stress at the point of interest. Since the envelope curves do not contain any information about when the peaks occur, it is assumed a worst-case scenario where all three are in phase contributing to the total tension at the same time.

The same assumption is used when calculating the shear stress. Maximum torsional moment and vertical shear force is assumed to be in phase with the mentioned forces. Horizontal shear force is ignored since the shear stress caused by it is insignificant.

Figure 7.37 shows the result for the dynamic equivalent stress along the bridge girder. Looking back at the static equivalent stresses, it is noticed that the difference is relatively small. At some of the towers, the dynamic equivalent stress exceed 500 MPa, which is beyond the allowed stress according to von Mises yield criterion.

When comparing the static and dynamic results, it becomes clear how large the static bending moment about the y-axis and vertical shear stress is. It is also worth mentioning that the dynamic equivalent stress is for waves with an amplitude of

3 m. When $H_s = 3$ m, waves will exceed this height and the dynamic response and corresponding equivalent stress will increase. The cross section used has to be modified in future models to avoid these high stresses.

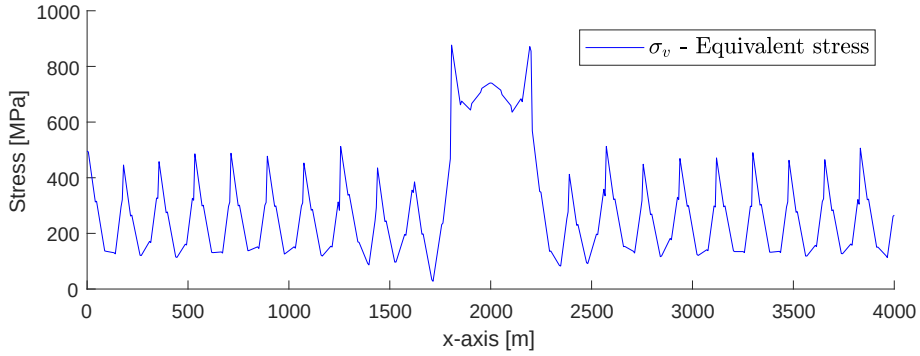

Figure 7.37: Dynamic equivalent stress in bridge girder

7.5.3 Dynamic Axial Force in Cables

As mentioned in Section 7.3.4, it is the dynamic part of the cable tension/compression that is of interest. Figure 7.38 shows the dynamic axial force response in the cables. The largest response is for cable number 3. This cable is connected to the pontoon with the largest horizontal motion as seen in Section 7.5.2.

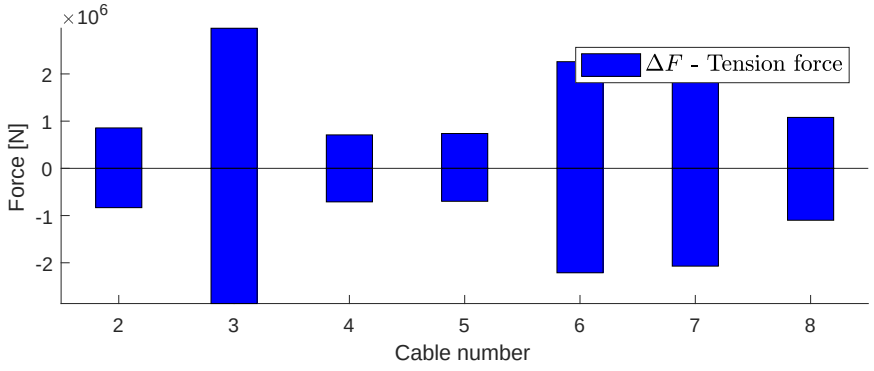

Figure 7.38: Dynamic axial force in cables for $H = 3$ m and $T = 6$ s.

To avoid snapping of the cable, the cable is supposed to be pre-tensioned. This pre-tension has to account for the compressive forces observed in these analyses. Meaning that the pretension has to correspond to at least a force of 2.97 MN (maximum observed value) in order to avoid any compression which will lead to sagging of the cables. This sagging could in turn lead to snapping of the cable if the distance between the bridge girders suddenly change.

With a pretension of 3 MPa, the total axial force would reach 6 MPa. The calculated cross section area of the cable is $A = 83.684\,\text{cm}$. This corresponds to a maximum stress, calculated according to Equation (3.17) in Section 3.2.1, of approximately 700 MPa. According to Gimsing and Georgakis (2012), the yield strength of a conventional cable of steel is in the order of magnitude of 1200 MPa. The observed tensional stress is therefore within the acceptable limits.

Linearity in Axial Forces

For regular waves with $T = 6\,\text{s}$ the wave height, H, is varied from 1 m to 11 m. The dynamic response in each cable has been plotted against the wave height in Figure 7.39. As seen in the figure, dynamic axial force in each cable vary linearly with increasing wave height. The dynamic results for a wave height can then be scaled to find the dynamic response for a wave with the same period but different wave height.

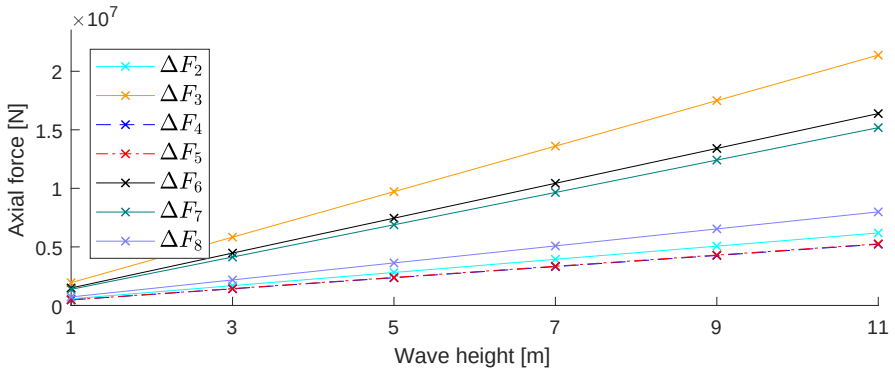

Figure 7.39: Difference in dynamic force in each cable for waves ranging from 1 m to 11 m with $T = 6$ s. Notice that the relative force plot for cable 3 and 4 are plotted on top of each other and that the cable numbering starts at 2. This is due to its connection to supernode number 2 in the model, where supernode 1 is the starting point on land.

Chapter 8

Conclusion and Further Work

As becomes clear in this report, design of a floating bridge includes an endless amount of aspects. This report covers just a fraction of all the considerations that has to be done for a floating bridge.

As the results showed, the model behaves linearly for the investigated quantities. This is a useful result, as it makes it possible to say something about the response for several wave heights with the same wave period.

The static analysis shows that the static bending moment about the y-axis and static shear stress in the vertical direction dominates the forces in the bridge girder. Both components have their maximum values at the tower connections, causing the equivalent stress to be large at these points.

The main reason for the high equivalent stresses is the thin wall thickness of the bridge girder. This causes large shear forces at the same locations as where the maximum stresses due to bending occur. The wall thickness should therefore be increased in order to reduce the shear stress and hence reduce the equivalent stresses.

The dynamic addition in response for regular waves are relatively small compared to the static values. A good starting point for new designs might therefore be to reduce the static stresses either by changing the main dimensions like span length, or by changing the cross section of the bridge girder.

The eigenvalue analysis showed that the bridge has several horizontal mode shapes in the range of wind loads with long periods. The bridge also has vertical mode shapes in the range of wind driven sea.

It is unclear from the results whether the cables have any contribution to reducing the axial compressive forces in the bridge girder. An idea could be to perform an analysis of a similar model without cables in order to investigate if there is reduction in forces.

8.1 Recommendations for Further Work

The linearity has only been investigated for some parameters with wave heading perpendicular on the model. For an analysis with different headings, it should be performed more test to verify the linearity.

The pontoons have only been investigated briefly in this report. As indicated in the report, there are many variables to decide for the pontoons, and a larger study should be conducted in order to optimize the design and dimensions. The possibility of using other materials as steel could also be investigated.

As the X-Bridge concept differs from other floating bride concepts, there are many aspects that should be given special attention in a further investigation. Especially the cable system and how these actually perform would be of interest in a further study. This should eventually be combined with the spring solution at the bridge end in order to see if this solution is an effective way of reducing the compression forces in the bridge girders.

Rotations and motions of the bridge girder should also be addressed further in order to make sure the road is safe to drive on.

In hindsight, it would have been a good idea to minimize complexity of the model in order to make it easier to identity the unique properties of the X-Bridge. As an example, the navigation channel can be omitted in a new model, as this disturbs the results.

When performing the dynamic analysis, the phase between the loads should be

considered in order to avoid too conservative results. Dynamic analysis should also include changes in the wave heading and periods.

By reducing the complexity of the model, or having axes to a more powerful computer, would make irregular dynamic analysis possible. This is important to perform on new concepts in order to investigate the response spectrum.

Another problem that has not been addressed in the report is the environmental footprint of the bridge. With end connections separated by a distance of 500 m, the impact on land will become much larger than for the more traditionally concepts.

Bibliography

Aas-Jakobsen. (n.d.). Nordhordland bridge - reference portifolio. Online. Retrieved November 7, 2016, from http://www.aaj.no/bruer/pdf/Nordhordland_flyt_eng.pdf

Aas-Jakobsen, COWI, Johs Holt, & Global Maritime. (2016a, February 15). *Curved Bridge - Navigation Channel in South*.

Aas-Jakobsen, COWI, Johs Holt, & Global Maritime. (2016b, February 19). Straight Bridge - Navigation Channel in South. Tech. rep. Retrieved December 9, 2016, from http://www.vegvesen.no/_attachment/1605065/binary/1145263?fast_title=Bj%C3%B8rnafjorden+Sideforankret+flytebru+-+oppsumering+av+analyser.pdf

Amdahl, J. (2005, January 19). *TMR4205 Buckling and Ultimate Strength of Marine Structures*.

Bauchau, O. A. & Craig, J. I. (2009, August 3). *Structural analysis*. Springer Netherlands. Retrieved from http://www.ebook.de/de/product/19293637/olivier_a_bauchau_james_i_craig_structural_analysis.html

Bostic, S. W. (1991). Lanczos eigensolution method for high-performance computers.

Damkilde, L. (2000, November). Stress and stiffness analysis of beam-sections. Department of Structural Engineering and Materials, Technical University of Denmark. Retrieved May 2, 2017, from http://homes.civil.aau.dk/lda/Notes/CROSS.pdf

DNV. (2010a, October). Recommended Practice, DNV-RP-F205: Global performance analysis of deepwater floating structures. Retrieved December 13, 2016, from https://rules.dnvgl.com/docs/pdf/DNV/codes/docs/2010-10/RP-F205.pdf

DNV. (2010b, January 2). Sesam User Manual - Wadam: Wave Analysis by Diffraction and Morison Theory. Retrieved December 13, 2016, from https://projects.dnvgl.com/sesam/manuals/Wadam_UM.pdf

DNV. (2013, June). *DNV-RP-C208: Environmental conditions and environmental loads*. Retrieved November 21, 2016, from http://rules.dnvgl.com/docs/pdf/DNV/codes/docs/2014-04/RP-C205.pdf

Ellevset, O. (2012). Project overview - Coastal highway route E39. The Norwegian Public Roads Administration.

Faltinsen, O. M. (1993, September 23). *Sea loads on ships and offshore structures*. Cambridge University Press.

Gillesvik, K. (2017, March 10). Tror ikke på fergefri e39 på 20 år [do not believe in ferry free e39 within 20 years]. Retrieved from http://www.bt.no/nyheter/innenriks/Tror-ikke-pa-fergefri-E39-pa-20-ar-331611b.html

Gimsing, N. J. & Georgakis, C. T. (2012, January 6). *Cable supported bridges: Concept and design*. JOHN WILEY & SONS INC. Retrieved from http://www.ebook.de/de/product/16212810/niels_j_gimsing_christos_t_georgakis_cable_supported_bridges_concept_and_design.html

Gutierrez, S. (2012, February 29). Washington: Floating bridge capitol of the world. Retrieved December 1, 2016, from http://www.seattlepi.com/local/transportation/article/Floating-bridges-of-the-world-2971885.php

Haque, A. (2016, October 26). *Introduction to Timoshenko Beam Theory*. Retrieved April 2, 2017, from http://www.clearlyimpossible.com/ahaque/timoshenko.pdf

Ibrahim, R. A. & Grace, I. M. (2010). Modeling of ship roll dynamics and its coupling with heave and pitch. *Mathematical Problems in Engineering*, *2010*, 1–32. doi:10.1155/2010/934714

Irgens, F. (1999a). *Fasthetslære [Mechanics of Materials]*. Retrieved June 3, 2017, from http://www.nb.no/nbsok/nb/90594336fd9b02d0f4aff326e58b91a5.nbdigital?lang=no#0

Irgens, F. (1999b). *Formelsamling [Handbook of Mechanical Formulas]* (3rd ed.). Tapir Akademiske Forlag.

Langen, I. (1981). *On dynamic analysis of floating bridges*. Division of Structural Mechanics, The Norwegian Institute of Technology, The University of Trondheim, Norway.

Langen, I. & Sigbjørnsson, R. (1979). *Dynamisk analyse av konstruksjoner [Dynamic analysis of structures]*. Tapir.

Larssen, R. M., Larsen, P. N., Strømsem, K., & Sørby, B. (2016, May 16). *Design basis*. Retrieved February 22, 2017, from http://www.vegvesen.no/_attachment/1605052/binary/1145248?fast_title=Bj%C3%B8rnafjorden+Flytebru+Design+Basis.pdf

Leira, B. J. (2014, January). *Marine structures, basic course*. Kompendieforlaget.

Lindblom, M. (2016, January 13). New 520 bridge to open in April; walkers, bicyclists get to try it first. *The Seattle Times*. Retrieved November 8, 2016, from http://www.seattletimes.com/seattle-news/transportation/new-520-bridge-to-open-in-april-walkers-bikes-will-get-to-try-it-first/

Lwin, M. M. (1999). Floating bridges. In *Bridge engineering handbook*. Informa UK Limited. doi:10.1201/9781420049596.ch22

MARINTEK. (2016, April 21). *RIFLEX 4.8.1 Theory Manual*.

MARINTEK. (2016, April 21). *RIFLEX 4.8.1 User Guide*.

Marit Irene Kvittem. (2014). *Modelling and response analysis for fatigue design of a semi-submersible wind turbine* (Doctoral dissertation, Norwegian University of Science, Technology, Faculty of Engineering Science, and Technology, Department of Marine Technology).

Narayanan, R., Kalyanaraman, V., Santhakumar, A., S.Seetharaman, Kumar, S. S., Jayachandran, S. A., & Senthil, R. (2011). Beams subjected to torsion and bending -i. Institute for Steel Development & Growth. Retrieved June 2, 2017, from http://www.steel-insdag.org/TeachingMaterial/Chapter17.pdf

Nedrebø, Ø. (2016, September 20). Floating bridge E39 Bjørnafjorden. Presentation. Retrieved October 13, 2016, from http://www.vegvesen.no/_attachment/1545428/binary/1135143?fast_title=14+Flytebru.pdf

Newman, J. (2005, March). Efficient hydrodynamic analysis of very large floating structures. *Marine Structures*, *18*(2), 169–180. doi:10.1016/j.marstruc.2005.07.003

Norsk Standard. (2003). Eurocode 1: Actions on structures - part 2: Traffic loads on bridges: Ns-en 1991-2:2003+na:2010.

Norwegian Ministry of Transport and Communications. (2013). National transport plan 2014–2023 english version. Research rep.

Norwegian Public Roads Administration. (1994). The Nordhordland Bridge. Retrieved November 7, 2016, from https://web.archive.org/web/20060209233657/http://www.vegvesen.no/region_vest/prosjekter/nordhordlandsbrua/brosjyre_1994.pdf

Norwegian Public Roads Administration. (2012). Stor bransjeinteresse for Ferjefri E39 [Great interest in Ferry free E39 in the industry]. Retrieved April 11, 2017, from http://www.vegvesen.no/vegprosjekter/ferjefriE39/Nyhetsarkiv/stor-bransjeinteresse-for-ferjefri-e39

Norwegian Public Roads Administration. (2015a). *Bruprosjektering - Prosjektering av bruer, ferjekaier og andre bærende konstruksjoner [Bridge Design - Design of Bridges, ferry quays, and other load-bearing constructions]: Håndbok N400 [Manual N400].* Retrieved November 19, 2016, from http://www.vegvesen.no/_attachment/865860/binary/1030718?fast_title=H%C3%A5ndbok+N400+Bruprosjektering.pdf

Norwegian Public Roads Administration. (2015b). *Na-rundskriv 2015/2 - fartsgrenser og motorveger - ny dimensjoneringsklasse for motorveg med fartsgrense 110 km/t [speed limits and motorway - new dimensioning class for motorway with speed limit 110 km/h].* Retrieved April 21, 2017, from http://www.vegvesen.no/_attachment/766252/binary/1010085?fast_title=NA - rundskriv + 2015 % 2F2+ - +Fartsgrenser + og + motorveger+ - +Ny + dimensjoneringsklasse+for+motorveg+med+fartsgrense+110+km%2Ft.pdf

Norwegian Public Roads Administration. (2015c, May). Statusrapport Ferjefri E39 [project status report Ferry-free coastal route E39]. Tech. rep.

Norwegian Public Roads Administration. (2016, September 6). Subproject: Fiord Crossings – technology development for extreme fiord crossings. Retrieved February 9, 2017, from http://www.vegvesen.no/vegprosjekter/ferjefriE39/English/subprojects/Fjordcrossings

Øderud, H. T. & Nordahl, R. S. (2006, December 30). Bro [Bridge]. Retrieved April 27, 2017, from https://snl.no/bro

Pettersen, B. (2014). *Tmr4247, marin teknikk 3, hydrodynamic.*

Rydland, S. & Sado, F. (2016, March 23). - Kostnadssprekk på veiene et stort demokratisk problem [- Budget deficit on roads are a big democratic issue]. Retrieved May 11, 2017, from https://www.nrk.no/hordaland/_-kostnadssprekk-pa-veiene-et-stort-demokratisk-problem-1.12868584

Vugts, J. (1968, January). *The hydrodynamic coefficients for swaying, heaving and rolling cylinders in a free surface*. Report // Nederlands Scheepsstudiecentrum TNO. Delft : Netherlands Ship Research Centre TNO, Shipbuilding Department. Retrieved from https://books.google.no/books?id=--A%5C_HAAACAAJ

Wang, C. & Tay, Z. (2011). Very Large Floating Structures: Applications, Research and Development. *Procedia Engineering*, *14*, 62–72. doi:10.1016/j.proeng.2011.07.007

Washington State Department of Transportation. (n.d.-a). SR 520 - Floating Bridge and Landings Project: Construction Overview. Retrieved November 8, 2016, from http://www.wsdot.wa.gov/Projects/SR520Bridge/BridgeAndLandings/StepByStep.htm

Washington State Department of Transportation. (n.d.-b). Sr 520 - floating bridge facts. Retrieved November 8, 2016, from http://www.wsdot.wa.gov/Projects/SR520Bridge/About/BridgeFacts.htm

Watanabe, E. & Utsunomiya, T. (2003). Analysis and design of floating bridges. *Progress in Structural Engineering and Materials*, *5*(3), 127–144. doi:10.1002/pse.151

Wilson, E. L. (1999). *Three dimensional static and dynamic analysis of structures: A physical approach with emphasis on earthquake engineering*. Computers and Structures. Retrieved April 8, 2017, from ftp://ceres.udc.es/Doctorado/Estructuras2/analisis_no_lineal/Wilsonbook.pdf

Witoś, M. & Stefaniuk, M. (2011). Compressor blade fatigue diagnostics and modelling with the use of modal analysis. *Fatigue of Aircraft Structures*, *2011*(3). doi:10.2478/v10164-010-0044-4

Appendix A

Regular Wave Analysis in SIMO

In the current version of SIMO (version number of the different modules are summarised in Table A.1) the dynamic calculation for regular waves does not work.

Table A.1: Program versions

Program	Version
MARINTEK COUPLED RIFLEX - SIMO	2.0.1
MARINTEK SIMO	4.0.0
RIFLEX	7.1.1

A.1 Workaround

The regular wave analysis is performed by setting the wave type to Joint North Sea Wave Observation Project (JONSWAP), choosing unidirectional (long crested) with the chosen direction. The significant wave height and peak period is set to arbitrary values.

In the *Dynamic Calculation* settings, the "trick" to make the wave regular is found under the *SIMO parameters* tab. Here it is possible to choose *Wave time series*

from file. By choosing that option, it is possible to choose a wave time series created as a regular wave.

The wave time series is generated in MATLAB by scaling a sinus function according to the wave height and period. The result is written to a *.dat file containing two columns; time and wave elevation.

Appendix B

Static Results

B.1 Hydrostatic Stiffness Matrices

Table B.1: Hydrostatic stiffness matrix from Wadam analysis for the medium pontoon.

	1, Surge	2, Sway	3, Heave	4, Roll	5, Pitch	6, Yaw
1, Surge	0	0	0	0	0	0
2, Sway	0	0	0	0	0	0
3, Heave	0	0	1.39×10^7	0	0	0
4, Roll	0	0	0	3.02×10^8	0	0
5, Pitch	0	0	0	0	3.28×10^9	0
6, Yaw	0	0	0	0	0	0

Table B.2: Hydrostatic stiffness matrix corrected for buoyancy compensation force for the medium pontoon.

	1, Surge	2, Sway	3, Heave	4, Roll	5, Pitch	6, Yaw
1, Surge	0	0	0	0	0	0
2, Sway	0	0	0	0	0	0
3, Heave	0	0	1.39×10^7	0	0	0
4, Roll	0	0	0	6.59×10^8	0	0
5, Pitch	0	0	0	0	3.63×10^9	0
6, Yaw	0	0	0	0	0	0

Table B.3: Hydrostatic stiffness matrix from Wadam analysis for the large pontoon.

	1, Surge	2, Sway	3, Heave	4, Roll	5, Pitch	6, Yaw
1, Surge	0	0	0	0	0	0
2, Sway	0	0	0	0	0	0
3, Heave	0	0	1.75×10^7	0	0	0
4, Roll	0	0	0	4.62×10^8	0	0
5, Pitch	0	0	0	0	5.18×10^9	0
6, Yaw	0	0	0	0	0	0

Table B.4: Hydrostatic stiffness matrix corrected for buoyancy compensation force for the medium pontoon.

	1, Surge	2, Sway	3, Heave	4, Roll	5, Pitch	6, Yaw
1, Surge	0	0	0	0	0	0
2, Sway	0	0	0	0	0	0
3, Heave	0	0	1.75×10^7	0	0	0
4, Roll	0	0	0	1.04×10^9	0	0
5, Pitch	0	0	0	0	5.75×10^9	0
6, Yaw	0	0	0	0	0	0

B.2 Static Moment and Stress in Towers

[Intentionally blank page]

Table B.5: Tower heigh, maximum moment and stress about y- and z-axis and location for maximum for arch 2. Local y-axis is along negative global y-axis and local z-axis is along global x-axis.

Tower	Height [m]	$M_{y\max}$ [N m]	$\sigma_{y\max}$ [MPa]	Location [m]	$M_{z\max}$ [N m]	$\sigma_{z\max}$ [MPa]	Location [m]
n02a2tow	8.67	-8.02×10^5	0.3	8.67	-3.60×10^6	1.5	8.67
n03a2tow	8.67	-7.37×10^5	0.3	8.67	-5.72×10^6	2.4	8.67
n04a2tow	8.67	-7.85×10^5	0.3	8.67	-6.63×10^6	2.7	8.67
n05a2tow	8.67	-7.15×10^5	0.3	8.67	-6.92×10^6	2.9	8.67
n06a2tow	8.67	-5.34×10^5	0.2	8.67	-6.69×10^6	2.8	8.67
n07a2tow	8.67	-7.61×10^5	0.3	8.67	-5.67×10^6	2.4	8.67
n08a2tow	16.16	-1.18×10^6	0.5	16.16	-4.18×10^6	1.7	16.16
n09a2tow	24.25	7.92×10^4	0.0	24.25	-1.57×10^6	0.7	24.25
n10a2tow	31.74	6.49×10^6	2.7	31.74	-4.96×10^6	2.1	31.74
n11a2tow	38.56	-3.66×10^7	15.2	38.56	-2.01×10^6	0.8	38.56
n13a2tow	38.56	3.66×10^7	15.2	38.56	-2.01×10^6	0.8	38.56
n14a2tow	31.74	-6.49×10^6	2.7	31.74	-4.96×10^6	2.1	31.74
n15a2tow	24.25	-7.90×10^4	0.0	24.25	-1.57×10^6	0.7	24.25
n16a2tow	16.16	1.18×10^6	0.5	16.16	-4.18×10^6	1.7	16.16
n17a2tow	8.67	7.61×10^5	0.3	8.67	-5.67×10^6	2.4	8.67
n18a2tow	8.67	5.34×10^5	0.2	8.67	-6.69×10^6	2.8	8.67
n19a2tow	8.67	7.15×10^5	0.3	8.67	-6.92×10^6	2.9	8.67
n20a2tow	8.67	7.85×10^5	0.3	8.67	-6.63×10^6	2.7	8.67
n21a2tow	8.67	7.37×10^5	0.3	8.67	-5.72×10^6	2.4	8.67
n22a2tow	8.67	8.02×10^5	0.3	8.67	-3.60×10^6	1.5	8.67

Appendix C

Modelling Limitations in SIMA

The cables connecting the two bridge girders were initially modelled as *simplified wire connections* in SIMA. This was done in order to be able to add some pre-tension to the cables.

But, when the wires where shortened in order to obtain this tension, the analysis started to fail. The only error message provided by the software was that the rotations at some of the nodes where too large in order to obtain convergence in the results.

One theory is that this error was caused by the way the wire was connected to the model. Since the *simple wire connection* is a part of the SIMO package, the wire had to be connected to the floating bodies. In order to lift the wire to the desired height, the wire was connected to an off-body point on the floating body. As the pre-tension was introduced, this causes a large moment which has to be taken by the pontoon and tower, in order to transfer the forces to the girder.

This may have led to the error. Eventually it was decided, in agreement with supervisor, to discard the simple wire connections and replace them with bar elements.

Appendix D

Eigenmodes

D.1 Eignmode Frequencies and Periods

Mode	Frequency [Hz]	Frequency [rad/s]	Period [s]
1	0.0129	0.0811	77.52
2	0.0215	0.1351	46.51
3	0.0264	0.1659	37.88
4	0.0328	0.2061	30.49
5	0.0507	0.3186	19.72
6	0.0555	0.3487	18.02
7	0.0592	0.3720	16.89
8	0.0733	0.4606	13.64
9	0.0841	0.5284	11.89
10	0.0925	0.5812	10.81
11	0.0953	0.5988	10.49
12	0.1012	0.6359	9.88
13	0.1045	0.6566	9.57
14	0.1062	0.6673	9.42
15	0.1073	0.6742	9.32
16	0.1105	0.6943	9.05
17	0.1172	0.7364	8.53

18	0.1199	0.7534	8.34
19	0.1199	0.7534	8.34
20	0.1199	0.7534	8.34
21	0.1201	0.7546	8.33
22	0.1206	0.7578	8.29
23	0.1206	0.7578	8.29
24	0.1212	0.7615	8.25
25	0.1228	0.7716	8.14
26	0.1229	0.7722	8.14
27	0.1231	0.7735	8.12
28	0.1244	0.7816	8.04
29	0.1277	0.8024	7.83
30	0.1284	0.8068	7.79
31	0.1294	0.8130	7.73
32	0.1322	0.8306	7.56
33	0.1338	0.8407	7.47
34	0.1346	0.8457	7.43
35	0.1349	0.8476	7.41
36	0.1367	0.8589	7.32
37	0.1376	0.8646	7.27
38	0.1418	0.8910	7.05
39	0.1433	0.9004	6.98
40	0.1442	0.9060	6.93
41	0.1448	0.9098	6.91
42	0.1467	0.9217	6.82
43	0.1495	0.9393	6.69
44	0.1498	0.9412	6.68
45	0.1503	0.9444	6.65
46	0.1544	0.9701	6.48
47	0.1563	0.9821	6.40
48	0.1584	0.9953	6.31
49	0.1617	1.0160	6.18
50	0.1623	1.0198	6.16
51	0.1631	1.0248	6.13

52	0.1682	1.0568	5.95
53	0.1688	1.0606	5.92
54	0.1709	1.0738	5.85
55	0.1721	1.0813	5.81
56	0.1757	1.1040	5.69
57	0.1785	1.1215	5.60
58	0.1840	1.1561	5.43
59	0.1856	1.1662	5.39
60	0.1880	1.1812	5.32
61	0.1914	1.2026	5.22
62	0.1984	1.2466	5.04
63	0.2025	1.2723	4.94
64	0.2033	1.2774	4.92
65	0.2056	1.2918	4.86
66	0.2192	1.3773	4.56
67	0.2248	1.4125	4.45
68	0.2269	1.4257	4.41
69	0.2278	1.4313	4.39
70	0.2340	1.4703	4.27
71	0.2417	1.5186	4.14
72	0.2499	1.5702	4.00
73	0.2530	1.5896	3.95
74	0.2567	1.6129	3.90
75	0.2610	1.6399	3.83
76	0.2638	1.6575	3.79
77	0.2649	1.6644	3.78
78	0.2695	1.6933	3.71
79	0.2767	1.7386	3.61
80	0.2804	1.7618	3.57
81	0.2889	1.8152	3.46
82	0.2896	1.8196	3.45
83	0.2923	1.8366	3.42
84	0.2964	1.8623	3.37
85	0.3037	1.9082	3.29

86	0.3102	1.9490	3.22
87	0.3286	2.0647	3.04
88	0.3349	2.1042	2.99
89	0.3439	2.1608	2.91
90	0.3493	2.1947	2.86
91	0.3535	2.2211	2.83
92	0.3576	2.2469	2.80
93	0.3687	2.3166	2.71
94	0.3727	2.3417	2.68
95	0.3811	2.3945	2.62
96	0.3827	2.4046	2.61
97	0.3849	2.4184	2.60
98	0.3909	2.4561	2.56
99	0.3986	2.5045	2.51
100	0.3996	2.5108	2.50
101	0.4038	2.5372	2.48
102	0.4048	2.5434	2.47
103	0.4101	2.5767	2.44
104	0.4122	2.5899	2.43
105	0.4274	2.6854	2.34
106	0.4314	2.7106	2.32
107	0.4447	2.7941	2.25
108	0.4465	2.8054	2.24
109	0.4471	2.8092	2.24
110	0.4476	2.8124	2.23
111	0.4548	2.8576	2.20
112	0.4655	2.9248	2.15
113	0.4751	2.9851	2.10
114	0.4836	3.0385	2.07
115	0.4882	3.0675	2.05
116	0.4904	3.0813	2.04
117	0.4983	3.1309	2.01
118	0.5081	3.1925	1.97
119	0.5189	3.2603	1.93

120	0.5237	3.2905	1.91
121	0.5302	3.3313	1.89
122	0.5413	3.4011	1.85
123	0.5441	3.4187	1.84
124	0.5445	3.4212	1.84
125	0.5460	3.4306	1.83
126	0.5485	3.4463	1.82
127	0.5666	3.5601	1.76
128	0.5814	3.6530	1.72
129	0.5899	3.7065	1.70
130	0.6021	3.7831	1.66
131	0.6035	3.7919	1.66
132	0.6047	3.7994	1.65
133	0.6121	3.8459	1.63
134	0.6322	3.9722	1.58
135	0.6345	3.9867	1.58
136	0.6353	3.9917	1.57
137	0.6353	3.9917	1.57
138	0.6592	4.1419	1.52
139	0.6813	4.2807	1.47
140	0.6844	4.3002	1.46
141	0.7752	4.8707	1.29
142	0.7778	4.8871	1.29
143	0.7850	4.9323	1.27
144	0.8158	5.1258	1.23
145	0.8515	5.3501	1.17
146	0.8551	5.3728	1.17
147	0.8658	5.4400	1.16
148	0.9200	5.7805	1.09
149	0.9400	5.9062	1.06
150	0.9448	5.9364	1.06

Table D.1: Eigenmode frequencies and periods.

D.2 Mode shape Plots

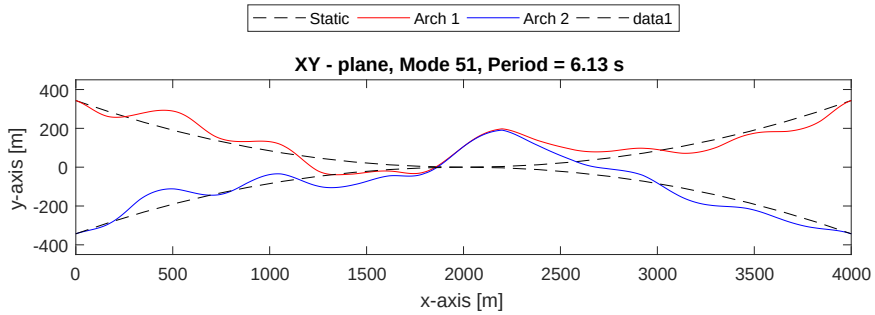

(a) Horizontal

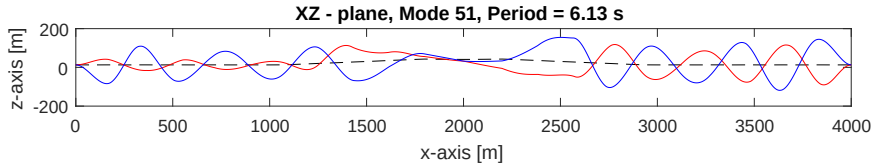

(b) Vertical

Figure D.1: Mode 51 dominated by vertical motions

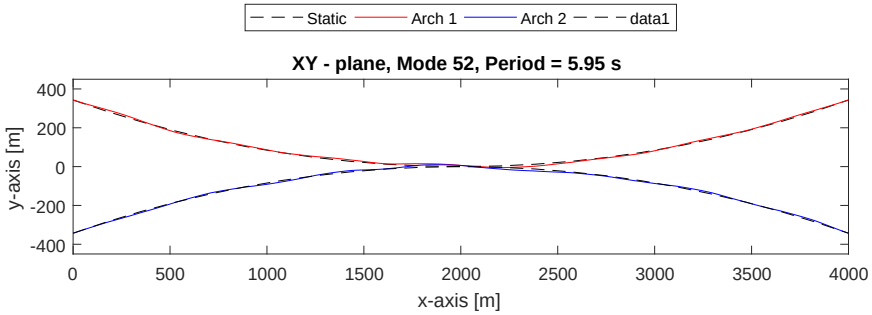

(a) Horizontal

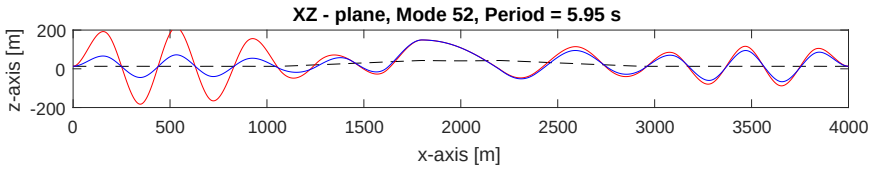

(b) Vertical

Figure D.2: Mode 52 dominated by vertical motions

D.3 All Mode Shape Plots

All mode shapes identified in the analysis can be found in the electronically attachment to this report.

Appendix E

Electronic Attachments

- Mode shape figures
- Sima model
- Hydrodynamic results
- Poster
- Cross sections